BIOREFINERY SYSTEMS ENGINEERING: FROM FACILITY LOCATION TO PROCESS SYNTHESIS AND DESIGN

A DISSERTATION
SUBMITTED TO THE FACULTY OF THE GRADUATE SCHOOL
OF THE UNIVERSITY OF MINNESOTA
BY

Adam J. Kelloway

IN PARTIAL FULFILLMENT OF THE REQUIREMENTS
FOR THE DEGREE OF
Doctor of Philosophy

Advised by Prodromos Daoutidis

May, 2015

Acknowledgments

I would like to thank my adviser, Professor Prodromos Daoutidis, for giving me the opportunity to work on interesting and challenging projects but also for teaching me to question the usefulness/appropriateness of every word, written or spoken in a professional setting -"words are like money, spend them wisely!"

I would also like thank Professor Michael Tsapatsis with whom I have worked closely over the last two years of my Ph.D. on the membrane modelling and techno-economic analysis work.

I would like to acknowledge my Daoutidis group office-mates over the years Dr. Fernando V. Lima, Dr. Milana Trifkovic, Dr. Ana I. Torres, Dr. Dimitris Georgis, Dr. Srinivas Rangarajan, Seongmin Heo, Abdulla Malek, Nahla Al Amoodi, Michael Zachar, Udit Gupta, Mustafa Caglayan, Nitish Mittal and Andrew Allman. I have been very lucky to share an office with friends who have always been generous with their time. In particular, I've enjoyed collaborating with Alex on biorefinery process design, and Nitish on membrane modelling. I will particularly miss our group's lively discussions and 2pm coffee break with Ian Hill and Samia Illias.

A special thanks to the members of the CEMS Graduate Student Committee and I wish you all continued success in our objectives. Also, I want to thank all my friends in CEMS who have made my graduate student life extraordinary, particularly Dr. Garrett Swindlehurst and Dr. Alex Marvin for some memorable times as housemates. I would

also like to acknowledge Laura Lennartson without whose generosity during my internship in Minnesota in 2009 I may never have applied to the Ph.D. program at the University of Minnesota.

And last but by no means least, my Mum who has always supported my decisions no matter how far away from home they have taken me.

For My Mum

Abstract

This thesis applies concepts, tools and techniques of Process Systems Engineering to problems arising from the conversion of biomass to fuel and chemical products.

Waste grease produced in metropolitan areas needs to be treated before it can be disposed. One option is to convert it to biodiesel for resale to the local population. The optimal locations of small-scale facilities for this conversion within Greater London is studied. The technical and economic performance criteria of a small scale facility are initially determined. These are then used in the formulation of an optimization problem that finds the best locations of these small scale production facilities within Greater London such that delivery times and resource utilization are optimized.

Biorefineries have been identified as a promising alternative to crude oil refineries for the production of fuels and chemicals. Biorefineries convert renewable biomass resources using multiple chemical and physical transformations. Process synthesis is the optimal, according to a specific objective function, selection and arrangement of processing units. A systematic biorefinery process synthesis problem is formulated for finding which products and processes result in a biorefinery with the highest economic potential or carbon efficiency.

Membrane based technologies are capable of efficiently tackling separation processes that remain challenging for traditional distillation. A hollow-fiber supported zeolite membrane technology is initially modelled. Techno-economic analyses of the feasibility of these

membranes applied to the dehydration of ethanol and the separation of butane isomers are then performed.

Finally, the standard pressure-driven flux membrane models previously used are extended to include a mathematical description of adsorption-diffusion based flux. This allows for flux to be predicted directly from operating conditions such as pressures and temperatures rather than relying on fixed values of permeance and selectivity to predict flux through the membrane layer. A comparison of a pressure-driven flux model with this novel adsorption-diffusion model for butane isomer separation is performed.

Contents

List of Tables

List of Figures

CHAPTER 1

Introduction

Mathematical modelling, simulation, and optimization of real-world chemical processes has formed a core pillar of chemical engineering for the last 50 years or more [58]. Whilst these activities have academic interest, the results that these produce allow for faster, safer and cheaper development of new industrially relevant processes and the improvement of existing ones. This allows all of us access to safer, cheaper and more environmentally sustainable chemical products and their derivatives.

The unifying theme of the research presented in this thesis is biomass conversion technologies and processes. Specifically, problems concerning the energy use, environmental impact and economics of these processes are addressed. The promise of a world where biomass is used as a renewable carbon source for the production of fuels and chemicals in integrated, multiple-feedstock, multiple-product facilities known as biorefineries remains an elusive and challenging goal. As shown in figure 1.1, designing a biorefinery requires choices for location, scale, biomass feedstock, product portfolio, conversion technologies and chemistries, and is affected by external factors such as governmental policies, environmental considerations and market conditions. Process Systems Engineering (PSE) approaches are ideally suited to tackle such problems.

Most problems that fall under the umbrella of PSE can be divided into separate domains

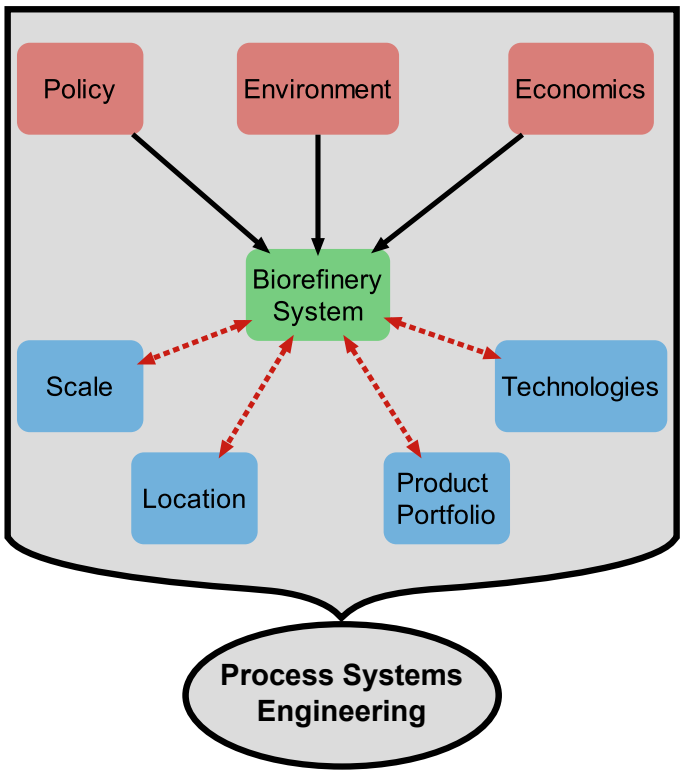

Figure 1.1: Process Systems Engineering for biorefineries [13]

(or levels) along characteristic length and time scales as shown in figure 1.2 [14]. Each domain provides relevant parameters for the analysis at higher levels whilst the higher domains provide constraints for the lower domain analyses. Key challenges addressing the conversion of biomass based feedstocks remain within each domain. At the chemistry scale, the challenge of elucidating the specific chemistry of biomass upgrading and its associated kinetic parameters remains. At the process and facility scales, the design of novel process equipment and separation technologies suited to the specific challenges associated with biomass based conversion technologies is required. At the enterprise level, the focus is on the design of biorefinery systems composed of multiple facilities where each is competing for limited and seasonal biomass resources but where each is also constrained by a limited demand for its products. While the ultimate goal of the biorefinery Process Systems Engineering community is to address all these challenges and domains simultaneously, this thesis tackles problems at the enterprise scale (chapter 2), facility scale (chapter 3), and process scale (chapters 4 and 5) separately. The overall objective in each of these is the development and better understanding of new technologies and processes with the aim of better resource utilization.

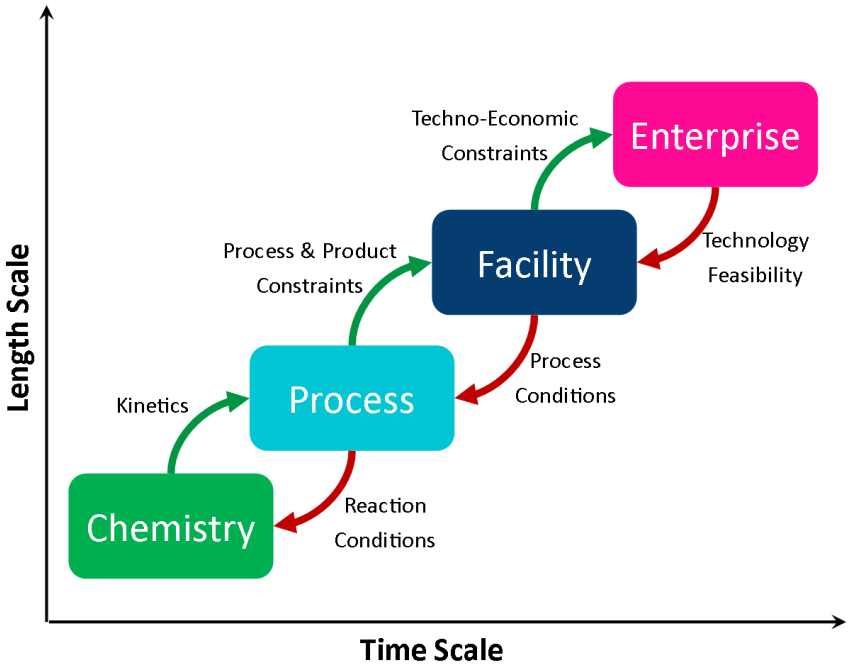

Figure 1.2: Length scales and time scales in Process Systems Engineering

Chapter 2 focuses on a small-scale waste grease to biodiesel facility location problem based in Greater London. Major cities produce a vast amount of waste grease annually which must be properly treated before it can be safely disposed of [73]. Recently, several companies have been created to convert their cities' waste grease into biodiesel for sale to local residents [73]. In the first part of this work, a novel process for the conversion of waste grease to biodiesel is modelled in Aspen HYSYS which allows for the calculation of process economics. Following this, a facility location problem is formulated based on the supply of waste grease, the demand for biodiesel in Greater London, and the aforementioned process economics.

Chapter 3 focuses on the process synthesis and analysis of biorefineries. The synthesis of integrated biorefineries, which akin to petroleum refineries, convert multiple feedstocks into multiple products through a broad set of physical and chemical processes, is an ambitious goal for this emerging industry. A schematic of this is shown in figure 1.3. Initial studies on process synthesis have focused on determining the single best technology for the production of single products, with emphasis on fuels [5, 44, 63]. Recent publications, however, have begun to consider process synthesis superstructures which include many technologies, feedstocks and products [43]. A key issue that needs to be addressed is the relationship (and competition) between chemicals and fuels production. The National

Renewable Energy Laboratory (NREL) suggests that chemicals (or more generally low-volume, high-value products) will play an important role in the overall profitability of the biorefinery, with the chemical products driving the profitability of the system and the fuels driving the capital expenditure. A comprehensive assessment of the economics of such biorefineries is currently lacking. This becomes the motivating statement of this work, which aims at elucidating the interplay between fuels and chemicals in a multi-feed, multi-product biorefinery facility.

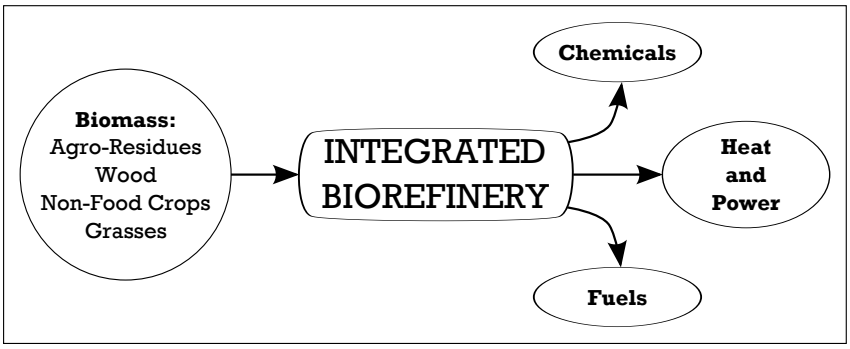

Figure 1.3: Biorefinery concept

A mixed integer non-linear process synthesis problem is formulated based on a multi-feed, multi-product facility which is capable of producing a broad set of fuel and chemical products from four biomass feedstocks. The selection of products is guided by the NREL's top value added products from biomass [72]. In addition to these several fuel products are also included. Two objective functions are considered. The first is an economic objective based on the facility's net present value while the second is an environmental objective based on carbon efficiency which seeks to maximize the utilization of feedstock carbon.

Chapter 4 focuses on a techno-economic analysis of a novel hollow-fiber supported zeolite membrane technology. The objective of this study is the generation of appropriate performance targets, in terms of membrane characteristics (flux, selectivity and costs), necessary to achieve economically competitive membrane-based processes compared to existing technologies. In the first part of this chapter, a model of a hollow-fiber supported zeolite membrane unit is developed in gPROMS. This model is used to analyze two specific case studies. The first addresses the dehydration of ethanol and the second focuses on the separation of butane isomers.

Corn ethanol is a \$20 billion business in the U.S.A. The separation of ethanol from water is energy intensive due to the azeotrope that forms between the two components at approximately 95wt% ethanol. Currently, ethanol is separated from water in a series of

distillation columns followed by a molecular sieve unit. The proposed approach involves eliminating some or all of the distillation columns and replacing them with a much smaller and less energy intensive membrane separation unit.

Butanes are produced from natural gas wells, as well as other petroleum refining operations. Butane isomers must be separated before they can be used for downstream production needs. n-Butane is used for gasoline blending and for the production of ethylene and butadiene, both important industrial chemical precursor molecules. It is predicted that a large market exists for membranes capable of separating condensible vapours such as n-butane and i-butane as well as other short chain hydrocarbons [3]. These close-boiling mixtures are separated on a very large scale in the synthesis of important chemical feedstocks [3]. The separation of butane isomers is traditionally accomplished via a distillation process. This process is energy and capital intensive because of the closeness of the isomers' boiling points.

For both case studies, net present value savings over existing technologies are calculated. These allow for the development of appropriate targets for several key membrane performance characteristics. These targets can then be used for laboratory-based development of the hollow-fiber supported zeolite-based membranes.

In chapter 5, the membrane model developed in the previous chapter is extended. The previously used model is based on a traditional, pressure-driven flux, formulation. Instead of this definition of flux through the membrane layer, an adsorption-diffusion model is formulated which includes adsorprtion-diffusion onto and through the zeolite layer, and molecular and Knudson diffusion through the support layer. Flux through zeolite membranes is driven by surface adsorption processes which are non-linear with respect to pressure [9]. Current membrane models use linear relationships between pressure and flux. These opposing statements suggest the need for the inclusion of advanced adsoprtion-diffusion models [35] into traditional membrane models. Furthermore, the negligible pressure drop assumption previously used is dropped in this work to further improve the accuracy of the model.

The objective of this chapter is two fold; firstly to develop the adsorption-diffusion model of a membrane unit and secondly to compare results of membrane performance between the new model and existing model formulations.

CHAPTER 2

Process Design and Supply Chain Optimization of Supercritical Biodiesel Synthesis from Waste Cooking Oils *

2.1 Introduction

Biodiesel has been identified as a viable alternative to fossil derived diesel fuel. Biodiesel produced from soybean oil, the industrially established method, can yield more energy than is invested in its production (the biofuel energy content exceeds the fossil energy inputs) by 93% and can reduce (through biological carbon dioxide fixation) the greenhouse gas emissions caused by its production and combustion by up to 41% [28]. Although potentially environmentally preferable to fossil based fuels, soybean biodiesel costs more than fossil diesel. At 2005 prices, soybean biodiesel production costs are \$0.55 per diesel EEL (energy equivalent liter) whereas the wholesale diesel price average was \$0.46/liter [28]. Subsidies play an important part in driving the production of biofuels; indeed, in the U.S.A. biodiesel receives a \$0.29/EEL federal government subsidy in addition to benefiting from subsidized soybean crops [10].

*Reprinted from *Chemical Engineering Research and Design*, **91**, 8, Adam Kelloway, W. Alex Marvin, Lanny D. Schmidt, and Prodromos Doaoutidis, Process design and supply chain optimization of supercritical biodiesel synthesis from waste cooking oils, 1456-1466 Copyright © 2013, with permission from The Institution of Chemical Engineers.

Soybean oil purchasing can make up to 84% of the total operating costs of a biodiesel production facility [21]. It has been suggested that yellow grease can be used instead of soybean oil for the production of biodiesel. Yellow grease is derived from waste vegetable cooking oil and is considerably cheaper than soybean oil [21].

The conversion of oils to biodiesel is performed using basic homogeneous catalysts to convert oils to fatty acid methyl esters (biodiesel) at moderate conditions (338°K, 1 atm). The base catalyzed process is preferable to the alternative acid catalyzed process as this reaction is slower and higher temperatures are required for similar biodiesel yields [22, 69, 70]. A saponification side reaction occurs when the traditional biodiesel production methods are applied to feeds high in free fatty acids (such as waste cooking oil). This reduces the biodiesel yield and complicates downstream separation processes. The saponification reaction occurs when free fatty acids are neutralized by the basic catalysts to free fatty acid salts (essentially forming soaps). The Mcgyan process [41] is a patented supercritical process that can avoid the saponification problems by performing the reactions over a proprietary heterogeneous catalyst at supercritical conditions.

Soybeans are a distributed resource and therefore, smaller, distributed biodiesel production facilities may prove to be economically favourable compared to the increasing cost of transportation associated with collecting the soybeans and delivering them to a centralized processing facility. Fore et al. [19, 20] have investigated both the economics and the energy balance of this idea for the production of soybean or canola oil based biodiesel using a yield based conversion efficiency to estimate the production flows. They concluded that the economic viability of these systems is heavily dependent on the price of petroleum diesel and the initial capital expenditure involved.

The principal objective of the work presented here is to investigate whether small scale biodiesel production is feasible and economical. The scale of each process was limited to a feed rate of 20kg/hr of either soybean oil or waste cooking oil. This scale was chosen such that each facility can be trailer mounted to retain the possibility of easy transportation between potential production sites. In order to accomplish this objective, we first simulated (in the HYSYS process simulation software) a Mcgyan process for the production of biodiesel from either virgin soybean oil or waste vegetable cooking oil. Using the results obtained from the HYSYS simulation, we performed a basic techno-economic analysis on each process to calculate the capital and operating costs such that the operating profit could also be calculated. We used the operating profit and capital costs in a discounted cash-flow analysis to find the net present value (NPV) for each case. The HYSYS process simulation results and techno-economic analyses were used as the

base case in the investigation of the economic feasibility of a distributed system of small scale biodiesel production facilities based in the Greater London area of the U.K.

2.2 Process design

The Mcgyan process is unique among commercial biodiesel processes for its ability to utilize low quality, high free fatty acid content oils as well as the traditional soybean oils. Furthermore, the catalyst used has been shown to catalyze both transesterification and esterification reactions simultaneously [41]. In this study, two extreme feedstocks are considered: pure triolein and pure oleic acid (a free fatty acid). Triolein is the triglyceride formed from three oleic acid molecules and glycerol. Triolein is used to simulate soybean oils and oleic acid is used to simulate waste cooking oils.

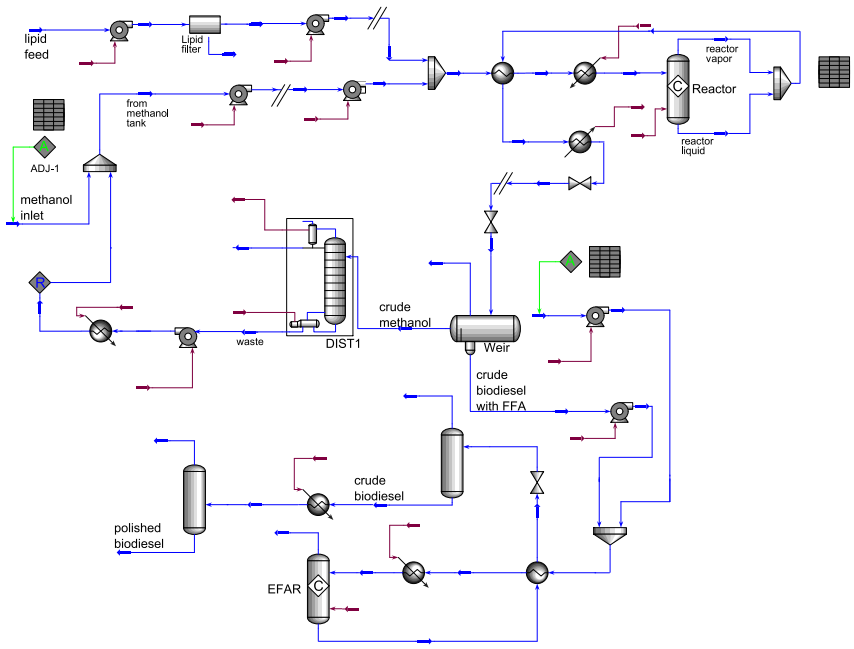

Figure 2.1: Biodiesel production system HYSYS flowsheet.

The Mcgyan process was designed in HYSYS and is shown in figure 2.1. The two feedstock cases examined differ in the composition of the stream "lipid feed", methanol to oil ratio in the reactor feed and reaction conversion in the "Reactor" unit. The specifics of the reaction conditions (temperatures and pressures) and specific flow compositions are omitted due to the proprietary nature of the Mcgyan process. However, we have worked closely with Sartec Inc., a Mcgyan process operator, to ensure that the HYSYS

simulations accurately predict the operating and performance parameters found in their production facility. The overall process proceeds as follows. The oil and methanol are mixed, pressurized and brought up to reaction temperature from where they are passed to the reactor unit. The reactor effluent is used in a reactor feed-effluent heat exchanger and then further cooled and passed to a weir separation tank which separates leftover methanol from crude biodiesel. The crude biodiesel is further reacted with a methylating agent to polish off any remaining free fatty acids. Finally, the polished crude biodiesel is distilled to fuel grade purity.

The non-random two liquid (NRTL) model was selected for the estimation of thermodynamic properties due to the presence of polar compounds (e.g. methanol and glycerol). Unavailable binary interaction parameters were estimated using UNIFAC liquid-liquid equilibrium (calculated at 40°C) as the methanol/biodiesel phase separation was important in most of the process. Equilibrium between vapour and liquid phase was important in the methanol distillation unit, so a separate NRTL model with UNIFAC vapour-liquid equilibrium parameters was used there. The Soave-Redlich-Kwong (SRK) equation of state was used for the supercritical alcoholysis reactor section where methanol is supercritical.

2.3 Economic analysis

The HYSYS models were used as a base for an economic assessment of the processes. All processes were assumed to run for 8,000 hr/yr and produce biodiesel that is up to ASTM (American Society for Testing and Materials) specifications. For the economic analyses, the pure triolein case was assumed to be soybean oil and the pure oleic acid case was assumed to be waste oil collected by Sartec, Inc.. Initially the capital costs of the processes were estimated and the operating costs were found using the unit costs shown in table 2.1. Having estimated the capital and operating costs (and operating profits), a discounted cash flow analysis was performed to find the net present value (NPV) of the processes. Finally, the sensitivity of this NPV to the main operating costs was investigated.

Table 2.1: Unit costs

Material Costs		
Methanol [30]	$ 0.17	$/lb
Virgin Soybean Oil [64]	$ 0.55	$/lb
Waste Oil [55]	$ 0.12	$/lb
Methylating agent [55]	$ 0.72	$/lb
Product Price		
Biodiesel [30]	$ 0.51	$/lb
Utilities [65]		
Cooling Water (400kpa, 6°C)	$ 0.01	$/m3
Electricity	$ 0.06	$/kW h
Low Pressure Steam (450kpa, 210°C)	$ 26.63	$/tonne
Refrigeration	$ 0.17	$/tonne
Waste Treatment [65]		
Liquid (Hazardous)	$ 200.00	$/tonne

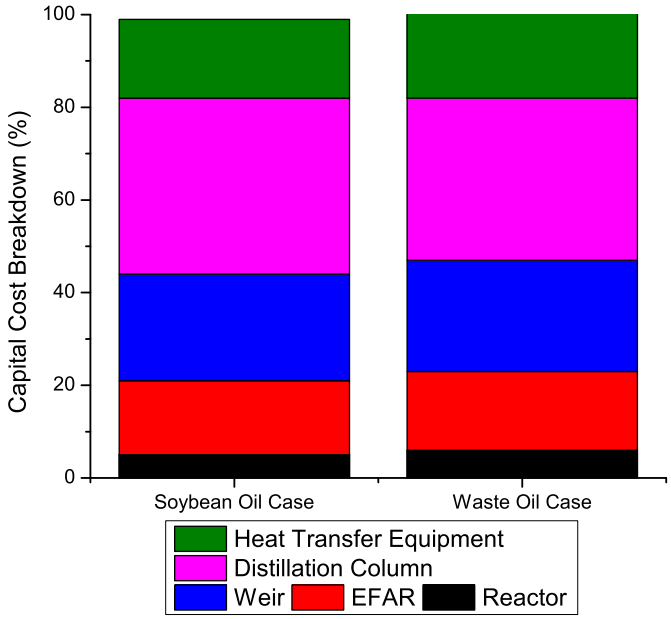

Figure 2.2: Capital cost breakdown

2.3.1 Capital cost estimates

The Guthrie [25] correlations taken from [18] were used throughout to estimate the purchase and installed costs of all capital equipment used in the process. The dimensions of the reactors and weir tank were acquired directly from Sartec Inc. and used in the

Guthrie correlations. The material and energy flows through the heater, coolers and heat exchangers were taken from the HYSYS model and used in conjunction with heat transfer coefficients estimated from [48] to estimate the heat transfer surface area needed. This can then be used in the Guthrie correlations to estimate the purchase and installed costs of the heat transfer equipment. The break down of capital cost expenditure for the main process equipment is shown in figure 2.2 where the total capital expenditure is $97,600 and $94,000 for the soybean and waste oil cases respectively. The most important factors that are missing from these capital cost estimates are land, piping and instrumentation costs. Figure 2.2 clearly shows that the differences between the total capital cost distributions between the soybean and waste oil cases are minimal.

2.3.2 Operating cost estimates

The flowrate of material feeds and the electricity usage were taken directly from the HYSYS simulation. The flow rates of high and low pressure steam and cooling water were estimated using the energy requirements of each heat transfer unit found in the HYSYS simulation. A figure showing the sources of operating costs is shown in figure 2.3 where the total operating cost is $222,000 and $87,800 for the soybean and waste oil cases, respectively. A summary of the gross operating profits can be found in table 2.2.

Table 2.2: Gross operating profit

	Soybean Oil ($/yr)	**Waste Oil Case ($/yr)**
Expenditure	$222,000	$87,800
Revenue	$175,800	$185,000
Gross Profit	**($46,500)**	**$97,000**

In contrast to the capital costs, figure 2.3 clearly shows that there are major differences in both the magnitude and distribution of operating costs between the soybean and waste oil cases. This fact will play a crucial role in determining the economic feasibility of the individual processes.

From table 2.2, it is noted that the soybean oil case generates a gross operating loss of approximately $46.5K whereas the waste oil case generates a gross operating profit of approximately $97K. The most important factors missing from this analysis are taxes, labour, insurance, supplies and maintenance.

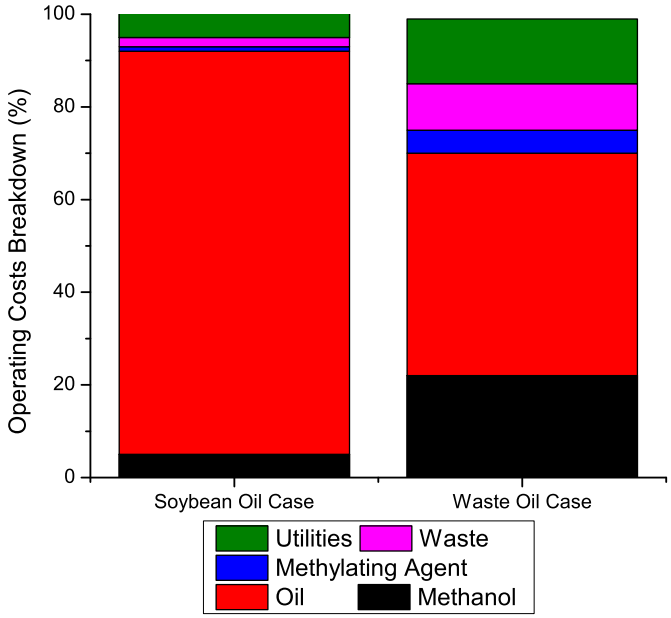

Figure 2.3: Operating cost breakdown

2.3.3 Net present value calculation

For the sake of NPV calculation, the capital expenditure of both scenarios was rounded up to \$120K. This was done in an attempt to account for some of the initial start-up expenses such as contingency, auxiliary and contractor fees but also to mitigate the fact that the Guthrie correlations tend to underestimate process equipment costs at these smaller scales. NPV was calculated (3.46) based on an annual discount rate of 10% over 15 years of operation where it was assumed that all the capital is spent in year one and full operation is established at the beginning of year two.

The NPV for the base case with virgin soybean oil was -\$474K and therefore we can say that small scale soybean oil based biodiesel product is not economically feasible. However, for the waste oil case the NPV was \$618K and the internal rate of return was calculated to be 80%. These NPV calculations do not take into account the depreciation of the capital equipment as well as the factors previously mentioned in the capital and operating costs estimate sections.

2.3.4 Sensitivities

Having established the base scenario economic estimates for both capital and operating costs and calculated the NPV of the plant, a sensitivity analysis was undertaken to investigate how changes in key economic variables affect the NPV of the processes. The key economic values identified for this study are: capital costs, methylating agent price, feed oil price, methanol price and biodiesel selling price.

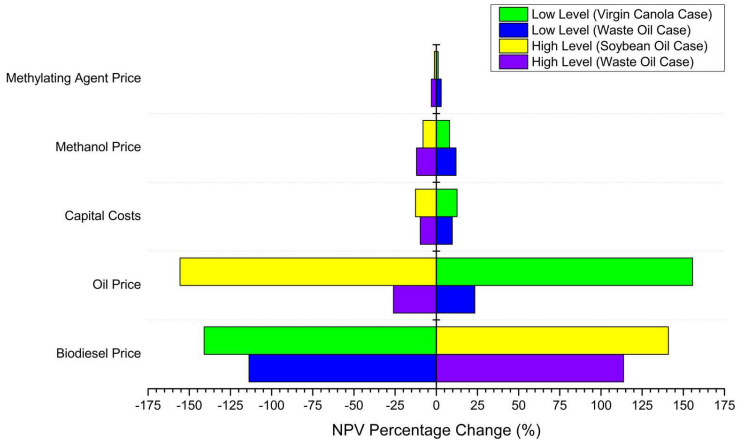

Figure 2.4: Sensitivity analysis results

The results of the sensitivity analysis are shown in figure 2.4 where each of the key variables identified increased to a high level value of 50% above their base value and a low level value of 50% below their base value. The sensitivity analyses clearly show that using waste oil results in a process that is much less sensitive to external cost factors when compared to the virgin soybean oil case. For the virgin soybean oil case the process is most sensitive to the soybean purchase price whereas for the waste oil case it is most sensitive to the biodiesel price. In fact, the break even (NPV=0) soybean oil price is \$0.42/lb - representing a 24% decrease from the base case. The break even biodiesel price for the soybean oil case is \$4.77/gal - representing a 26.5% increase from the base case. The break even price of biodiesel for the waste oil case was calculated to be \$1.79/gal.

The results of the process simulation, techno-economic analysis and associated sensitivity studies show that the waste cooking oil based biodiesel process is both more economically favourable and more robust to external parameters such as material costs than the virgin soybean oils based process.

In the following sections, we explore the feasibility of a system of small scale biodiesel

production facilities. The waste cooking oil based biodiesel process is chosen over the soybean based process because of its superior economics and robustness. The choice of waste cooking oil based facilities suggests focusing the study region on a large city with an abundance of waste oil supply and potential biodiesel consumers.

2.4 Facility location and supply chain optimization

In this section, we investigate the economic feasibility of a distributed network of biodiesel production facilities installed in the Greater London area of the UK. This location is chosen in order to take advantage of the availability of waste cooking oil. There are over 8000 fast food outlets in Greater London [2] as well as numerous other restaurants and office canteens all of which have the potential to be sources of used cooking oil. This location is also used to take advantage of the concentrated demand for biodiesel and economies of "mass" produced capital equipment when a large number of similar facilities are built. The biodiesel facility location problem is formulated as a mixed integer linear program (MILP) with the objective to maximize system-wide NPV. Total capital investment is described as a function of installed capacity using a general piecewise linear function and thus allowing for the effect of capital cost reductions due to mass production to be addressed.

The model of the Mcgyan process described above using waste cooking oil feedstock is used as the base case technology in each installed facility. The scale of each facility is that of the trailer mounted system at Sartec Inc., MN, U.S.A.. This small scale is chosen to ensure that installing these facilities in Greater London remains feasible given land limitations. Due to the lack of detailed biodiesel demand data, a uniform demand across Greater London is also assumed. This assumption leads to fixed facility locations in the problem formulation.

2.4.1 Problem formulation

The problem is formulated as a facility location problem with the objective function to maximize NPV for the entire region. Greater London is divided into its 649 electoral wards and each of these is considered as a potential customer source (where $w \in \{1 \dots W\}$ is the set of all customers) and facility site (where $i \in \{1 \dots I\}$ is the set of all potential facility locations). NPV is calculated over a T=15 year time horizon with a discount rate

r=10%. Depreciation is not considered. All the plants are installed in the first year, start producing in year two and then have constant annual profit. NPV is defined as follows:

$$NPV = \theta \sum_i P_i - TCI \tag{2.1}$$

where θ is a discounting factor to account for discounting of the future annual profits to year one:

$$\theta = \frac{(1+r)^T - 1}{r(1+r)^T}$$

The decision variables are the quantity of annual biodiesel shipments ($Ship_{i,j}$), number of installed facilities (where x_i is the binary which takes a value of 1 when there is a facility installed at ward i) and their locations in Greater London. Biodiesel shipments cannot exceed the maximum biodiesel demand at each ward (2.2) or the facility production capacity (2.3):

$$\sum_i Ship_{i,j} \leq D_w \quad \forall w \tag{2.2}$$

$$\sum_w Ship_{i,w} \leq CAP \cdot x_i \quad \forall i \tag{2.3}$$

Annual profit for each facility is defined with sales revenue R reduced proportionally (by the factor DC) to the distance a customer must travel to purchase biodiesel and an operating cost (OC) such that:

$$P_i = \sum_w (R - DC \cdot Dist_{i,w}) - OC \sum_w Ship_{i,w} \quad \forall i \tag{2.4}$$

Biodiesel shipments are nonnegative such that:

$$Ship_{i,w} \geq 0 \quad \forall i, w \tag{2.5}$$

Binary decision variables denote facility installation at each of Greater London's 649 electoral wards and therefore:

$$x_i \in \{0, 1\} \quad \forall i \tag{2.6}$$

A complete list of sets, parameters and decision variables is shown in section 2.6.

To take into account the potential savings associated with mass produced capital

equipment, we define the total capital investment (TCI) for the entire region as a function of the number of installed facilities. The capital investment associated with installing an M_j number of facilities is $C_j = C_0(M_j)^{1+b}$, where C_0 is the single facility capital cost. There is a discount per plant if $b < 0$. This discount is described by the progress ratio $PR = 2^b$ [27]. Having a PR of 0.97 is equivalent to a 3% cost savings for each doubling of the number of installed facilities. The total capital costs no longer follow a linear relationship to total number of facilities and the resulting relationship is shown in figure 2.5.

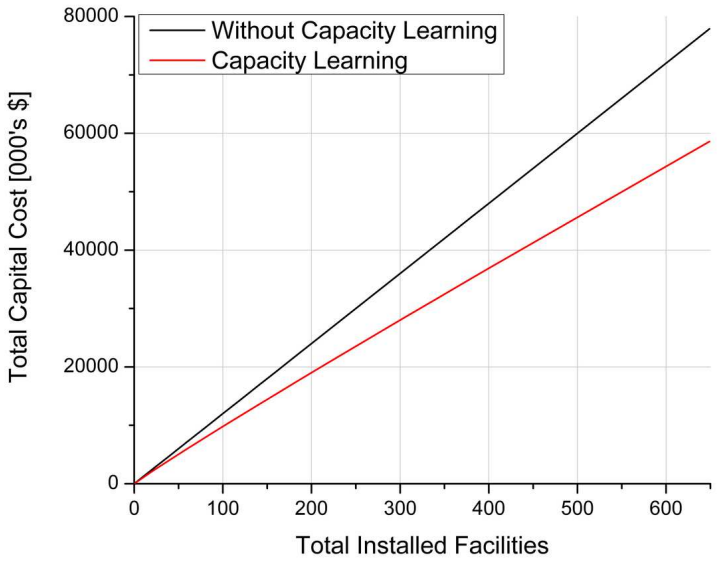

Figure 2.5: Comparison of total capital costs with and without capacity learning

To implement this non-linear total capital costs relationship while still maintaining an overall linear program, we introduce a general piecewise linear function that passes through a set of J points $\{(Mj, Cj); j \in \{1, \ldots, J\}\}$. It should be noted that this set of points are model parameters, and are calculated prior to optimization. For our purposes, we choose a set of $\{M_j\}$ to be spaced between M_1=0 (zero plant installations) and M_J=649 (maximum installations with one facility per candidate site). Our formulation allows for any functional relationship between C_j and M_j to be used, but we used a power law relationship described by the progress ratio discussed above. This is implemented by introducing variables λ_j that determine the position along the curve (eqs. (2.7) and (2.8)) and are constrained (using binary variables y_j) to be a special ordered set of type 2 (eqs. (2.9) to (2.12)). The variables λ_j represent fractional weights of the (M_j,C_j) points of the piecewise linear function (eqs. (2.13) and (2.14)).

$$TCI = \sum_j C_j \cdot \lambda_j \tag{2.7}$$

$$\sum_i x_i = \sum_j M_j \cdot \lambda_j \tag{2.8}$$

$$\lambda_j - y_{j-1} - y_j \leq 0 \quad \forall j \tag{2.9}$$

$$y_0 = y_J = 0 \tag{2.10}$$

$$\sum_j y_j = 1 \tag{2.11}$$

$$y_j \in \{0, 1\} \quad \forall j \tag{2.12}$$

$$\sum_j \lambda_j = 1 \tag{2.13}$$

$$0 \leq \lambda_j \leq 1 \quad \forall j \tag{2.14}$$

Each ward is a candidate facility location. Straight-line travel distances between ward centroids were calculated from UK ordinance survey coordinates. Inner ward travel distance was approximated as the average within a circle of equal area to that ward. Maximum biodiesel demand D_w for each ward is proportional to its population, Pop_w (2001 census), using the UK average petroleum diesel consumption per capita of $D = 324.3 L.(p.yr)^{-1}$ from Earth Trends. In particular, $D_w = Mpen \cdot D \cdot Pop_w$ where $Mpen$ is the maximum biodiesel market penetration. All other parameters are shown in Table 2. The MILP (eqs. (2.2) to (2.14) and (3.46)) is formulated in *GAMS v23.5.2* and solved using *CPLEX v12.1.*

Annual maximum biodiesel demand density ($L.(ha.yr)^{-1}$) is an important metric for this facility location problem, because a shorter customer transportation distance translates into a higher biodiesel selling price. Figure 2.6 shows the biodiesel demand density scaled to the highest value of $7.89 \cdot 10^5 L.(ha.yr)^{-1}$ in Cordwainer Ward in the City of London. Demand density is most concentrated near the center of London.

2.4.2 Results

Initially, we assume there is no mass production of the capital equipment and therefore no associated capital cost savings. Thus $PR = 1$, $b = 0$, and any set of $\{M_j\}$ such that $M_1 = 0$ and $M_J = 649$ will yield the same capital cost per facility. The total capital

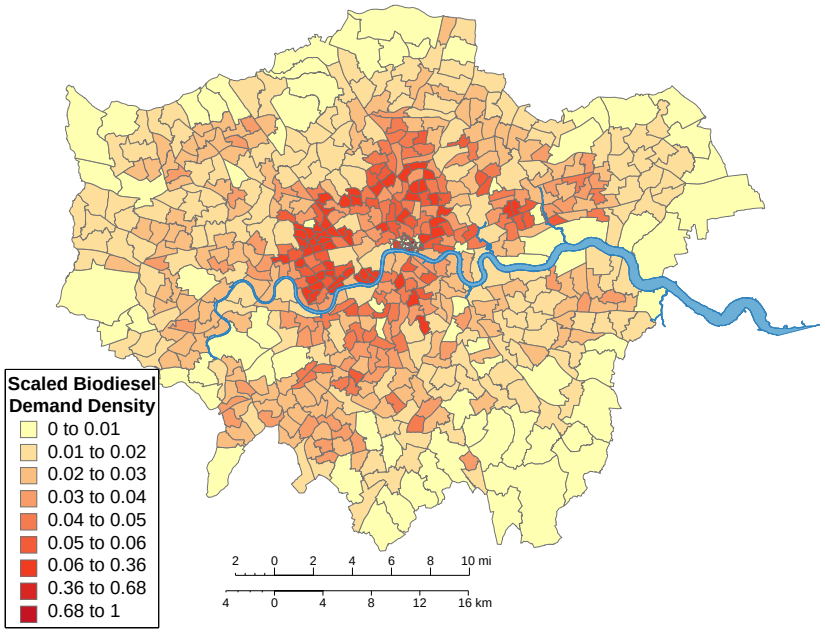

Figure 2.6: Scaled biodiesel demand

investment is thus defined in this part as follows:

$$TCI = CAPEX \cdot \sum_{i} x_i \tag{2.15}$$

where $CAPEX$ is the capital cost of one facility ($120K).

Table 2.3: Parameter values used

Parameter	Value
$Mpen$	0.3
R	0.99
DC	0.3
OC	0.474

In this first scenario we use the parameters in table 2.3. The MILP involves 422,501 decision variables and 649 binary variables constrained by 1,949 equations and *CPLEX* converged to a relative optimality gap of 1% within one minute.

The resulting facility locations are shown in figure 2.7 and in figure 2.8 overlaid with the percentage demand satisfaction of each ward. Biodiesel shipments from facilities to

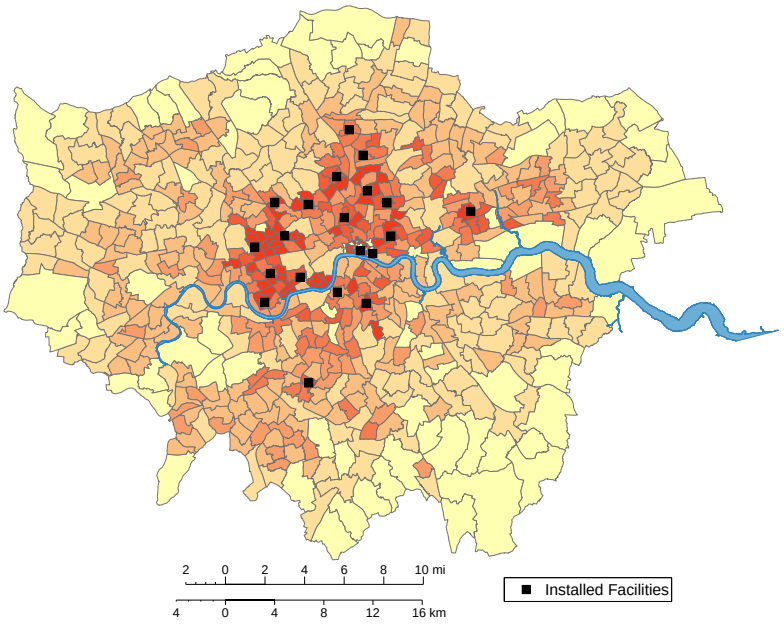

Figure 2.7: Results - first scenario (no capital costs savings modelled)

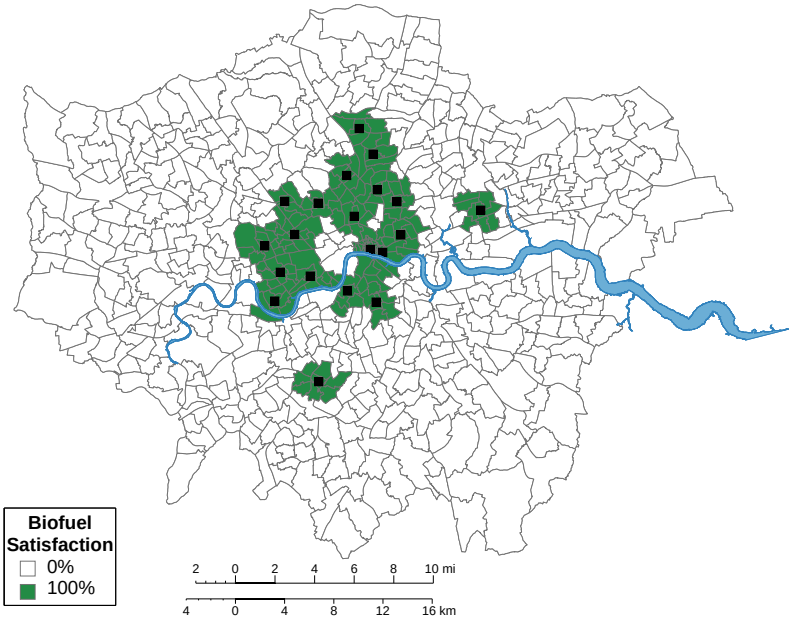

Figure 2.8: Results - first scenario - demand satisfaction

wards are not shown for simplicity. There are 20 installed facilities that satisfy 26.6% of the maximum biodiesel demand for the whole region, and the NPV is \$1.1MM with

an initial capital investment of $TCI = \$2.4MM$. As expected, higher demand density regions are preferred for facility installation. On average each facility only uses 52.1% of its maximum capacity.

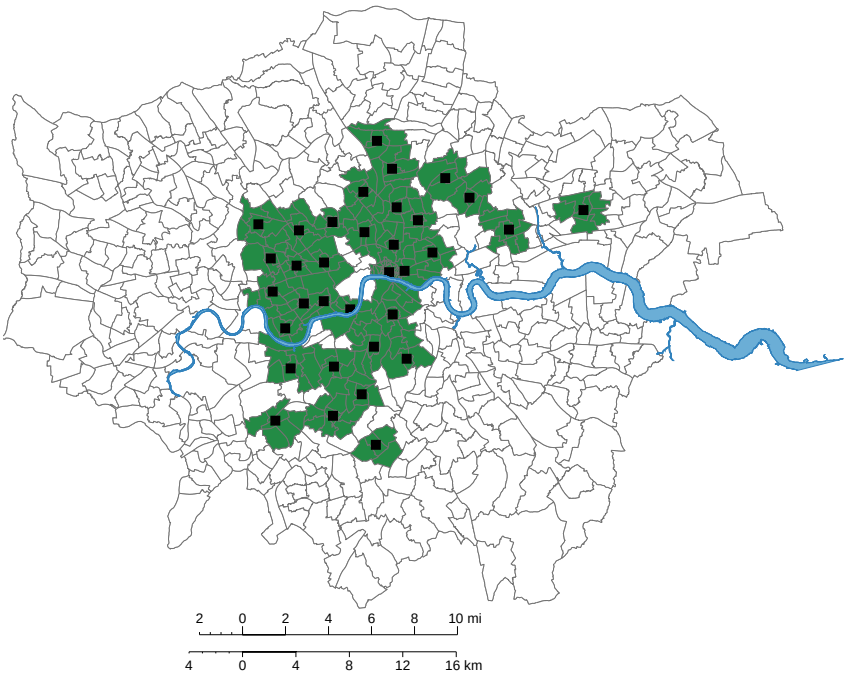

Figure 2.9: Results: capacity learning run - demand satisfaction

Next, we consider the potential savings associated with mass produced capital equipment as described above in eqs. (2.7) to (2.14) using the same basic operating cost parameters as above (table 2.3). The results in figure 2.9 show that the number of plants has now increased to 34. The demand satisfaction and NPV both increased to 37.1% and \$1.5MM respectively. TCI increased to \$3.5MM but represents a reduction in TCI per plant from \$0.12MM to \$0.10MM with capacity learning.

It is interesting to note that all the wards receiving biodiesel have 100% of their demand satisfied. The formulation is such that there is no equality constraint on biodiesel demand. There is such a high cost associated with customer transportation (DC) that it is advantageous only to sell to nearby customers and operate the facility under capacity, rather than operating at full capacity and having to find customers further away. In this case, each facility only uses 42.7% of its capacity - a reduction from the previous scenario.

Finally, we reduce the distance based cost parameters (DC) to 0.1 with the cost reduction scheme still in place. The solution now has an increased number of installs to 54 and an increased NPV of \$13MM with an increased average capacity utilization of 72.4%. This

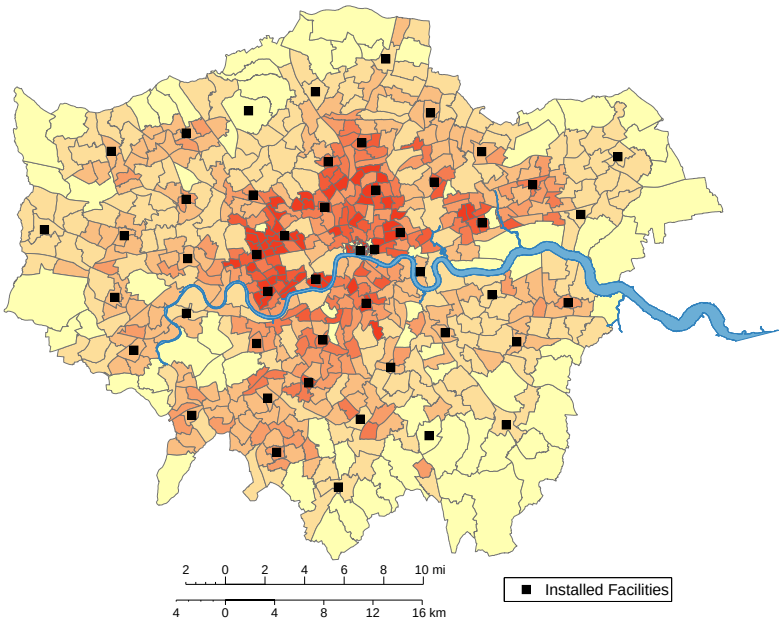

Figure 2.10: Results: third run - reduced DC value

second set of results is shown in figure 2.10. The installed facilities in these results are more spread out across the region than in the earlier results; this is indicative of the reduced distance based cost parameter DC.

2.4.3 Monte Carlo analysis

In the final phase of the study we investigated how variability of key economic parameters affects the overall solution. Using the capacity learning model, a normal distribution of parameters R, DC, OC is sampled. The sample for each run is taken randomly from a normal distribution of each parameter with the mean taken as the original value in table 2.3 and standard deviation as 10% of the mean value. The results are shown in figure 2.11. Only one ward (Tower Ward in the Hammersmith and Fulham District) has an installed facility more than 80% of the samples. The NPV is found to range from \$0.02MM to \$15.8MM and the total number of installed facilities ranges from 1 to 115. Following this initial study where we sampled over the three parameters simultaneously, we further investigated the specific source of the variability that led to the broad range of solutions found. This is accomplished by sampling over each parameter individually. When a normal distribution of R is sampled we get the distribution of NPV shown in

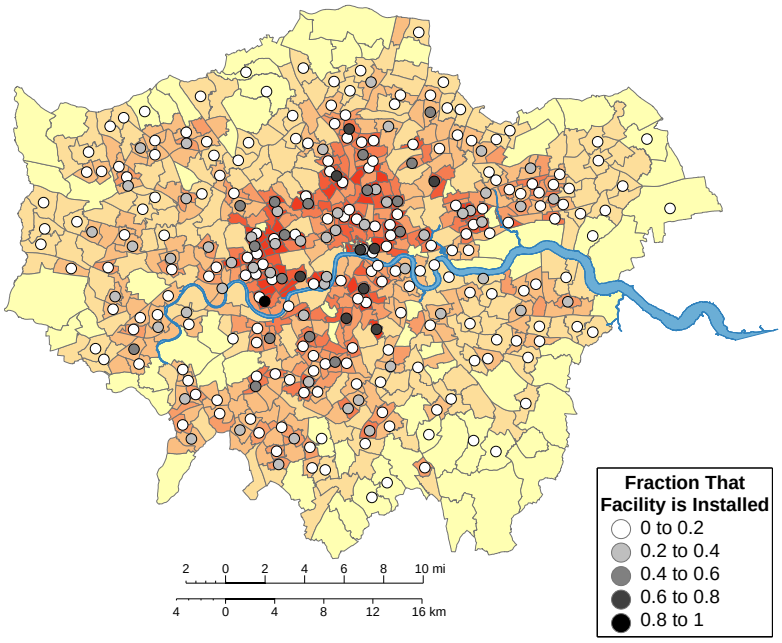

Figure 2.11: Results - Monte Carlo run sampling over R, DC and OC simultaneously

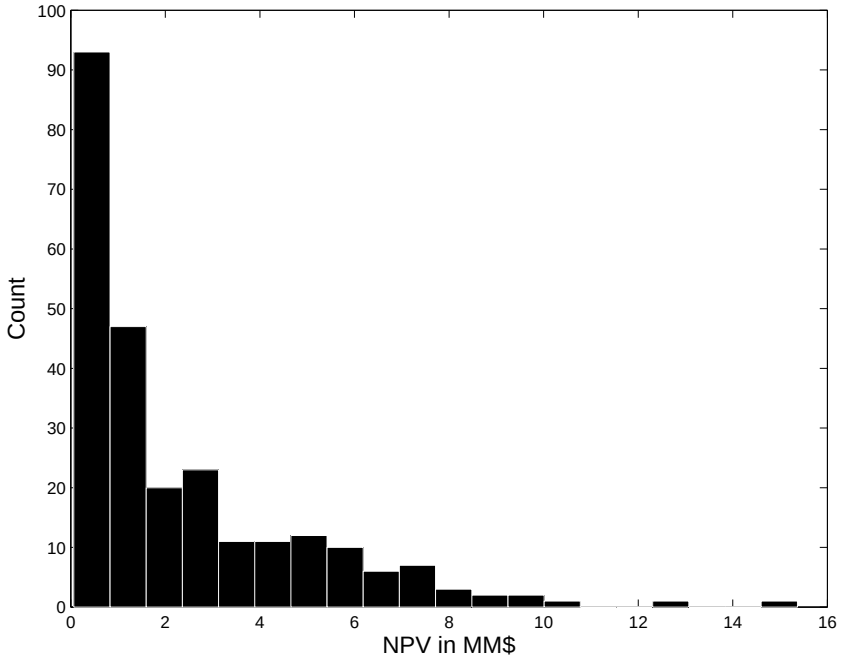

Figure 2.12: NPV distribution on sampling of R - min: 0.07, max: 15.4

figure 2.12 with a minimum NPV of \$0.07MM and a maximum of \$15.4MM. When we sample *DC* instead we get the distribution of NPV shown in figure 2.13 with a minimum

NPV of \$0.5MM and a maximum of \$4.0MM. Finally, when we sample OC we get the distribution shown in figure 2.14 with a minimum NPV of \$0.2MM and a maximum of \$5.5MM. It can be seen from these figures that the sensitivity of the process to economic parameters is driven by variability in the revenue, R. An increase in the revenue (driven by an increased biodiesel sale price) leads, as expected, to large changes in the overall NPV (by more than 1000% in extreme cases); indeed, this means that the process is most sensitive to the sale price of biodiesel as shown in the single facility analysis. The important point of these Monte Carlo analyses is that in no individual sample was the NPV negative and thus it can be said that under a broad range of economic parameters the waste cooking oil to biodiesel process is profitable and economically feasible.

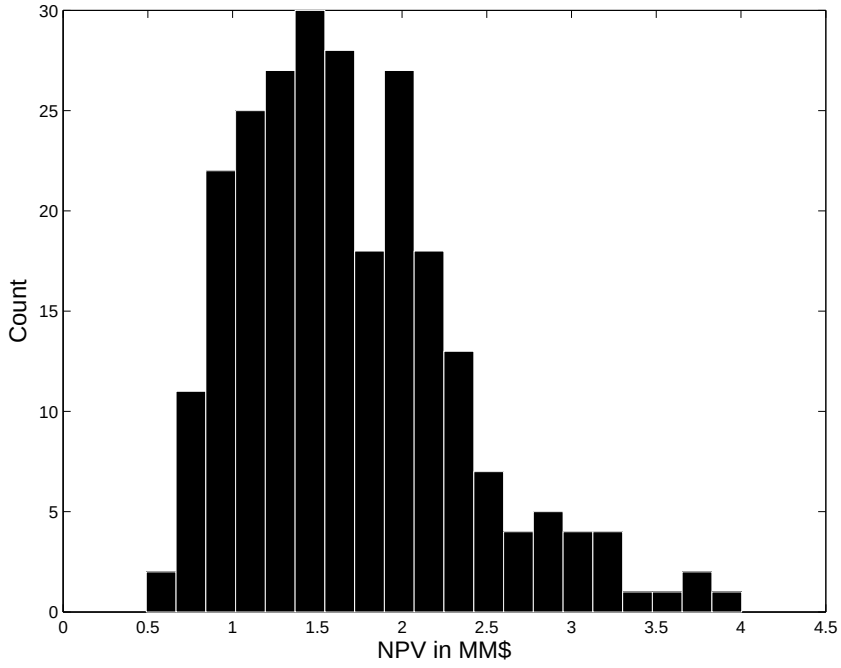

Figure 2.13: NPV distribution on sampling of DC - min: 0.5, max: 4.0

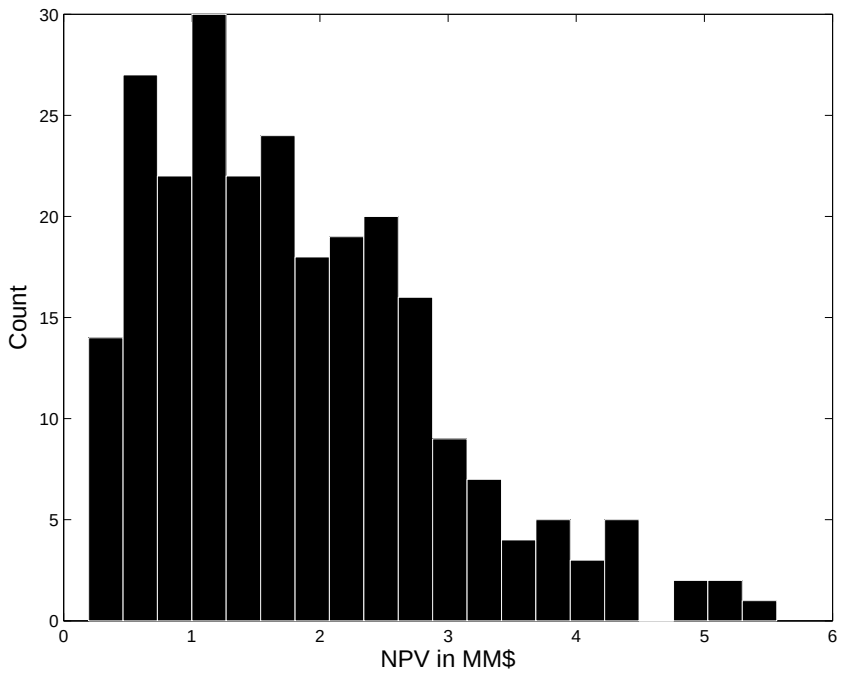

Figure 2.14: NPV distribution on sampling of OC - min: 0.2, max: 5.5

2.5 Conclusions

We initially developed designs based on the Mcgyan process for the production of biodiesel, using virgin soybean oil and waste cooking oil as the principal feedstock. It was determined that a system operating on a 20kg/hr feed of waste cooking oil has an NPV of $618K based on a 15 year project horizon; whereas, when operating on virgin soybean oil the NPV is -$474K. The analysis shows that the low purchase cost of waste cooking oil ($0.12/lb) is the principal driver of the positive economic potential of this scenario. The high purchase costs of soybean oil ($0.55/lb) is the principal reason behind the negative economic potential of that scenario. Furthermore, the Mcgyan process is ideally suited for waste cooking oil feeds as it can handle the high concentration of free fatty acids found in these oils. This makes it more profitable than the traditional biodiesel process when using the cheap waste oil as a feedstock.

We then formulated a MILP to solve a facility location problem that involves finding the optimal locations and capacities for a set of small scale production facilities using the Mcgyan process to convert waste restaurant grease into biodiesel in the Greater London area. A Monte Carlo analysis showed that the system is most sensitive to changes in revenue but also that under all parameters sampled the system was profitable and

economically feasible and can, therefore, be seen as a possible step towards a more locally focused fuels supply network.

This research has shown that small scale distributed production of biodiesel is economically feasible in a large city. Biodiesel production may contribute to the reduction of CO_2 emissions from fossil fuel based diesel production and consumption. Perhaps more importantly, this process can help reduce cooking oil waste processing by converting it into biodiesel that is sourced, produced and sold locally.

2.6 Notation

The definitions and descriptions of the sets, parameters, and variables used in this chapter are shown in table 2.4

Table 2.4: Desciption of sets, parameters, and variables used in chapter 2

Sets	**Description**
$w \in \{1, \ldots, W\}$	Demand sources
$i \in \{1, \ldots, I\}$	Candidate facilities
$j \in \{1, \ldots, J\}$	Set of logicals for capacity learning
Parameters	**Description**
θ	Discount factor [yr]
CAP	Capacity [L]
R	Revenue per biodiesel liter [$/yr]
DC	Distance based cost [$/mile.L]
D_w	Demand at source w [L/yr]
OC	Operating cost per biodiesel liter [$/L]
$Dist_{i,w}$	Distance from i to w [mile]
$CAPEX$	Capital cost of one facility [$]
r	Discount rate [%]
T	Time horizon [yr]
Variables	**Description**
NPV	System net present value [$]
P_i	Profit at facility i [$/yr]
$Ship_{i,w}$	Shipment from facility i to demand w [L/yr]
x_i	Installation binary
TCI	Total capital investment [$]
C_j	Capital costs [$]
M_j	Installed plants in piecewise linearization
λ_j	Piecewise linearization factor
y_j	Logicals binary

CHAPTER 3

Process Synthesis of Biorefineries: Optimization of Biomass Conversion to Fuels and Chemicals *

3.1 Introduction

The concept of a biorefinery as a biomass-based parallel to the petroleum refinery has emerged as a strategy to mitigate increased levels of carbon dioxide in the atmosphere, depletion of easily recoverable crude oil, and uncertainties in energy supply. The current state of U.S. biofuels/biochemicals production is dominated by the production of first generation biofuels that compete for feedstocks with the food and feed industries. Research has focused on the production of second and third generation biofuels and biochemicals from lignocellulosic materials, woody crops, agricultural wastes and residues. These products may not compete for the same such feedstocks as current ethanol and biodiesel production methods. Biorefineries are envisioned to use such non-food biomass feedstocks to produce a portfolio of fuels and chemicals through a broad set of physical, chemical and biological processes [8].

In 2004, the United States Department of Energy (DOE) produced a report detailing

*Reprinted (adapted) with permission from Adam Kelloway, and Prodromos Doaoutidis, *Industrial & Engineering Chemistry Research*, **53**, 13, 5261-5273 (2014) Copyright © 2013 American Chemical Society.

the top value-added chemicals from biomass [72]. This report also identifies the most important technologies within the biorefinery landscape. These include: fermentation, gasification, pyrolysis and aqueous-catalytic technologies. This report, as well as others [32], identified potential products from potential feedstocks but also concluded that the chemical conversion pathways for these transformations can be quite complicated. To address this complexity from a systems perspective, several authors have investigated the synthesis of such reaction pathways. A rule-based software tool for systematically generating these pathways has recently been proposed [51]. This tool has been applied to the generation and optimal selection of biofuel-gasoline blends [40]. Thermodynamic feasibility [61,62] or hierarchical optimization approaches [52,53] to generate and evaluate feasible reaction pathways have also been proposed. Finally, a systematic "forward-backwards" synthesis approach to generating possible reaction pathways in a biorefinery has been proposed [49]. A broad discussion of the systems challenges involved in designing biomass conversion processes and facilities can be found in [15]. A collection of papers addressing issues related to product and process design, feedstock selection, supply-chains and process synthesis can be found in [59].

Combining the complex biomass conversion pathways and processes into integrated biorefinery configurations remains a challenge [78]. The process synthesis of gasification based biorefineries using a fuzzy optimization approach has been studied in [63]. An automated targeting framework for the synthesis of biorefinery configurations has been proposed in [44] and applied to a gasification based case study. The synthesis of biomass derived liquid fuels was addressed in [5]. The synthesis of multiple feedstock biorefineries producing ethanol, hydrogen and biodiesel has been studied in [54], also considering the trade-offs between economic and environmental objectives. In a similar study [43] a generalized disjunctive programming approach for the process synthesis of biorefineries was proposed and applied to a case study based in Mexico.

The goal of this chapter is to expand upon the previous studies and propose an optimization based process synthesis formulation applied to biorefineries that produce a multitude of chemicals and fuels from multiple feedstocks. We select chemical products from the DOE top value-added biomass derived products. To this list we add gasoline, diesel and Fischer-Tropsch fuel products. We select these products such that they span the most frequently cited biorefinery products [32] with equal importance given to fuels and chemicals. With these chosen products we formulate a biorefinery superstructure comprised of the feasible inter-connections between the different technologies selected. We then formulate and solve the resulting mixed integer non-linear program (MINLP) to obtain a base case solution configuration. Next, we undertake a set of sensitivity analyses

which involve the systematic variation of parameters and the subsequent investigation of their effects on the overall solution. This allows us to elaborate on which technologies are most profitable for different values of the economic parameters. We also formulate a multi-objective mixed integer non-linear program (MoMINLP) by maximizing both NPV and carbon efficiency and we identify trade-offs between these two objectives, finding the Pareto frontier of best feasible solutions. Finally, we perform a Monte Carlo sampling of the parameter space which involves randomly sampling a distribution of economic parameters and again investigating the subsequent solutions. This indicates which products and technologies are most likely to lead to biorefinery configurations with maximized economic potentials.

Our approach allows for the systematic and explicit evaluation and comparison of different biorefinery configurations. It also allows us to investigate the relationship (and competition) between chemicals and fuels production. This information can be valuable for future investment and/or policy decisions in this emerging industry.

3.2 Biorefinery superstructure

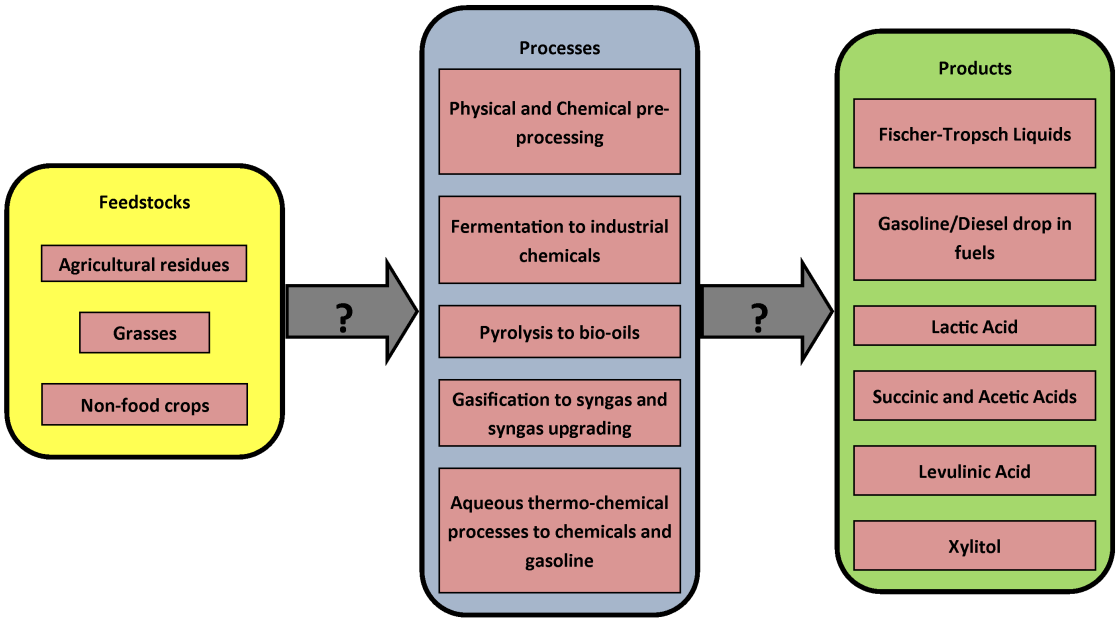

Figure 3.1: Overview of proposed biorefinery concept

In figure 3.1 we present the feedstocks, technologies and principal products considered throughout this chapter. These products span both fuels and chemicals and can be

produced from a variety of feedstocks.

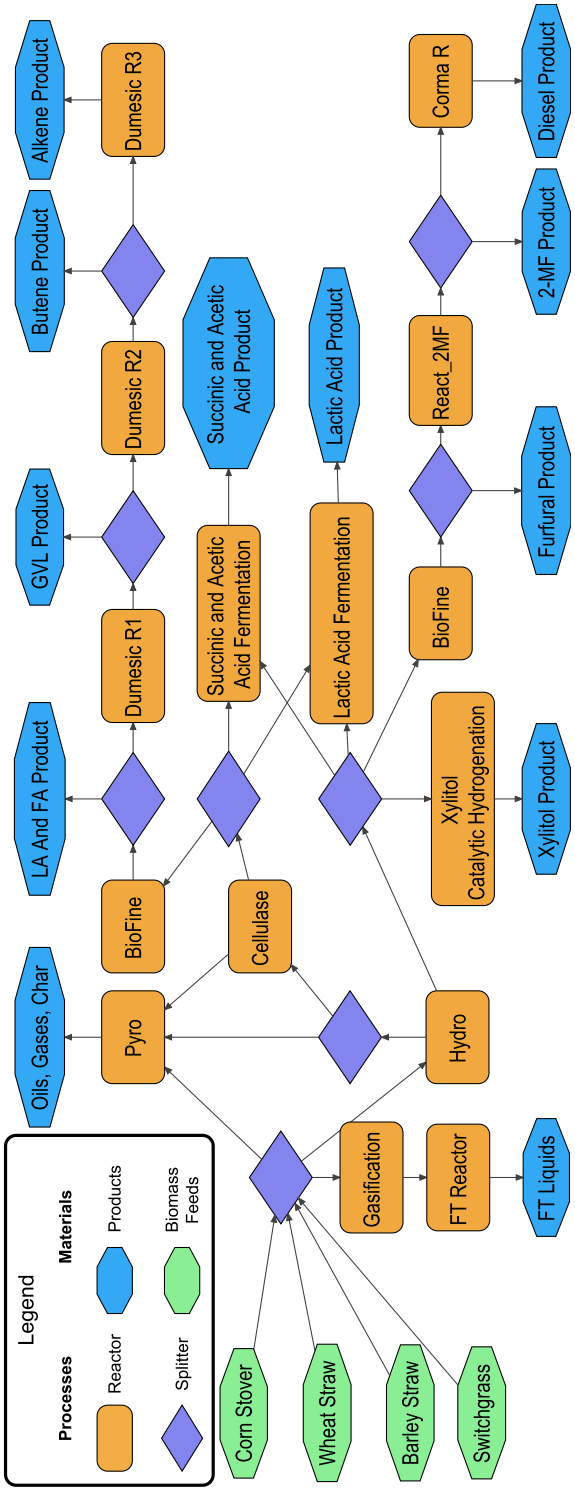

Figure 3.2: Schematic representation of the biorefinery superstructure

The technologies in figure 3.1 are combined into a biorefinery superstructure in figure 3.2 which represents all the possible processing routes. The following is a walkthrough detailing the choices that can be made throughout the superstructure.

The first decision to be made is which biomass feed(s) should be used. The biomass feeds considered are shown in table 3.1. The feed biomass can be either directly gasified or pyrolyzed. Alternatively, it can be broken down by hydrolysis; this yields hemicellulose rich and lignin-cellulose rich streams. The lignin-cellulose rich stream can be pyrolyzed or further treated with an enzymatic hydrolysis process. The hemicellulose stream can either be further converted to furfural through a BioFine® [26] process or be sent to the fermentation or xylose hydrogenation processes. The effluent of the enzymatic hydrolysis process is a lignin rich stream which can be pyrolyzed, and a cellulose rich stream which can either be sent to the fermentation processes or be converted to levulinic and formic acids through another BioFine® process. The fermentation process takes hemicellulose and cellulose and produces either lactic acid or succinic and acetic acids. The xylose hydrogenation converts the hemicellulose to xylitol through conventional catalytic hydrogenation. The remaining two processes take either furfural or levulinic and formic acids and convert them to gasoline or diesel replacements.

Table 3.1: Biomass feed characteristics [54]

	Composition [%]				
Feed	Cellulose	Hemicellulose	Lignin	Char	Cost [$/ton]
Corn Stover	38	26	19	17	39.06
Wheat Straw	38	29	15	18	45.57
Barley Straw	42	28	0	30	59.96
Switch Grass	37	29	19	15	59.87

In the following section we describe the main characteristics of each technology and discuss in further detail how they are modelled and implemented.

3.3 Process descriptions

In formulating the process models in our superstructure we use different model types. For the gasification and pyrolysis units we implement temperature dependent equilibrium and kinetics models respectively. For all other processes we use yield and conversion relations as detailed kinetic models are not available in the literature.

3.3.1 Biomass gasification

The gasification reactor converts biomass feedstocks to syngas. In this work, we follow the model in [62] which assumes that chemical equilibrium is reached among the gasification products (H_2, CO, CO_2, H_2O and CH_4). The reactions considered are:

$$\begin{aligned}
\text{Boudard equilibrium:} \quad & C_{(s)} + CO_2 \overset{K_1}{\leftrightarrow} 2CO \\
\text{Hydrogenating gasification/methanation:} \quad & C_{(s)} + 2H_2 \overset{K_2}{\leftrightarrow} CH_4 \\
\text{Methane decomposition:} \quad & CH_4 + H_2O \overset{K_2}{\leftrightarrow} CO + 3H_2 \\
\text{Water gas shift reaction:} \quad & CO + H_2O \overset{K_4}{\leftrightarrow} CO_2 + H_2 \\
\text{Heterogeneous water gas shift reaction:} \quad & C_{(s)} + H_2O \overset{K_5}{\leftrightarrow} CO + H_2
\end{aligned} \tag{3.1}$$

For each of the gasification reactions the corresponding equilibrium constants are given as follows:

$$\begin{aligned}
K_1 &= \frac{x_{CO}^2 \cdot P}{x_{CO_2}} \\
K_2 &= \frac{x_{CH_4}}{x_{H_2}^2 \cdot P} \\
K_3 &= \frac{x_{H2}^3 \cdot x_{CO} \cdot P^2}{x_{H_2O} \cdot x_{CH_4}} \\
K_4 &= \frac{x_{CO_2} \cdot x_{H_2}}{x_{CO} \cdot x_{H_2O}} \\
K_5 &= \frac{x_{H2} \cdot x_{CO} \cdot P}{x_{H_2O}}
\end{aligned} \tag{3.2}$$

where x_i is the molar fraction of component i and P is the operating pressure.

The equilibrium constants for each of the gasification reactions are obtained from the following thermodynamic relation [6]:

$$K_{\text{equil}} = \exp\left(- \left[\sum_{i=1}^{N_c} v_i \Delta G^{\circ}_{i,\text{prod}} - \sum_{j=1}^{N_c} v_j \Delta G^{\circ}_{j,\text{react}} \right] / RT \right) \tag{3.3}$$

where K_{equil} is the equilibrium constant for each gasification reaction, and v_i and v_j are the stoichiometric coefficients of components i (products) and j (reactants) respectively. N_c is the number of components in the system. R is the ideal gas constant and T is the reaction temperature. $\Delta G^{\circ}_{\text{i}}$ is the standard free energy of formation of component i.

These have the following polynomial temperature dependence [6]:

$$-\frac{\Delta G_i^{\circ}}{RT} = b_1 T^{-1} + b_2 \ln T + b_3 T + b_4 T^2 + b_5 T^3 \tag{3.4}$$

with T in °K. The values of the coefficients in equation 3.4 are shown in table 3.2.

Table 3.2: Coefficients used in free-energy expansion (eq.3.4)

Component (i)	b_1	b_2	b_3 ($\cdot 10^{-3}$)	b_4 ($\cdot 10^{-6}$)	b_5 ($\cdot 10^{-10}$)
H_2O	28780	- 0.69477	- 1.4283	0.74925	- 1.3785
CH_4	8372.2	- 1.0769	- 5.6435	2.9046	- 5.2351
CO	13612	- 1.8317	- 2.7584	0.6536	- 0.78772
CO_2	47280	- 0.1322	- 0.94025	0.45112	- 0.91901

Equations 3.1 through 3.4 are solved for the equilibrium composition of species H_2, CO, CO_2, H_2O and CH_4 as a function of temperature.

We add to the model an overall mass balance:

$$\sum_{k=in} F_k = \sum_{k=out} F_k \tag{3.5}$$

where F_k is a stream mass flow rate, in denotes inlet streams and out denotes outlet streams. We complete the model with three atom balances for carbon, hydrogen and oxygen:

$$\sum_{k=in} \sum_{i}^{Nc} \frac{Fc_{k,i} \cdot \#\mathrm{a}_{n,i}}{MW_i} = \sum_{k=out} \sum_{i}^{Nc} \frac{Fc_{k,i} \cdot \#\mathrm{a}_{n,i}}{MW_i} \tag{3.6}$$

where MW_i is the molecular weight of componet i, n is the atom index and $\#a_{n,j}$ is the number of atoms of type n in component i.

3.3.2 Fischer-Tropsch upgrading

The Fischer-Tropsch (FT) reactor takes the syngas produced by the gasification reactor and converts it into a range of hydrocarbon products. We first formulate the reaction equations occurring within the Fischer-Tropsch reactor:

$$nCO + (2n+1)H_2 \rightarrow C_nH_{2n+2} + nH_2O \tag{3.7}$$

$$nCO + 2.5nH_2 \rightarrow C_nH_{2n} + nH_2O \tag{3.8}$$

for paraffins and olefins respectively. The distribution of these hydrocarbon products is modelled to follow an Anderson-Shultz-Flory (ASF) distribution. The ASF distribution is based on a chain growth probability value and is modelled as follows:

$$W_n = n(1-\alpha)^2\alpha^{n-1} \tag{3.9}$$

where W_n is the mass fraction of the species with carbon number n ($n \in [1, \ldots, 29]$) and α is the chain growth probability, which is the probability that the hydrocarbon chain will continue to react forming a longer hydrocarbon chain. In general, α is a function of the catalyst and the specific process conditions. In this chapter we implement a modified ASF distribution as described in [4]. The value of α used is 0.7 with a fractional conversion of carbon monoxide of 80 mol%. Oxygenated species are also produced in the FT reactor. These are represented by pseudo-components produced in the vapour, aqueous and organic phases respectively, expressed as:

$$2.43CO + 4.275H_2 \rightarrow C_{2.43}H_{5.69}O_{1.43} + 1.43H_2O \tag{3.10}$$

$$1.95CO + 3.815H_2 \rightarrow C_{1.95}H_{5.77}O_{1.02} + 1.93H_2O \tag{3.11}$$

$$4.78CO + 9.25H_2 \rightarrow C_{4.78}H_{11.14}O_{1.1} + 3.68H_2O \tag{3.12}$$

The total converted carbon present in these pseudo-components is 0.1%, 1.0% and 0.4% respectively.

The distribution of products described in equation 3.9 under-predicts the yields of lighter hydrocarbons. The modified value of W_n for these is given by the following equations [81]:

$$W_1 = \frac{1}{2}\left(1 - \sum_{n=5}^{\infty} W_n\right) \tag{3.13}$$

$$W_{2,3,4} = \frac{1}{6}\left(1 - \sum_{n=5}^{\infty} W_n\right) \tag{3.14}$$

All C_{30+} compounds are represented by a generic wax pseudo-component as follows:

$$C_{52.524}H_{105.648}O_{0.335}$$

which has the following definition of W_n:

$$W_{\text{wax}} = \sum_{n=30}^{\infty} n(1-\alpha)^2\alpha^{n-1} \tag{3.15}$$

Using the definitions of W_n described above, the total converted fraction of carbon at each value of n is defined as follows:

$$cr_n = \frac{nW_n}{\sum_{n=1}^{29} nW_n + n_{\text{wax}}W_{\text{wax}}} \tag{3.16}$$

Finally, the fraction of carbon in the paraffin form is 20% for C_2-C_4 , 25% for C_5-C_6 and 30% for C_7-C_{29} hydrocarbons with the remainder being in the olefin form.

3.3.3 Fast pyrolysis of biomass compounds

Fast pyrolysis converts biomass to bio-oils, light hydrocarbon gases and heavy hydrocarbon tars. Bio-oils are an acidic heterogeneous mixture of hydrocarbon liquids.

There are several lumped parameter kinetic models that are used to model the complex network of reactions that occur during fast pyrolysis. In this study we use the kinetics presented and discussed in [77]. These allow for a balance between computational complexity and model accuracy to experimental data.

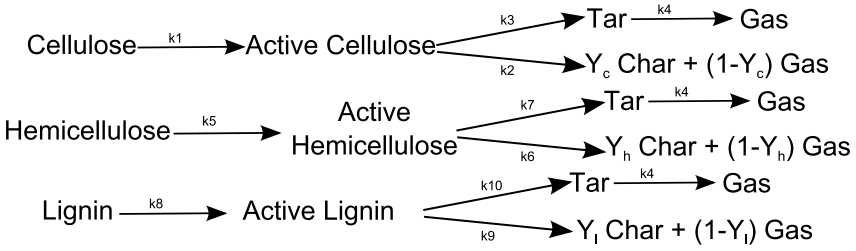

Figure 3.3: Kinetic scheme for pyrolysis where Y_i are the yield coefficients.

The fast pyrolysis model follows the reaction scheme in figure 3.3. Each of these reactions is assumed to be first order such that rate of formation of species in table 3.3 are written as follows:

$$r_1 = -k_1 m_1 \tag{3.17}$$

$$r_2 = -k_5 m_2 \tag{3.18}$$

$$r_3 = -k_8 m_3 \tag{3.19}$$

$$r_4 = k_1 m_1 - (k_2 + k_3) m_4 \tag{3.20}$$

$$r_5 = k_1 m_1 - (k_5 + k_6) m_5 \tag{3.21}$$

Table 3.3: Pyrolysis Species and Indexes

Components	Index
Cellulose	1
Hemicellulose	2
Lignin	3
Active Cellulose	4
Active Hemicellulose	5
Active Lignin	6
Tar	7
Gas	8
Char	9

$$r_6 = k_1 m_1 - (k_8 + k_9) m_6 \tag{3.22}$$

$$r_7 = k_2 m_4 + k_5 m_5 + k_8 m_6 - k_{10} m_7 \tag{3.23}$$

$$\begin{aligned} r_8 = {} & m_4 \left((1 - Y_1) k_3 + \frac{\rho_g}{\rho_b}(k_2 + k_3) + \frac{\rho_g}{\rho_c} \left(Y_1 k_3 - \frac{\rho_g}{\rho_b}(k_2 + k_3) \right) \left(\frac{1}{1 + \frac{\rho_g}{\rho_c}} \right) \right) \\ & + m_5 \left((1 - Y_2) k_6 + \frac{\rho_g}{\rho_b}(k_5 + k_6) + \frac{\rho_g}{\rho_c} \left(Y_2 k_6 - \frac{\rho_g}{\rho_b}(k_5 + k_6) \right) \left(\frac{1}{1 + \frac{\rho_g}{\rho_c}} \right) \right) \\ & + m_6 \left((1 - Y_3) k_9 + \frac{\rho_g}{\rho_b}(k_8 + k_9) + \frac{\rho_g}{\rho_c} \left(Y_3 k_9 - \frac{\rho_g}{\rho_b}(k_8 + k_9) \right) \left(\frac{1}{1 + \frac{\rho_g}{\rho_c}} \right) \right) \\ & + k_{10} m_7 \end{aligned} \tag{3.24}$$

$$\begin{aligned} r_9 = {} & m_4 \left(\left(Y_1 k_3 - \frac{\rho_g}{\rho_b}(k_2 + k_3) \right) \left(\frac{1}{1 + \frac{\rho_g}{\rho_c}} \right) \right) \\ & + m_5 \left(\left(Y_2 k_6 - \frac{\rho_g}{\rho_b}(k_5 + k_6 \right) \left(\frac{1}{1 + \frac{\rho_g}{\rho_c}} \right) \right) \\ & + m_6 \left(\left(Y_3 k_9 - \frac{\rho_g}{\rho_b}(k_8 + k_9) \right) \left(\frac{1}{1 + \frac{\rho_g}{\rho_c}} \right) \right) \end{aligned} \tag{3.25}$$

where r_i is the rate of formation of species i, and ρ_b, ρ_g and ρ_c are the densities of the biomass, gases and char respectively.

The reaction rate constants are assumed to have a standard Arrhenius form:

$$k_i = A_i e^{\frac{E_i}{RT}} \tag{3.26}$$

where A_i is the pre-exponential factor, E_i is the activation energy, R is the ideal gas constant and T is the pyrolysis temperature. The Arrhenius coefficients for the reactions are shown in table 3.4.

Table 3.4: Pyrolysis Reaction Constants [77]

Components	Reaction	Y	A(s^{-1})	E(MJ/kmol)
Cellulose	k_1	-	2.8 x 10^{19}	242.4
	k_2	-	3.28 x 10^{14}	196.5
	k_3	0.35	1.3 x 10^{10}	150.5
Hemicellulose	k_5	-	2.1 x 10^{16}	186.7
	k_6	-	8.75 x 10^{15}	202.4
	k_7	0.60	2.6 x 10^{11}	145.7
Lignin	k_8	-	9.6 x 10^{8}	107.6
	k_9	-	1.5 x 10^{9}	143.8
	k_{10}	0.75	7.7 x 10^{6}	111.4
Tar	k_4	-	4.25 x 10^{6}	108.0

We model the reactor as an ideal plug flow reactor, modeled at steady state by:

$$\frac{dM}{dV_r} = A \cdot M \tag{3.27}$$

where A is the matrix of kinetic rate constants, yield and densities, M is the vector of species masses and V_r is the volume of the reactor.

We can solve this system analytically:

$$M = V \cdot e^{DV_r} \cdot V^{-1} \cdot Mo \tag{3.28}$$

where V is the matrix formed by vertically stacking the eigenvectors of M, D is the diagonal matrix formed of eigenvalues of M, and Mo is the vector of feed species masses. As an example, we solve the system with initial masses of cellulose, hemicellulose and lignin of 0.5, 0.3 and 0.2 respectively and plot the temperature dependent results in figure 3.4.

The implementation of the analytical solution (eq. 3.28) in GAMS proved computationally intractable when placed within the superstructure.

In order to overcome this, we identified the temperature of operation that corresponds to the maximum yield of bio-oil (the principal product) for a range of initial conditions. We fit a linear multi-variate model for this temperature which depends on the feed mass fractions ($X_{o,i}$). This model is as follows:

$$T_{pyrolysis} = 725.26X_{o,cellulose} + 754.83X_{o,hemicellulose} + 884.94X_{o,lignin} \tag{3.29}$$

This temperature is used as a lower bound estimate in the GAMS implementation of the pyrolysis reactor. Similar models were fitted for the production rates of bio-oils and hydrocarbon gases. These models were fitted to the feed mass flow rates and the pyrolysis temperature as follows:

$$\begin{aligned} Fc_{oils} = {} & Fc_{cell} \cdot \left(-229.0 + 0.831 \cdot T - 9.95 \cdot 10^{-4} \cdot T^2 + 3.94 \cdot 10^{-7} \cdot T^3\right) && (3.30)\\ & Fc_{hemi} \cdot \left(-14.0 + 0.0388 \cdot T - 2.56 \cdot 10^{-5} \cdot T^2\right) && (3.31)\\ & Fc_{lig} \cdot \left(+143.0 - 0.551 \cdot T + 7.05 \cdot 10^{-4} \cdot T^2 - 2.99 \cdot 10^{-7} \cdot T^3\right) && (3.32)\\ & +3.85 \cdot T - 0.00724 \cdot T^2 + 6.04 \cdot 10^{-6} \cdot T^3 - 1.88 \cdot 10^{-9} \cdot T^4 - 767.0 && (3.33)\\ & && (3.34) \end{aligned}$$

$$\begin{aligned} Fc_{gas} = {} & Fc_{cell} \cdot (-2.6 + 0.0036 \cdot T) && (3.35)\\ & Fc_{hemi} \cdot \left(+11.7 - 0.0317 \cdot T + 2.17 \cdot 10^{-5} \cdot T^2\right) && (3.36)\\ & Fc_{lig} \cdot \left(+11.4 - 0.0309 \cdot T + 2.09 \cdot 10^{-5} \cdot T^2\right) && (3.37)\\ & +0.0404 \cdot T - 5.96 \cdot 10^{-5} \cdot T^2 + 2.86 \cdot 10^{-8} \cdot T^3 - 8.8 && (3.38)\\ & && (3.39) \end{aligned}$$

where Fc_{oils} and Fc_{gas} are the outlet flow rates of the pyrolysis oils and pyrolysis light hydrocarbon gases respectively, Fc_{cell}, Fc_{hemi}, Fc_{lig} are the inlet flow rates of cellulose, hemicellulose and lignin respectively and T (°K) is the reactor temperature.

3.3.4 Yield based reaction processes

We model the yield based reaction processes to have a fixed mass yield. The mass balances can be written as follows for each component (*comp*) participating in the reaction:

$$\sum_{k=out} Fc_{k,i} = \sum_{k=in} Fc_{k,i} - \sum_{k=in} Fc_{k,\text{key-comp}} \cdot \text{yield}_i \tag{3.40}$$

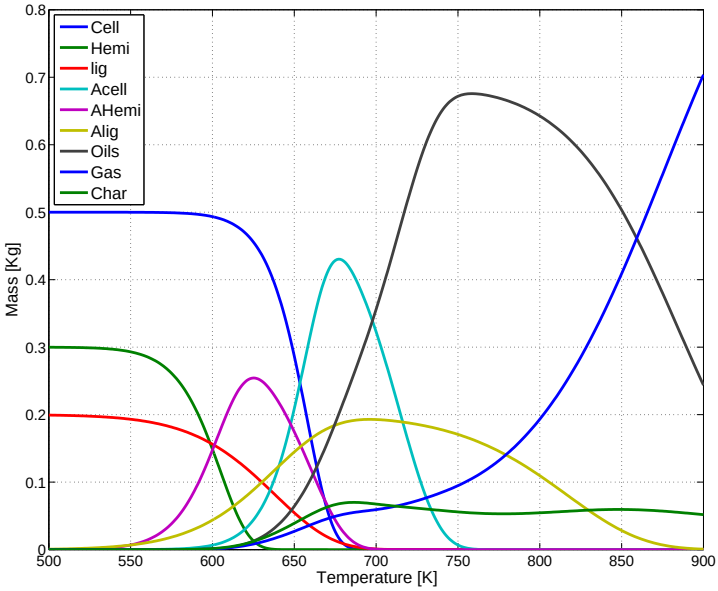

Figure 3.4: Solution to Pyrolysis Kinetic Model

where $Fc_{k,i}$ is the mass flow rate of component i in stream k and $Fc_{k,\text{key-comp}}$ is the flow rate of the key component in the reaction (i.e. the component with respect to which the yield is defined). Finally yield_i is the yield of component i from the key component in the reaction.

Following is a description of the yield based processes included in the superstructure.

Fermentation processes

Several fermentation processes have been included in the biorefinery superstructure. The production of lactic acid is modelled to have an overall yield of 65% from cellulose and hemicellulose [1]. We also include the fermentation of biomass for the production of succinic acid. It has been shown that sparging a fermentation tank loaded with *Escherichia coli* with CO_2 can increase the yield of succinic acid from 25% to 81% and the yield of acetic acid is 15% the yield of succinic acid [45]. In this chapter we use a binary variable to indicate the sparging of carbon dioxide or not, and also use this to set the yield to the appropriate value. We source our carbon dioxide for sparging from elsewhere in the superstructure.

Xylitol hydrogenation

The production of xylitol is accomplished by the hydrogenation of purified xylose at approximately 125°C. The overall xylitol yield is 55% from the total xylan (polysaccharide of xylose) present in the feed hemicellulose (assumed to be pure C_5 sugars here) [46].

BioFine® process

The BioFine® process is a patented process [26] composed of two reactors placed in series that convert cellulose and hemicellulose. The yield and products will depend on the type of feed used; when C_5 sugars (hemicellulose) are processed, furfural and char are produced in a 50-50 mass split whereas when C_6 sugars (cellulose) are processed, levulinic acid (LA) and formic acid (FA) are made as well as char in a 50-20-30 mass split, respectively.

3.3.5 Conversion based reaction processes

The remaining process units are modelled as conversion reactors whose mass balance takes the form:

$$\sum_{k=out} Fc_{k,i} = \sum_{k=in} Fc_{k,i} - \frac{\sum_{k=in} Fc_{k,\text{key-comp}} \cdot MW_i \cdot conv_i}{MW_{\text{key-comp}}} \tag{3.41}$$

The key component is the key reactant species with respect to which the conversion value is defined. Finally, $conv_i$ is the conversion of the key component to component i.

Diesel via 2-Methyl-Furan

It has been suggested that diesel range products can be formed in an energy efficient way by a set of reactions that involve hydrophobic intermediate species and produce nonpolar alkanes (i.e. diesel products). This strategy greatly reduces the energy requirements of the process when compared to other suggested routes to alkane products which require water separation by distillation [12].

The starting point for the scheme implemented here is 2-methylfuran (2MF). 2MF can be obtained from biomass via an established industrial process that initially produces furfural which can then be selectively converted to 2MF [23]. In the 2MF to diesel process, three moles of 2MF are hydroalkylated to 4-oxopentanal in the presence of concentrated

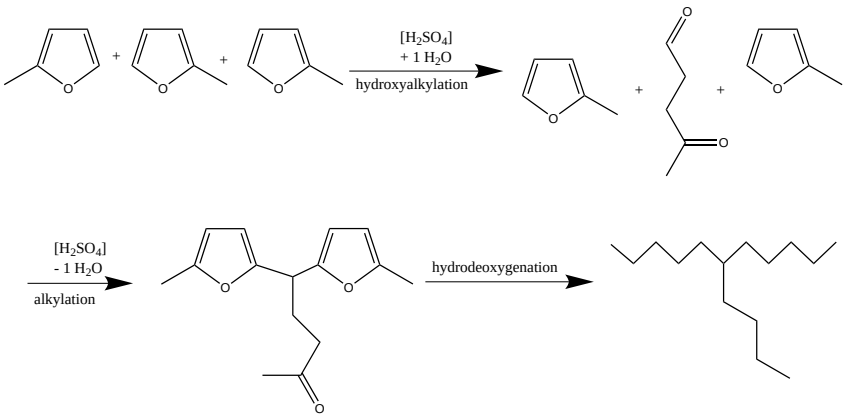

Figure 3.5: Diesel production from 2-Methyl-Furan

sulphuric acid. This is subsequently further alkylated and hydrodeoxygenated to the diesel product as shown in figure 3.5.

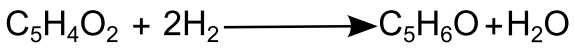

Figure 3.6: Furfural dehydrogenated to 2-Methyl-Furan (2MF)

The furfural produced by a BioFine® process is dehydrogenated to 2MF in an initial reactor (100% conversion) as shown in figure 3.6. The 2MF is then subjected to the set of reaction conditions described above with a conversion of 2MF to diesel of 87%.

Liquid hydrocarbon fuels from levulinic acid

A novel reaction scheme has been suggested [42] that converts levulinic acid into liquid hydrocarbon fuel products. This scheme takes levulinic and formic acids produced by a Biofine® process and initially converts these into γ-valerolactone (γVL) which is subsequently converted to butene. The butene undergoes oligomerization to produce the desired liquid hydrocarbon fuel products. The associated yields are as follows: the conversion of γVL from LA is 100%, the conversion of butene from γVL is 99% and the conversion of this to C_{8+} hydrocarbon liquids is 99% distributed between C_8(29.70%), C_{12}(25.74%), C_{16}(24.75%) and C_{20}(18.81%) hydrocarbons.

3.3.6 Ancillary models

Stream equations

For each stream in our superstructure we write the following mass balance equations:

$$F_k = \sum_{i=1}^{N_c} Fc_{k,i} \tag{3.42}$$

where F_k and $Fc_{k,i}$ are the total stream k flow rate, and the flow rate of component i in stream k.

Splitter

Each split point is modelled as follows:

$$Fc_{m,i} = \sum_{k=in} Fc_{k,i} \cdot e_m \tag{3.43}$$

where e_m is the split fraction (a continuous variable between 0 and 1), defined as the fraction of the inlet flow rate that is sent to stream m where is m denotes the set of outlet streams from the splitter.

Mixer

The mass balance used to model the mixer units has a similar form to equation 3.5. The energy balance is written as follows:

$$\sum_{k=in} F_k T_k Cp_k = \sum_{k=out} F_k T_k Cp_k \tag{3.44}$$

where T_{in} and T_{out} are the temperature of the inlet and outlet streams respectively and Cp is the stream average heat capacity.

Heater/Cooler

The mass balance used to model the heating and cooling units has a similar form to equation 3.5. The following energy balance is also written:

$$Q_{hx} = F \cdot Cp \cdot \Delta T \tag{3.45}$$

where Q_{hx} is the enthalpy flow in heat exchanger hx, F is the stream flow rate, Cp is the stream average heat capacity and ΔT is the temperature difference between inlet and outlet stream.

3.3.7 Capital cost calculations

Capital costs are initially calculated using the Douglas correlations [18] and other literature estimates [4]. Included in these capital costs calculations but not shown in the superstructure are the costs associated with drying and handling the biomass feeds. Measures to address the inaccuracy of capital cost estimates are discussed later. Biomass handling, drying and pretreatment technologies are included as a uniform component of the capital cost.

3.4 Problem formulation and solution strategy

We consider the NPV as an objective function which is defined as follows:

$$\text{NPV} = \theta \cdot \text{Profit} - \text{CAPEX} \tag{3.46}$$

where CAPEX is the total capital expenditure and θ is the discount factor. The profit of the biorefinery is defined as:

$$\text{Profit} = \sum_{i}^{N_c} P_i F c_{E,i} - \sum_{j}^{N_b} P_b F c_{I,b} - \sum_{k}^{N_{hx}} P_{hx} Q_{hx} \tag{3.47}$$

where N_b is the number of biomass feeds and N_{hx} is the number of heat exchangers (heaters and coolers), P_i, P_b and P_{hx} is the price of component i, biomass feed b and utility hx respectiverly. $Fc_{E,i}$ is the exit stream flow rate of component i, $Fc_{I,b}$ is the flow rate of biomass feed b, and Q_{hx} is the utility requirement of heat exchanger hx.

The discount factor is constant in this case as we assume a constant profit per year of operation and, for simplicity, no further discounting or amortization of the capital expenditure. The project horizon is set at 15 years with constant cost of capital (r) of 10%. The discount factor is calculated as follows:

$$\theta = \sum_{n=1}^{15} \frac{1}{(1+r)^n} \approx 7.61 \tag{3.48}$$

The CAPEX is simply the sum of all the capital costs of the individual process units. When a process unit is not used, its capital cost is set to zero. The capacity of the biorefinery is set at 1000 dry metric tons of biomass per day.

Carbon efficiency is a measure of how much carbon fed to the biorefinery is retained in the products. It is a useful metric of environmental performance. The specific definition used in the chapter as an alternative objective function is as follows:

$$C_{\text{eff}} = \frac{\sum_j^{N_b} (12 \cdot \#\text{a}_{C,j}/\text{MW}_j) F c_{j,I}}{\sum_i^{N_c} (12 \cdot \#\text{a}_{C,i}/\text{MW}_i) F c_{i,E}} \tag{3.49}$$

such that the numerator is the total amount of carbon leaving the system and the denominator is the total amount of carbon entering the system.

The process synthesis problem is formulated as an MINLP. The mass and energy balance equations for each process unit in the superstructure form a set of non-linear equality constraints. The problem is written in GAMS (v.23.9) and solved using the BARON (v.11.3) [60] solver package for the global optimum configuration. The decision variables are the split fractions at the split points (shown as diamonds in figure 3.2), the temperature of the gasification and pyrolysis units and the binary variables for streams being active or not. The complete model has 2133 variables of which 96 are binary, and 2249 equations. The sets used in the model are shown in table 3.5, the variables are shown in table 3.6 and the yield and conversion values are shown in table 3.7.

The BARON solver package guarantees that global optimality is reached when finite upper and lower bounds are available for all variables in the problem. In order to find these upper and lower bounds on the flow rate variables we formulated a simplified mass balance model in MATLAB. This not only guaranteed that global optimality was reached but also improved computational time. In order to further improve this time we normalized the feed to 1kg/hr of total biomass. We rescaled the solution flow rate to 1000 tons/day biomass feed before the capital costs and net present value were calculated. We further

improved the solution time during the sensitivity analyses, which require solving the MINLP many times with slightly different parameters, by initializing the problem with a previously found feasible solution.

In order to improve the accuracy of the capital costs calculations, we found existing literature estimates of the minimum selling prices (MSP) (where available) for the products - these are shown in table 3.8. The MSP is defined as the product price needed for the NPV to be zero. Using these literature MSP values we adjust the capital cost estimate calculations such that our superstructure replicates the MSP for each individual product considered. In the solutions and analyses of the biorefinery superstructure that follows we will continue using the literature MSP values as well as the adjusted capital cost calculations.

3.5 Base case solution

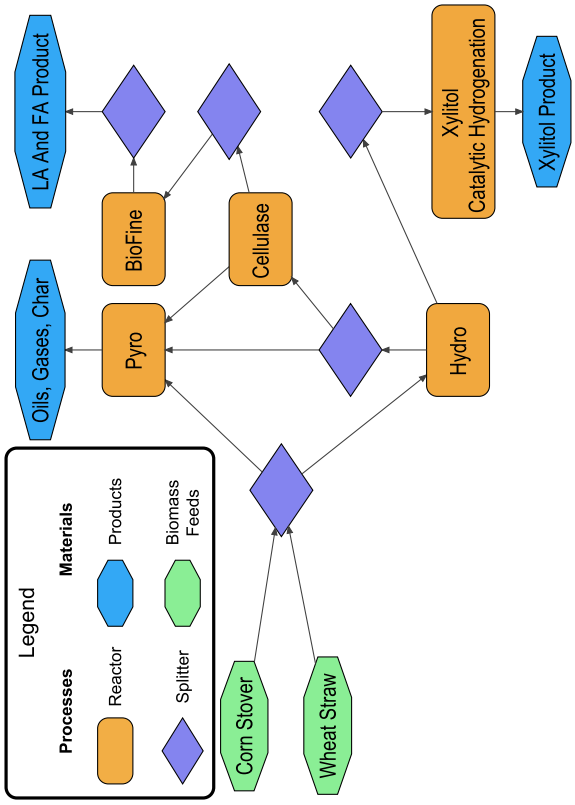

Figure 3.7: Base case solution of superstructure

Our base case solution is one that maximizes the NPV. The resulting solution to the

superstructure is found to have an NPV of $247.76 MM and favours the production of levulinic acid, formic acid and 2MF. The resulting biorefinery configuration is shown in figure 3.7. The carbon efficiency of this solution is found to be 37.1%.

When the objective function is changed to one that seeks to maximize carbon efficiency, the solution to the MINLP is one that has a carbon efficiency of 49.52% and converts all the incoming biomass through the first pyrolysis reactor.

These initial solutions are further analyzed by performing sensitivity and Pareto analyses in the following sections.

3.6 Solution analyses

3.6.1 Sensitivity analysis

The solutions presented so far are based on a large number of economic parameters such as product prices which are subject to variability and uncertainty. We perform sensitivity analyses by varying the values of these parameters and investigating their effect on the overall system configuration and economics. We can use these analyses to better understand how the profitability and configuration of the biorefinery respond to changing economic conditions.

Initially, we perform a sensitivity analysis on the material values (product prices and feedstock costs). In this analysis we uniformly vary these values from 50% to 150% of the values in tables 3.1 and 3.8, for the case where NPV is the objective function. It should be noted that the capital cost calculations do not change during this sensitivity analysis. In figure 3.8, we plot the relative change from the base case of the CAPEX, the profit and the NPV. We can identify four distinct regions at different percentages of the base case material values. Within each of these regions a new biorefinery configuration is found. Region I is found at material values between 50 and 88% of the base case values and is characterized by the production of levulinic acid, formic acids and 2-methylfuran (figure 3.9). Region II (the base case solution, figure 3.7) is characterized by the production of xylose, levulinic acid and formic acid. Region III is small and is found between an 18 and 24% increase from base case values and produces xylitol, lactic acid, levulinic and formic acids (figure 3.10). When the base material values are increased by 24%, the production of furfural and lactic acid is favoured in region IV (figure 3.11).

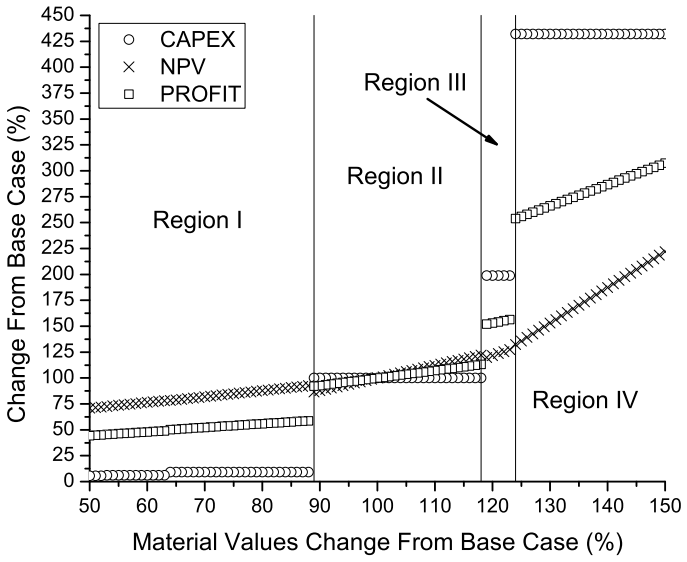

Figure 3.8: NPV sensitivity under variation in material values

Next, we examine the production of biofuels. Our initial superstructure solution (figure 3.7) does not produce any fuels. We investigate the increase in gasoline, FT liquids and diesel prices needed for the superstructure to start producing biofuels. In figure 3.12, we show that we can divide the results into three regions. Region I is small and represents the original base case solution. Region II is characterized by the production of the diesel product formed by the Corma process [12]. Finally, Region III is characterized by the production of gasoline formed by the Dumesic process [42]. Region II starts at an increase in the fuels price of \$0.05/kg and Region III starts at an increase of \$0.59/kg. It is interesting to note that only a small increase in fuels price ($\sim$5%) is needed to trigger the production of biofuels.

The fact that only a small increase in fuel prices is needed to trigger their production suggests that biofuels will still be an important part of future biorefineries. This demonstrates the importance of biorefinery configurations that produce both fuels and chemicals to the overall profitability of the system.

The final sensitivity analysis performed is one that focuses on FT liquids. These are frequently cited as playing an important role in biorefineries of the future and have been investigated in previous biorefinery process synthesis optimization studies [4, 63]. In this part of the study we investigate the increase in the FT liquids price needed for the

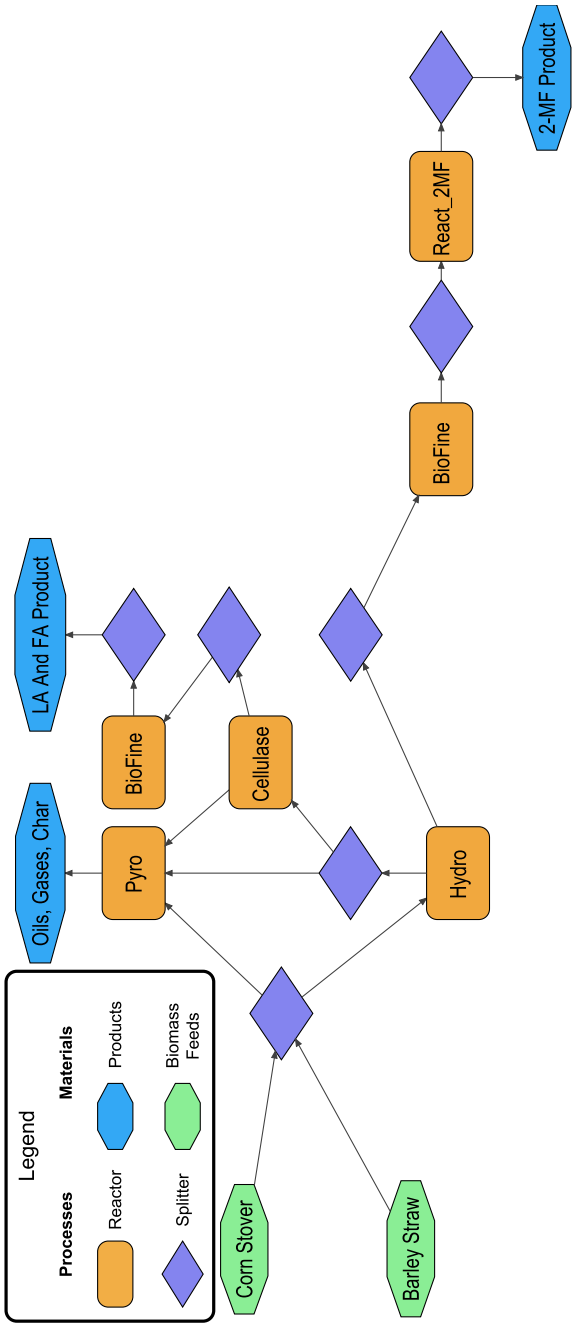

Figure 3.9: Region I

superstructure to find a solution that produces FT liquids. The result of this analysis is shown in figure 3.13. We see that the NPV remains at the original value of $247MM until the price of FT liquids reaches $1.35/kg after which the solution produces FT liquids and the NPV continues to increase linearly with FT liquid price as expected. The production

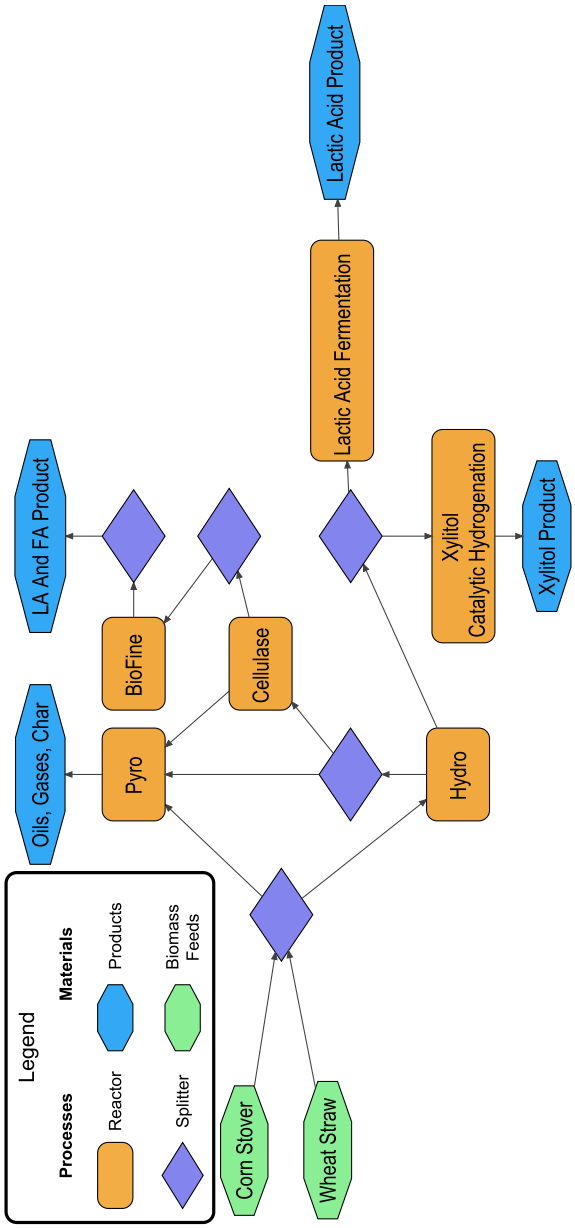

Figure 3.10: Region III

of FT liquids requires a 129% increase in the value of FT liquids with every other product staying at the base case values and can thus be deemed unlikely.

Our conclusions from these sensitivity analyses are three-fold. Firstly, we have shown that the integrated biorefinery has positive NPV over a wide range of material values. Secondly, we have demonstrated the importance of chemicals in the overall biorefinery configuration. Finally, the production of FT liquids has been shown to require a significant

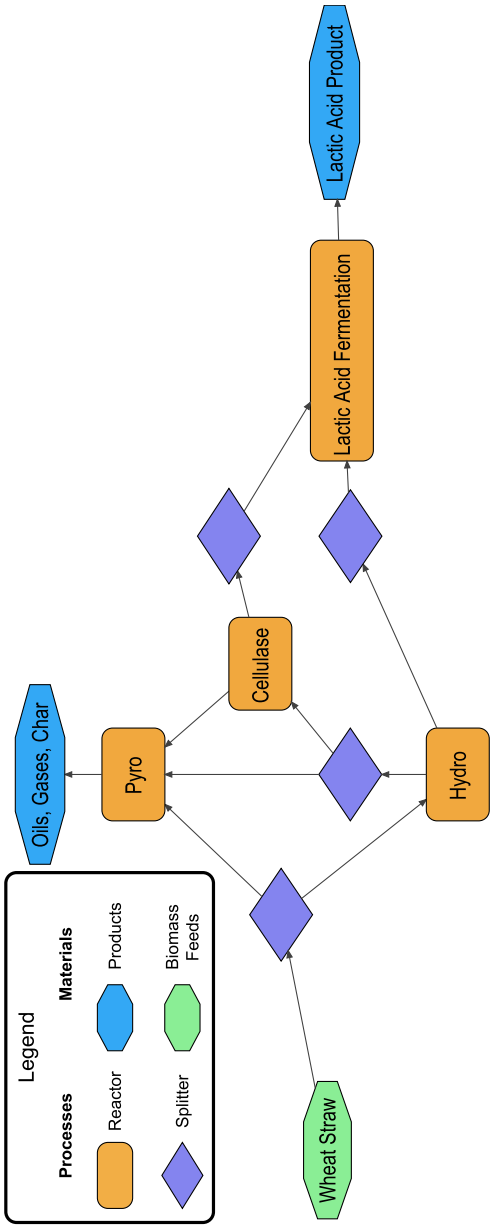

Figure 3.11: Region IV

increase in their value, making them unlikely to be part of future profitable biorefineries given the current state of technology. FT liquids can be produced more economically from natural gas sources, which are cheaper than biomass and also oxygen-free. This is consistent with assessments such as in [66] which argue that the biomass to FT liquids process cost is about twice as much as that of a natural gas based process.

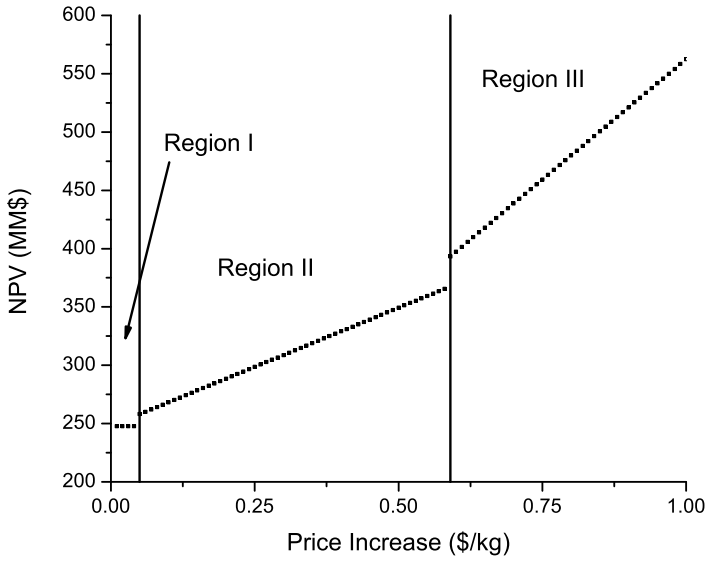

Figure 3.12: NPV sensitivity to fuels price increases

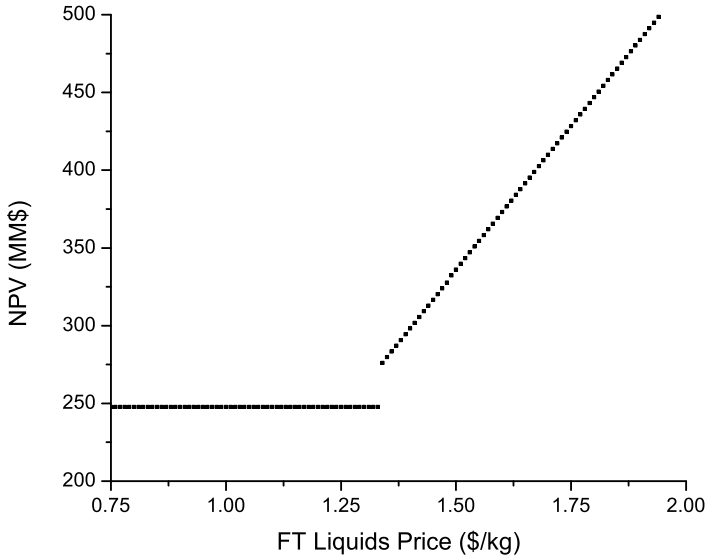

Figure 3.13: NPV sensitivity to FT liquids price

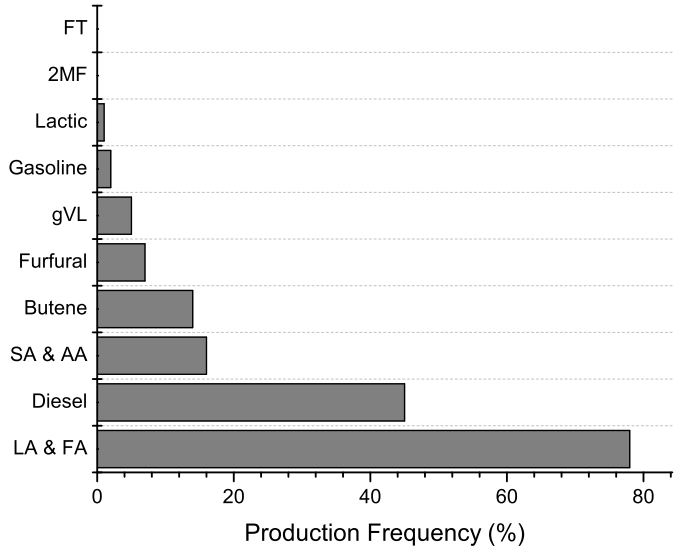

Figure 3.14: Production frequency during first Monte Carlo analysis

3.6.2 Monte Carlo sampling

In this section we sample a normal distribution of our product prices. For each price we assume a normal distribution with a mean equal to the values in table 3.8 and standard deviation of 10% of the mean value. This allows us to analyze the robustness of the biorefinery systems to economic uncertainty and changing economic conditions. In our first case study, we optimize the biorefinery superstructure by maximizing NPV for 100 rounds of independently selected economic parameters. The results presented in figure 3.14 show that levulinic and formic acids are the most frequently selected product, being produced in approximately 80% of the samples. Furthermore, we see that the second most frequent product is diesel. Again, we see that FT liquids are never selected.

For our next analysis we use the results of the first Monte Carlo analysis and construct a biorefinery configuration that can produce the most frequently selected products from our first analysis (namely, diesel, levulinic and formic acid). We accomplish this by fixing the values of the split fractions in order to achieve the configuration shown in figures 3.15. We then sample the distribution of product prices 10,000 times and investigate the resulting NPV. This produces the NPV distribution in figure 3.16 with a minimum value of \$148MM, a mean value of \$248MM and a maximum value of \$336MM. This shows that the biorefinery configuration shown in figure 3.15 which produces both fuels and chemicals

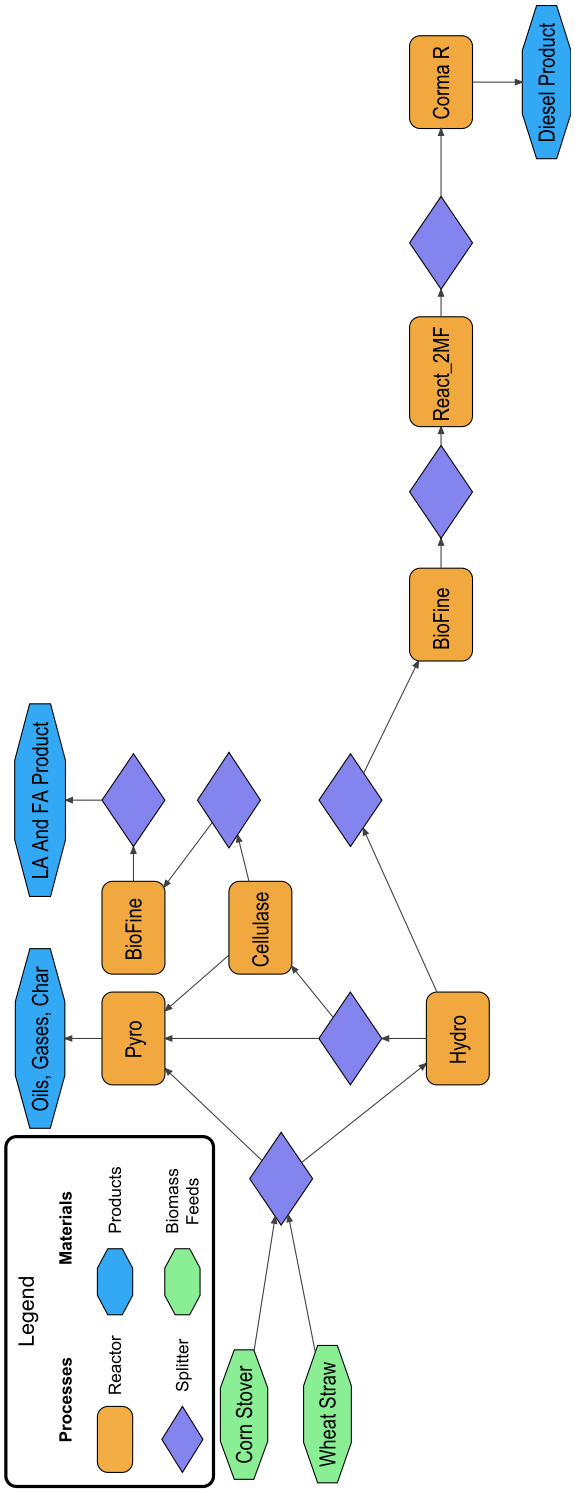

Figure 3.15: Monte Carlo

is robust to changes in economic operating parameters and can maintain a positive NPV in the face of economic variability.

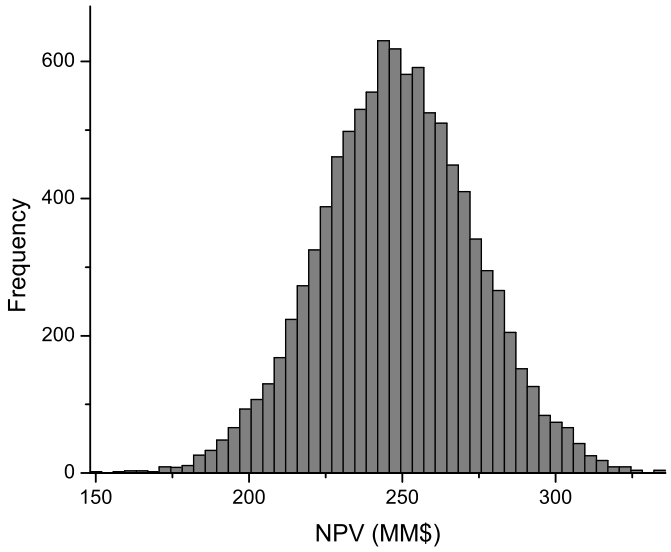

Figure 3.16: NPV distribution after second Monte Carlo analysis

3.6.3 Multi-objective optimization

In this section we consider the simultaneous optimization over two objective functions, specifically, carbon efficiency and NPV. Intuition would suggest that with increasing carbon efficiency, the maximum NPV attainable should decrease. The multi-objective optimization is implemented using the ϵ-constraint method [17]. In this method, we gradually increase the maximum allowable carbon efficiency (from 0.2 to 0.5) and seek the corresponding maximum value of NPV. The result of the multi-objective optimization is shown in figure 3.17.

The points shown on the figure are the feasible solutions found. The convex hull of these gives an estimate of the boundary to the region within which feasible biorefinery configurations are found. We see that there is a maximum in this boundary at point A on figure 3.17. The boundary curve to the right of point A is the Pareto frontier and represents the best compromise between NPV and carbon efficiency. As expected an increase in carbon efficiency drives the NPV lower. To the left of the point A is the boundary between feasible and infeasible biorefinery configurations but these are not

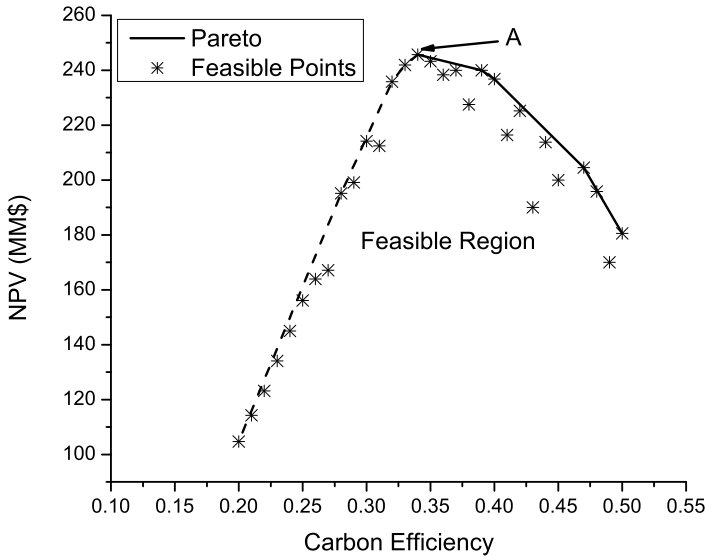

Figure 3.17: Pareto frontier of NPV against carbon efficiency

strictly part of the Pareto frontier as an increase in both NPV and carbon efficiency is possible from each point in this part of the boundary. In this region, the solution, to satisfy the carbon efficiency requirements, sends an increasing amount of carbon to the waste streams thereby satisfying the reduction in the carbon efficiency limit. However, importantly, no solution is found with negative NPV.

The highest values of NPV are achieved when each component of biomass (cellulose, hemicellulose and lignin) is used in a process that maximizes its contribution to the economic potential of the biorefinery system. At the maximum NPV value (in figure 3.17) the base case solution is found with a carbon efficiency of 37%. This configuration is found for carbon efficiencies ranging from 37% to 40%. For carbon efficiencies from 40% to 45% the production of LA, FA and 2MF is favoured. From 45% to the maximum achievable carbon efficiency (∼50%) all the biomass is converted in the pyrolysis reactor which is the most carbon efficient process included in our superstructure.

3.7 Conclusions

The aim of this work is a systematic analysis of the integrated biorefinery concept. We formulated a versatile superstructure that can produce both fuels and chemicals from

a variety of feedstocks. Our base case analysis showed that the production of xylitol, levulinic acid and formic acid is most favourable. This base case scenario has an NPV of $247MM and a carbon efficiency of 37%. When we turned our attention to maximizing carbon efficiency, the resulting configuration produced bio-oils from the pyrolysis reactor and a carbon efficiency of approximately 50%.

Several sensitivity analyses were performed in order to uncover how the superstructure reacts to different values of economic parameters. The initial sensitivity analysis performed on the material values showed that the chemical products produce a higher NPV than fuels. A second sensitivity analysis on the fuel prices showed that fuels play an important role in the profitability of biorefinery systems as only a small increase ($\sim$5%) was needed to trigger the production of fuel products. A Monte Carlo type sampling of the product prices highlighted the importance of fuels to overall biorefinery profitability. Including fuel and chemical products gave the biorefinery configuration flexibility to be profitable under a wide range of material values. Multi-objective optimization demonstrated the importance of multiple product biorefineries such that each component of the biomass is used to produce a product that maximizes its contribution to the system's economic potential.

3.8 Sets, variables and parameters

The definitions and descriptions of the sets used in this chapter are shown in table 3.5. The definitions and descriptions of the variables used in this chapter are shown in table 3.6. The values of the yield parameters used in this chapter are shown in table 3.7. Finally, the material values used in this chapter are shown in table 3.8

Table 3.5: Sets used in superstructure model formulation

Set Name	Description	Contents
str	Process Streams Set	{1 ... 96 }
Feed_str	Feed Streams Set	{1 ... 4 }
Comp	Component Set	{1 ... 40 }
Atoms	Atoms Set	{C, H, O }
Heh	Heater Units	{ 1 ... 10}
Hec	Cooler Units	{ 1 ... 8 }
Spl	Splitter Units	{ 1 ... 11}
Mxr	Mixer Units	{ 1 ... 7 }
CompSpl	Ideal Component Splitter Units	{ 1 ... 6 }
Enzym	Enzymatic Hydrolysis Units Units	{ 1 }
Hyd	Hydrolysis Units	{ 1 }
BioF	BioFine Units	{ 1 ... 2 }
Pyro	Pyrolysis Units	{ 1 ... 3 }
Gasi	Gasification Units	{ 1 }
FT_react	FT Reactor Units	{ 1 }
DUMR1	Dumesic 1st Reactor Units	{ 1 }
DUMR2	Dumesic 2nd Reactor Units	{ 1 }
DUMR3	Dumesic 3rd Reactor Units	{ 1 }
R_2MF	2MF Reactor Units	{ 1 }
CormaR	Corma Reactor Units	{ 1 }
Xyl	Xylose Reactor Units	{ 1 }
Lac_Ferm	Lactic Acid Fermentation Units	{ 1 }
SA_AA_Ferm	Succinic and Acetic Acid Fermentation Units	{ 1 }

Table 3.6: Variables used in superstructure model formulation

Variable Name (sets)	Description	Type
F(str)	Flow Rate	Continuous
Fc(str,comp)	Component Flow Rate	Continuous
T(str)	Stream Temperature	Continuous
e(spl,str)	Split fractions	Continuous
qh(heh)	Heater energy requirement	Continuous
qc(hec)	Cooler energy requirement	Continuous
pyroT(pyro)	Pyrolysis Unit Temperature	Continuous
SplT(spl)	Splitter Unit Temperature	Continuous
CompSplT(CompSpl)	Component Splitter Unit Temperature	Continuous
BioFT(BioF)	Biofine Unit Temperature	Continuous
GasiT(pyro)	Gasification Unit Temperature	Continuous
FT_ReactT(FT_React)	FT Reactor Unit Temperature	Continuous
DUMR1T(DUMR1)	Dumesic 1st Reactor Unit Temperature	Continuous
DUMR2T(DUMR2)	Dumesic 2nd Reactor Unit Temperature	Continuous
DUMR3T(DUMR3)	Dumesic 3rd Reactor Unit Temperature	Continuous
R_2MFT(R_2MF)	2MF Reactor Unit Temperature	Continuous
CormART(CormaR)	Corma Reactor Unit Temperature	Continuous
XylT(Xyl)	Xylose Reactor Unit Temperature	Continuous
Lac_FermT(Lac_Ferm)	Lactic Acid Fermentation Unit Temperature	Continuous
SA_AA_FermT(SA_AA_Ferm)	Succinic and Acetic Acid Fermentation Unit Temperature	Continuous
x(str,comp)	Mass Fraction of Component in Stream	Continuous
on(str)	Stream Inclusion Binary	Binary

Table 3.7: Yield and conversion values

Reaction	Yield/Conversion	Reference
Hydrolysis - cellulose from biomass	0.96	[31]
Hydrolysis - hemicellulose from biomass	0.801	[31]
Hydrolysis - lignin from biomass	0.885	[31]
Enzymatic hydrolysis - lignin from lignin-cellulose complex	0.83	[31]
Enzymatic hydrolysis -cellulose from lignin-cellulose complex	0.904	[31]
Biofine - Furfural from hemicellulose	0.5	[26]
Biofine - Char from hemicellulose	0.5	[26]
Biofine - Formic acid from cellulose	0.2	[26]
Biofine - LA from cellulose	0.5	[26]
Biofine - char from cellulose	0.3	[26]
Dumesic - γVL to LA	1	[42]
Dumesic - γVL to Butene	0.99	[42]
Dumesic - Butene to C4-C8	0.297	[42]
Dumesic - Butene to C8-C12	0.2574	[42]
Dumesic - Butene to C12-C16	0.2475	[42]
Dumesic - Butene to C16-C20	0.1881	[42]
Corma - 2MF from formic	1	[12]
Corma - Diesel from 2MF	0.87	[12]
Corma - Gases (C1-C4) from 2MF	0.02	[12]
Corma - hydrocarbons (C4-C8) from 2MF	0.02	[12]
Fermentation - Lactic acid	0.65	[29]
Fermentation - SA (no CO2)	0.33	[45]
Fermentation - SA (with CO2)	0.72	[45]
Fermentation - AA (no CO2) based on SA (gram per gram)	15.53667	[45]
Fermentation - AA (with CO2) based on SA (gram per gram)	7.08	[45]
Xylitol - Xylitol from xylose	0.55	[46]

Table 3.8: Material values

Material	**MSP [$/kg]**	Reference
Xylitol	8.56	[37]
Acetic Acid	0.46	[16]
Formic Acid	0.68	[57]
Butene	1.07	icis.com
2-Methyl-Furan	n/a	-
γValerolactone	n/a	-
Levulinic Acid	0.2	[50]
Furfural	1.02	[16]
FT Liquids	0.59	[74]
Succinic Acid	6.58	[56]
Succinic Acid	0.73	[79]
Lactic Acid	1.00	[1]
Bio-Oils	0.19	[75]
Drop-In Fuels		
Gasoline - Dec 2012 U.S. Energy Information Administration (EIA) gasoline price (excluding taxes) - 1.01$/kg		
Diesel - Dec 2012 U.S. Energy Information Administration (EIA) gasoline price (excluding taxes) - 1.11$/kg		

CHAPTER 4

Techno-Economic Analysis of Hollow Fiber Supported Zeolite Membranes

4.1 Introduction

Distillation is by far the most industrially important and effective separation process but its effectiveness can be limited by systems with close boiling points or azeotropes. Membrane technologies are not constrained by such limitations and can be an energy efficient solution to difficult separation requirements. Examples of successful industrial applications of membranes include hydrogen purification, air separation and carbon dioxide removal [3]. The size of the global membrane market is estimated to be $16.5 billion [24].

Techno-economic analyses have proven to be a useful tool for guiding the development of new technologies. Analyses of this sort allow researchers to systematically screen proposed technologies against a set of technical and economic objectives, thereby allowing for more focused technology development.

In the first part of this chapter, a membrane unit is modelled in gPROMS and is then used, in the second part of the chapter, to analyze the technical and economic merits

of membrane-based systems for two industrially important case studies. The first case study focuses on corn ethanol dehydration whilst the second looks at butane isomer separation. The specific objective of this work is to determine key performance targets for the development of hollow-fiber supported zeolite membranes which will render these technically and economically attractive compared to existing separation methods.

4.2 Membrane modelling

The membrane unit considered was modelled as a plug-flow counter-current hollow-fiber membrane module where the feed enters the hollow fibers (retentate side), ethanol permeates through the membrane and leaves in the product stream exiting the shell side (permeate side). Nitrogen is used as a sweep gas on the permeate side and assumed not to permeate through the membrane. A schematic of the membrane unit is shown in figure 4.1. The following simplifying assumptions are made:

- isothermal operation
- ideal gas equation of state is used to calculate appropriate physical properties
- negligible pressure drop along each side of the membrane
- feed uniformly divided between all hollow fibers
- constant permeance and selectivity along membrane length

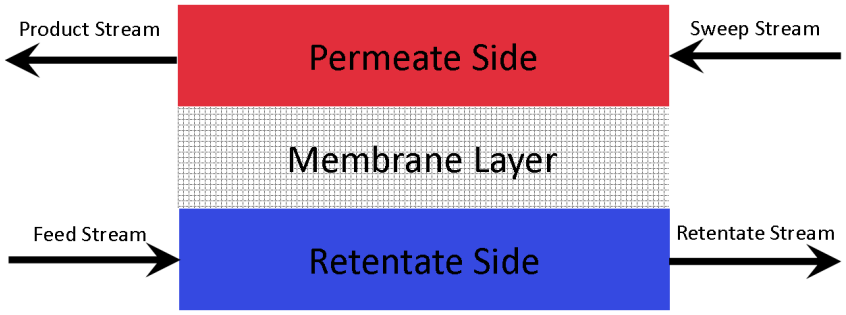

Figure 4.1: Schematic of membrane unit

The set of governing mass balance equations are formulated as follows:

$$\frac{dF_{k,i}}{dz} = -\pi d_t J_i \tag{4.1}$$

$$J_i = \mathcal{P}_i \left(P_{p,i} - P_{r,i} \right) \tag{4.2}$$

$$P_{k,i} = P_k^T x_{k,i} \tag{4.3}$$

$$\alpha = \frac{\mathcal{P}_i}{\mathcal{P}_j} \tag{4.4}$$

where, $F_{k,i}$ is the mass flow rate on side k (p: permeate, r: retentate) of component i, z is the axial coordinate ($z = 0$: retentate feed side, $z = L$: sweep feed side), J_i is the flux of species i through the membrane, $\mathcal{P}_i$ is the permeance of species i, $P_{k,i}$ is the partial pressure of component i on side k, P_k^T is the total pressure on side k, $x_{k,i}$ is the mole fraction of component i on side k, and α is the selectivity of species i to j.

The following boundary conditions are applied:

$$F_{r,i}|_{z=0} = F_{r,i}^0 \tag{4.5}$$

$$F_{p,i}|_{z=L} = F_{p,i}^0 \tag{4.6}$$

where L is the length of the membrane and $F_{k,i}^0$ is the feed flow rate of component i on side k.

The system of equations was solved in gPROMS v3.6 by discretization of the length of the membrane according to a Backward Finite Difference method using 50 uniformly distributed grid points. The key parameters of the membrane system are the total membrane area, key component permeance ($\mathcal{P}_i$) and selectivity (α).

4.3 Case study 1: corn ethanol dehydration

The first case study analyzes the dehydration of corn derived ethanol. The dehydration of ethanol is a crucial, energy intensive, step in the refining of corn derived ethanol which is a $20 billion business in the U.S.A.. This separation step is particularly energy intensive because of the azeotrope formed between ethanol and water at approximately 95wt% ethanol. Membrane technologies are not limited by this azeotropic behaviour and have been shown to be a promising alternative to traditional distillation technologies [47, 67]. A simulation study of the current technology, which is based on a three distillation column configuration, is initially carried out to establish, both technical and economic, performance benchmarks. These benchmarks become the yardstick by which the

membrane-based systems are judged. The technical and economic merits of the following membrane-based systems are studied:

1. a single membrane unit replacing all three columns
2. hybrid systems:
   (a) a membrane placed before column(s) to accomplish the initial portion of the separation requirements
   (b) a membrane placed after column(s) to finish the separation requirement:
      i. in single pass configuration
      ii. a recycle configuration where the membrane retentate is recycled to the distillation column feed

4.3.1 Base case: distillation modelling results

The current, state of the art, technology used to dehydrate ethanol produced by fermentation of corn sugars is a series of three distillation columns whose configuration is shown in figure 4.2 [36].

The feed to this system of columns is the fermentation tank effluent and contains 12wt% ethanol. The first column, known as the beer column, has 22 trays, a reboiler but no condenser. The column produces a vapour top product that contains the feed ethanol and approximately equal amounts of water. The steam flow to the reboiler is chosen such that 99% of the ethanol is recovered in the top product. The bottom product contains all the fermentation solids (corn kernels, yeast cells and corn oils) which, once dried, are sold as dry distillers grains with solubles (DDGS) to be used as animal feed. The revenues from DDGS contribute significantly towards the total revenue of these facilities and, as such, should be recovered in any membrane-based design configuration. The second column, the rectifying column, has 22 trays, a condenser but no reboiler. This column produces a top liquid product at the azeotropic ethanol concentration of 95wt%. The bottom liquid effluent is fed to the third column, the stripping column. The stripping column has 35 trays, a reboiler but no condenser. It produces a top vapour product which is fed to the bottom of the rectifying column. Again, the reboiler steam flowrate is chosen to recover 99% of the ethanol in the top product [36].

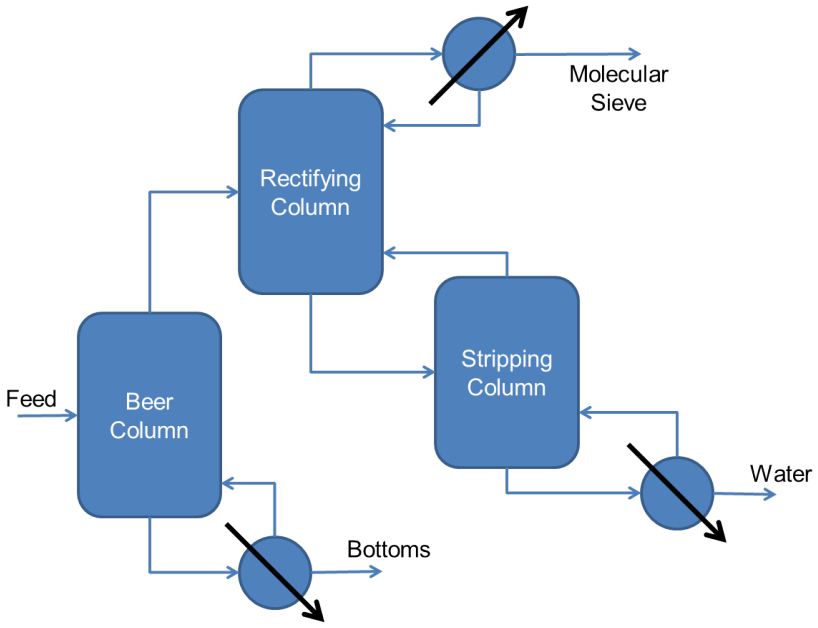

Figure 4.2: Process flowsheet for ethanol distillation base case

The three columns have been simulated in Aspen Plus. The overall recovery achieved is 99% and the top product purity is 95wt% ethanol. The reboiler energy costs are the largest operating expenses of these columns and outweighs the capital costs [36]. The Aspen Plus results show that the beer column uses 9.37MW and the stripping column uses 4.17MW of steam which costs \$1.66MM/year and \$0.74MM/year, respectively, assuming natural gas boilers operating at 80% efficiency and \$5.00/MMBTU natural gas price.

The key performance indicators that any membrane-based design must meet or exceed are an ethanol recovery of 99% with a final product purity of 95wt%. These values become the targets for the development of novel membrane based systems for the dehydration of ethanol.

4.3.2 Membrane results and discussion

As mentioned in section 4.1, several membrane-based systems are studied. The first was a stand-alone single membrane unit aimed at replacing all three distillation columns. Following this, hybrid systems composed of a membrane unit and distillation column(s) are studied. These include configurations with the membrane unit placed before and after distillation columns.

Stand-alone membrane system

A stand-alone membrane system capable of completely replacing all three distillation columns is initially investigated. The membrane model described in section 4.2 is applied to the ethanol dehydration system and solved in gPROMS v3.6. The membrane is given a relatively high permeance and selectivity values of 10kg/hr.m^2.atm and 1000, respectively. The feed to the membrane is assumed to be composed of only ethanol and water at the 12wt% ethanol fermentation product purity and completely vapourized at constant pressure before being sent to the membrane unit. The ethanol recovery and purity achieved as a function of membrane area are shown in figure 4.3 where the target recovery is that achieved in the distillation columns, namely, 99%.

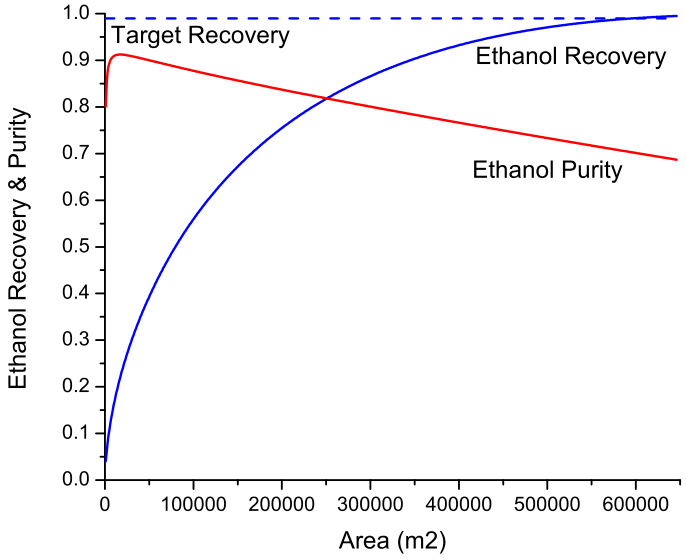

Figure 4.3: Single membrane results. selectivity: 1000, ethanol permeance: 10kg/m^2.hr.atm

The results show that as the membrane area increases more and more ethanol is recovered. However, with increasing membrane area more water is also recovered which reduces the product purity as membrane area increases. Given a target recovery of 99%, selected to match the distillation system's performance, the required membrane area is 598,000m^2. However, the achieved product purity at this membrane area is 70wt% which is below the target purity of 95wt%, again selected to match the distillation system's performance.

The fact that the product purity is below the target values and that a very high membrane

area is required indicate that the stand-alone membrane system should not be investigated further.

Hybrid systems

Having established that a stand-alone membrane system is incapable of economically replacing the distillation system, hybrid systems composed of distillation column(s) and a membrane unit are investigated.

As previously mentioned, two distinct hybrid systems are initially studied. These are shown in figure 4.4 and 4.5. The first such system is shown in figure 4.4, which places a membrane before the distillation column(s) and seeks to increase the concentration of ethanol in the distillation feed which should, in theory, reduce the cost of distillation. A similar system has been proposed previously [47]. In order to investigate the feasibility of this membrane pre-distillation system, the potential energy savings from the reduced distillation column are calculated. This is accomplished by investigating the effect on the distillation columns' energy requirement of an increase in the ethanol concentration in the beer column feed stream in Aspen Plus. The results, in figure 4.6 and generated using the Aspen Plus model of the three column system, show the total distillation energy required as a function of the ethanol mass fraction in the distillation feed. Also shown are the savings achieved by the increased feed ethanol concentration defined as the difference between the total energy required and the base case total energy required (13.54MW). The savings feasible when rectifying and stripping columns are eliminated (blue dashed line) are also included in the results figure. The inclusion of the savings achieved by removing the rectifying and stripping column is important as these are the savings achieved in the configuration shown in figure 4.5.

The results show that, as expected, increasing the ethanol concentration in the distillation feed stream reduced the total energy required. However, as highlighted by the blue dashed line in figure 4.6 the total savings are not more than those achieved by eliminating the rectifying and stripping columns. This blue dashed line also equals the total energy savings that a membrane unit placed after the beer column would have assuming that such a membrane could meet the required separation performance.

These results suggest that more energy can be saved when the membrane is placed after the beer column, which remains unchanged from the base case scenario. Further support for this configuration can be made by observing that the solids in the fermentation broth

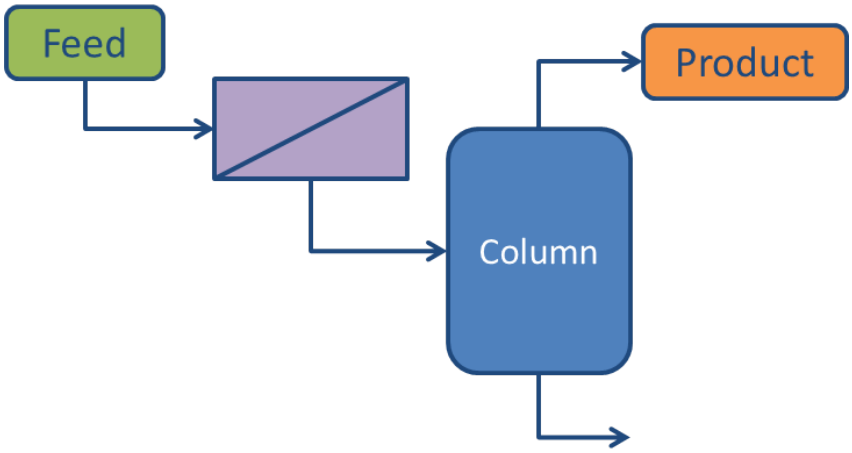

Figure 4.4: Schematic of hybrid system with membrane placed before column(s)

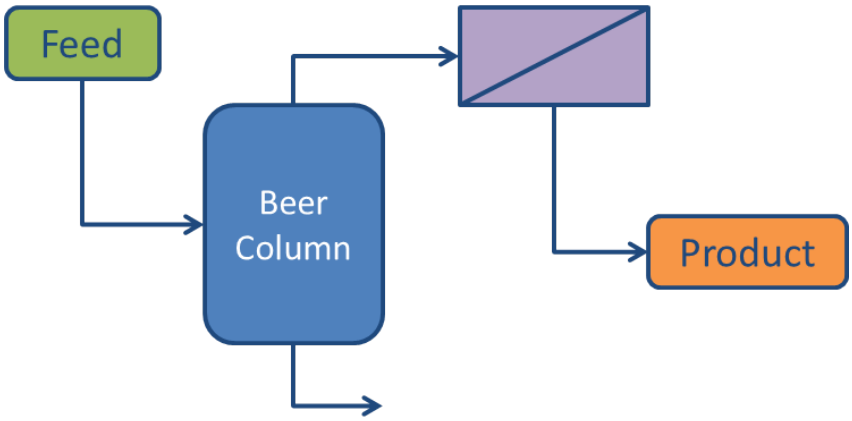

Figure 4.5: Schematic of hybrid system with membrane placed after column - single pass configuration

will negatively affect the membrane's performance. This issue is not found when the membrane is placed after the beer column as this column separates out all solids in its bottom stream.

To further understand the results, it is instructive to consider the ethanol-water vapour-liquid equilibrium (VLE) curve, shown in figure 4.7. The VLE curve exhibits a characteristic "bulge" at ethanol liquid mass fractions less than ~50wt%. This behaviour results in a large driving force for ethanol to be in the vapour phase at these concentrations. In turn, this suggests that distillation is better suited, at these concentrations, than other technologies. However, distillation becomes increasingly difficult (and expensive) as the ethanol concentration approaches the azeotrope at 95wt%.

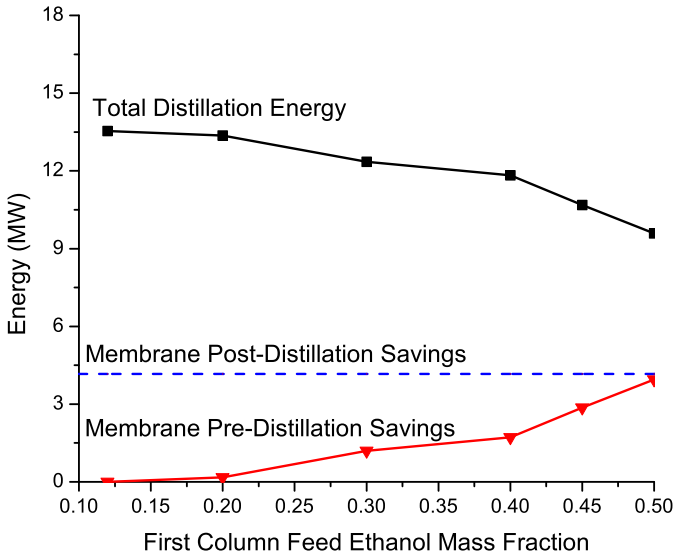

Figure 4.6: Distillation energy analysis

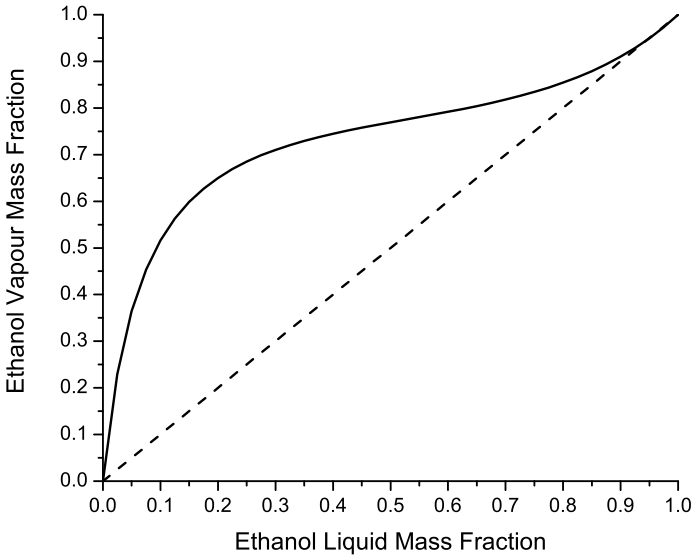

Figure 4.7: Ethanol-water vapour-liquid equilibrium at 2atm

The results in this section suggest that hybrid configurations with the membrane placed after the beer column are both technically and economically favourable. The analysis of this configuration is completed in the following section.

Post-distillation membrane systems

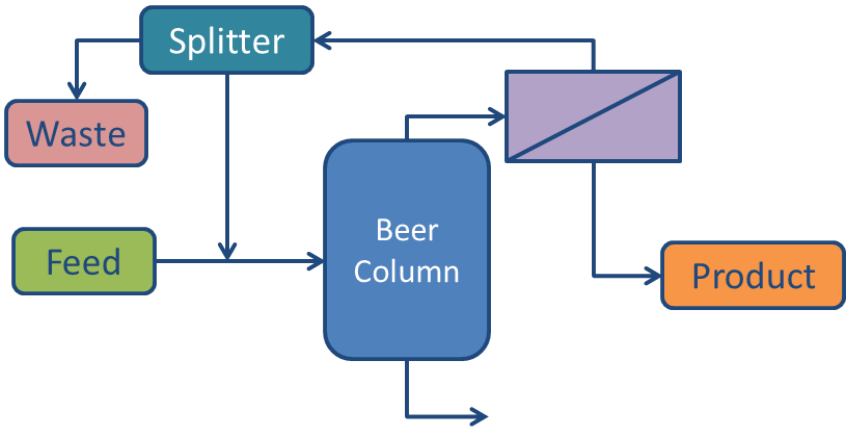

Figure 4.8: Process schematic for recycle scheme

We begin with the configuration shown in figure 4.5 which must achieve the required separation in a single pass. Figure 4.9 is an example of the type of results that are generated using the gPROMS model described in section 4.2 and shows the ethanol purity and recovery as a function of membrane area for a fixed permeance of 6kg/hr.m^2.atm and a selectivity of 250. In all cases in this section, the membrane is fed the beer column effluent which contains 56w% ethanol flowing at 5.43kg/sec which corresponds to a yearly production of 30 million gallons of dehydrated ethanol. In figure 4.9, the purity initially increases as more ethanol permeates through the membrane and dilutes the nitrogen sweep gas. At approximately 4,000m^2, the trend is reversed as an increasing amount of water permeates through the membrane and dilutes the ethanol product stream. The required membrane area is chosen as the area required to meet the 99% recovery target as shown by the black arrow in the figure. Once the required membrane area is found, the corresponding product purity can be read from the graph which in this case is just above 95%.

We can repeat the analysis for a range of permeances and selectivities and produce figure 4.10 which shows the final ethanol product purity achieved at the 99% recovery target for different values of permeance. The figure shows that the achieved product purity is a very weak function of permeance and that in order to achieve the desired 95wt% purity target a membrane with selectivity of at least 250 is required. Such a value can be considered unrealistic given the current state of membrane technology [80] and therefore a more reasonable value of 100 should be used. However, as shown in figure 4.10 the required purity and recovery cannot both be met in a single-pass membrane

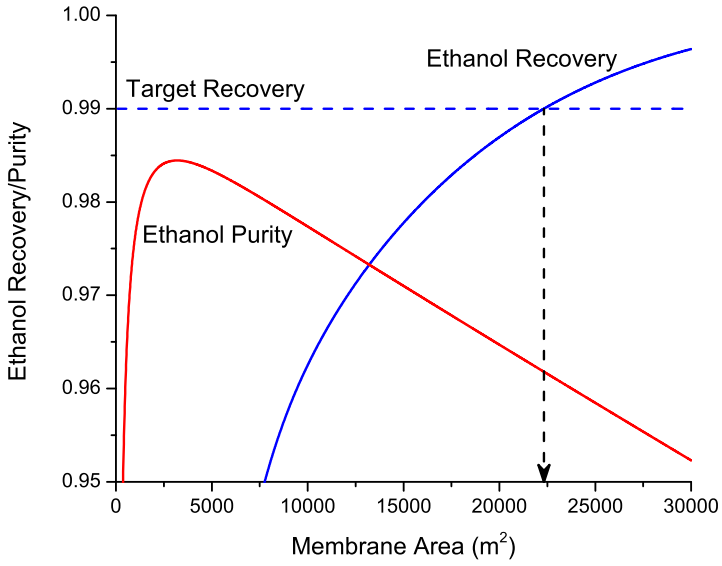

Figure 4.9: Ethanol product single pass recovery and purity vs. membrane area - selectivity: 250, ethanol permeance: 10kg/hr.m^2.atm

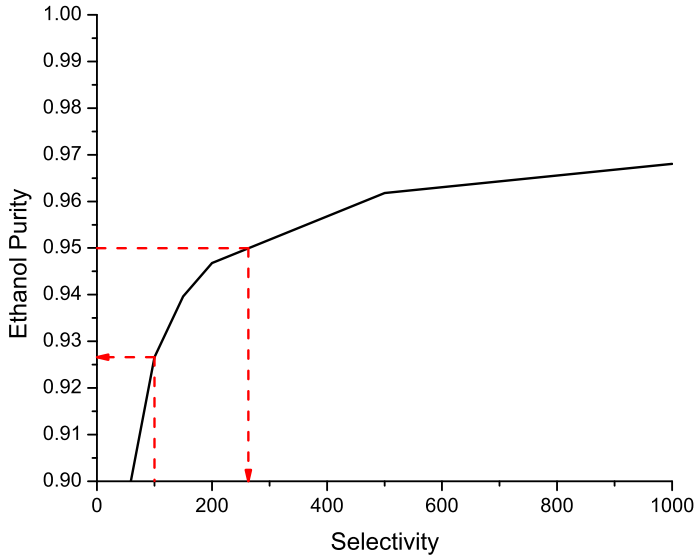

Figure 4.10: Ethanol product purity vs. membrane selectivity for ethanol permeances 1 to 10kg/hr.m^2.atm

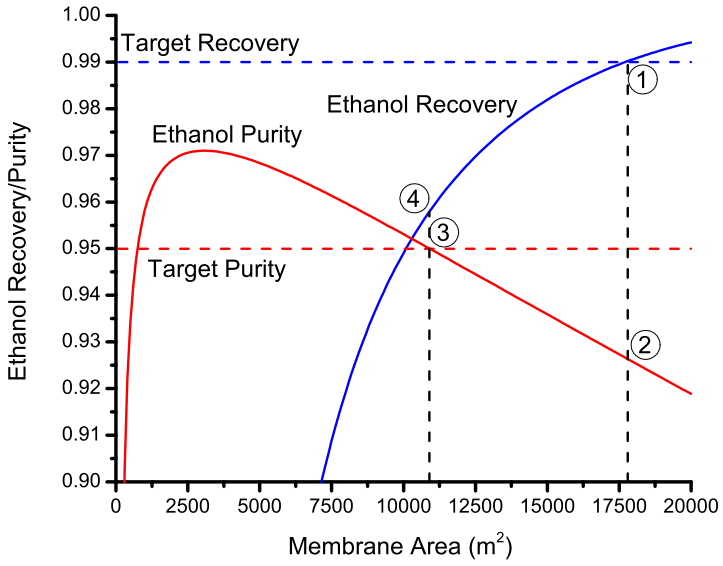

Figure 4.11: Ethanol product purity and recovery vs. membrane area - selectivity: 100, ethanol permeance: 6kg/hr.m^2.atm - target product purity shown by dashed red line

configuration with this selectivity.

Figure 4.11 shows ethanol product purity and recovery as a function of membrane area for a membrane with selectivity 100 and a permeance of 6kg/hr.m^2.atm. The single pass membrane configuration must be operated at point 1 (17,800m^2) for the required recovery to be achieved; however, this means that the achieved product purity (point 2, ∼93wt%) does not meet the 95wt% target. A smaller membrane can be used which achieves the required product purity at point 3 (10,900m^2) but does not achieve the required recovery at point 4 (∼96%).

In order to increase the overall recovery, a recycle loop is introduced as shown in figure 4.8 with a purge stream to avoid material accumulation. In this configuration, both the target purity and target recovery can be achieved with a membrane with selectivity 100.

The split fraction between the purge and recycled streams is set such that exactly 1% of the feed ethanol is in the purge stream and therefore the overall recovery target of 99% is achieved. As expected, the recycle stream will cause the beer column feed stream to increase in flow rate and decrease in ethanol concentration, and this is expected to increase the energy required in the beer column reboiler. The modified column is modelled in Aspen Plus and the energy requirement is shown in figure 4.12 as well as the

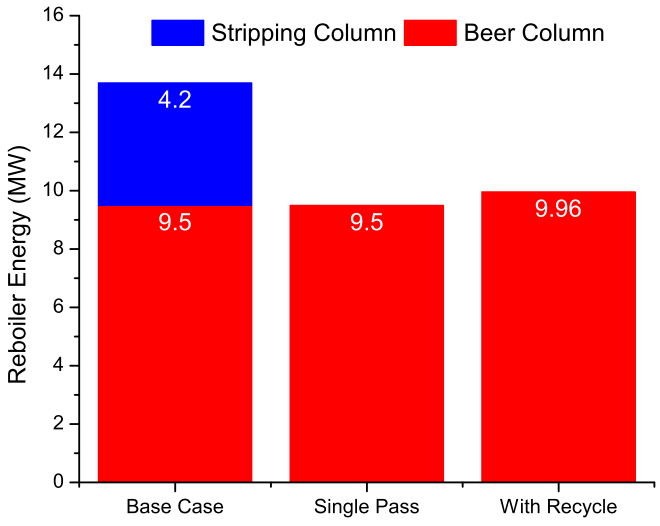

Figure 4.12: Column energy requirements for three scenarios

energy required in the base case and single pass configurations. The results show that, as expected, the beer column in the recycle scenario uses slightly more energy than in the single pass case. However, significant energy is saved compared to the base case. It was found that 3.77MW are saved which corresponds to a savings of $656,000/year.

4.3.3 Membrane economics

The net present value (NPV) savings defined as the net present value of the savings achieved over the current technology are calculated assuming a discount rate of 7%. The NPV saving projections over the course of an assumed 20 year project lifetime for a membrane cost of $\$100/m^2$ are shown in figure 4.13 for the same set of permeances studied above. It is assumed that the membrane tubes have a lifetime of five years and will cost half the initial investment to replace.

The NPV of the savings is calculated as follows:

$$NPV = \sum_{t=0}^{t=20} \frac{CF_t}{(1+r)^t} \tag{4.7}$$

where CF_t is the cash flow in year t and r is the discount rate. The value of CF_t will

depend on the specific year. For year 0:

$$CF_0 = -CAPEX_{mem} \tag{4.8}$$

where $CAPEX_{mem}$ is the capital cost of the membrane system which is calculated as the required membrane area multiplied by the membrane cost per square meter. For all years greater than 0 and except years 5, 10, 15, and 20, which are years in which the membrane must be replaced, the cash flow is defined as follows:

$$CF_t = OPEX_{dist} \tag{4.9}$$

where $OPEX_{dist}$ is the total energy saving of \$656,000/year. For years 5, 10, 15, and 20, the CAPEX associated with the replacement of the membrane unit is subtracted from the cash flow.

In figure 4.13, we see that each set of points follows a similar pattern which can be broken down as follows:

- initial investment in the membrane unit results in a negative NPV in the first month
- total energy savings of \$656,000/year are achieved over the next five years
- membrane tubes are assumed to have a lifetime of five years and cost half the initial investment to replace appropriately discounted
- this pattern is repeated for the next 15 years

Overall, we see that as the permeance increases, the system's economics improve because the required membrane area decreases.

Obviously, the results in figure 4.13 will change according to the assumed membrane cost. The process economics will improve with decreasing membrane costs as shown in figure 4.14 for membranes with permeance of 4kg/hr.m^2.atm.

In order to understand the trade-offs between increasing permeance or decreasing costs, we plot the breakeven time, defined as the time in years needed to reach an NPV of zero, against membrane costs for a set of permeances. These results are shown in figure 4.15. To further improve the clarity and usefulness of our results we suggest a new parameter termed "flow cost" which is calculated as the membrane cost (\$/m^2) divided by the membrane permeance (kg/hr.m^2.atm) and therefore has units of \$/kg/hr.atm. The flow

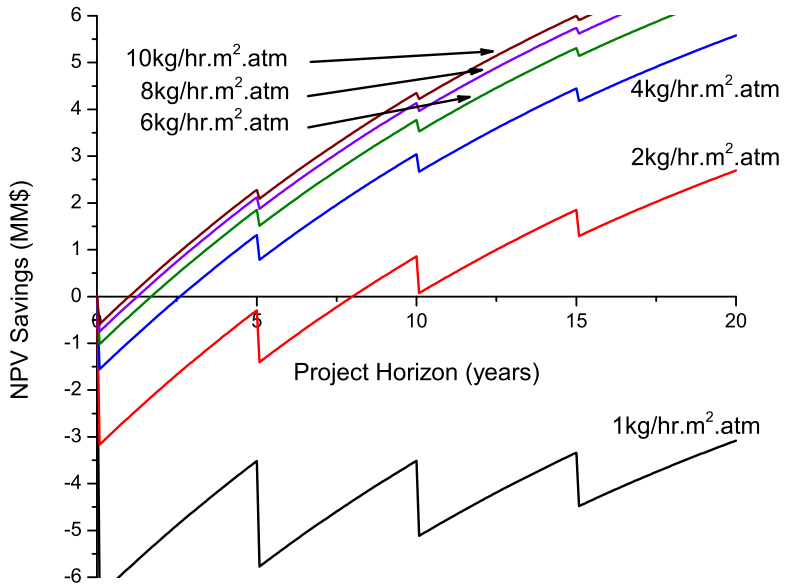

Figure 4.13: NPV savings projections for different ethanol permeance values - membrane cost: $100/m2

Figure 4.14: NPV savings projections for membrane cost values - ethanol permeance: 4 kg/hr.m^2.atm

cost can be thought of as the cost of ethanol flow rate through the membrane.

When the results shown in figure 4.15 are recast using this new parameter, the results shown in figure 4.16 are obtained. In this figure, all the points lie on a single line as long as the breakeven time is less than the lifetime of the membrane (assumed to be 5 years here). Results with breakeven times higher than five years correspond to scenarios that require at least one membrane replacement before breaking even and will result in a shift to the breakeven against flow cost curve. This is the case for the point at \$50/kg/hr in figure 4.15. The five year membrane lifetime assumption provides a reasonable upper bound on the required breakeven time. This breakeven upper bound sets a limit on the flow cost of \$42/kg/hr. Any membrane with a combination of membrane permeance and cost that achieves this upper bound flow cost limit will be economically attractive given the assumptions used.

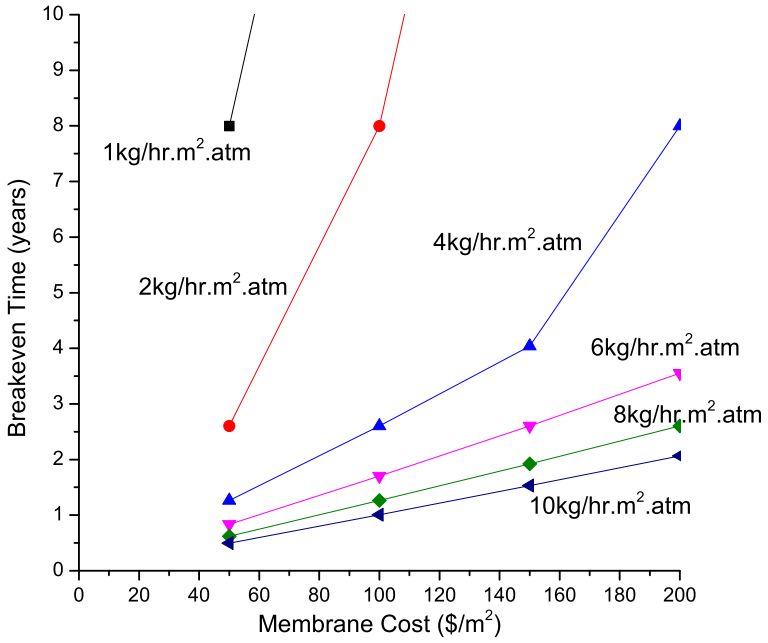

Figure 4.15: Breakeven time vs. membrane cost for different ethanol permeance values

It is interesting to investigate the sensitivity of the breakeven flow cost to the value of the membrane lifetime. These results are shown in figure 4.17. These show that maximizing the membrane lifetime greatly impacts the breakeven flow cost and breakeven time as this minimizes the number of membrane required over the course of the project.

In the results shown so far in this section, a selectivity of 100 is assumed. It is possible that such a selectivity cannot be achieved. In this case, the analyses presented above can

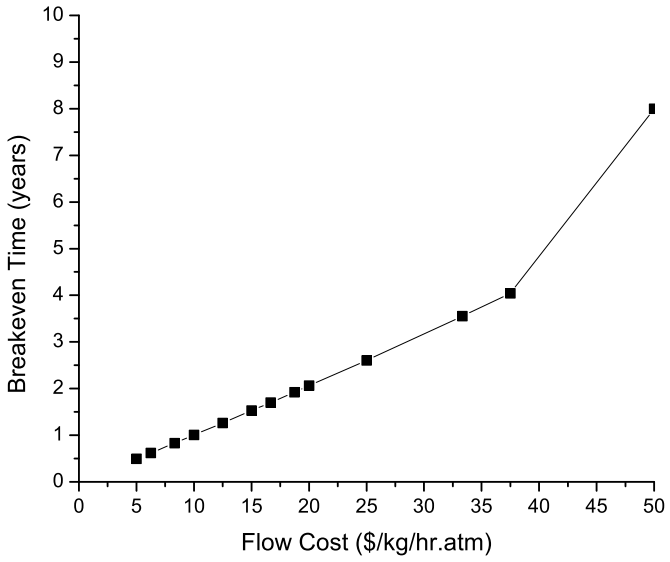

Figure 4.16: Breakeven time vs. flow cost

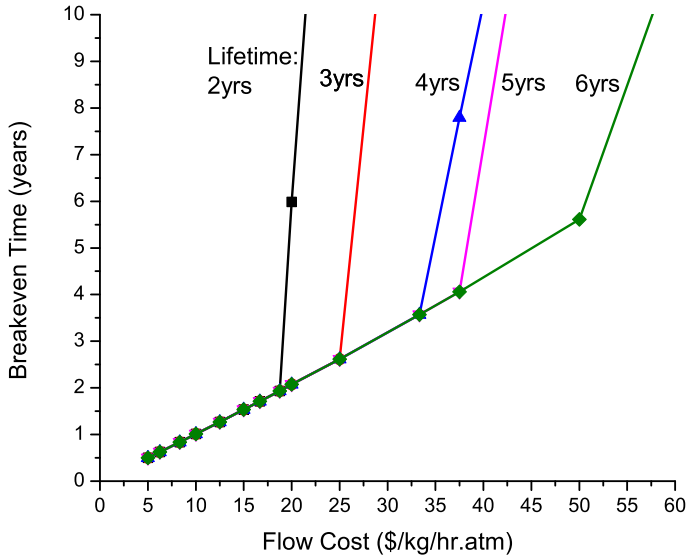

Figure 4.17: Breakeven time vs. flow cost for different membrane lifetimes

be repeated for a membrane with selectivity of 50. In this case, the energy required in the beer column increases to 11.14MW because more material is recycled. This has a knock-on effect on the NPV economics. The breakeven flow cost for both values of selectivity

is shown in figure 4.18. As expected, the membrane with a lower selectivity requires a smaller flow cost (i.e. a cheaper or higher permeance membrane) for the same breakeven time. However, this effect is not significant compared to the effect of membrane lifetime shown in figure 4.17.

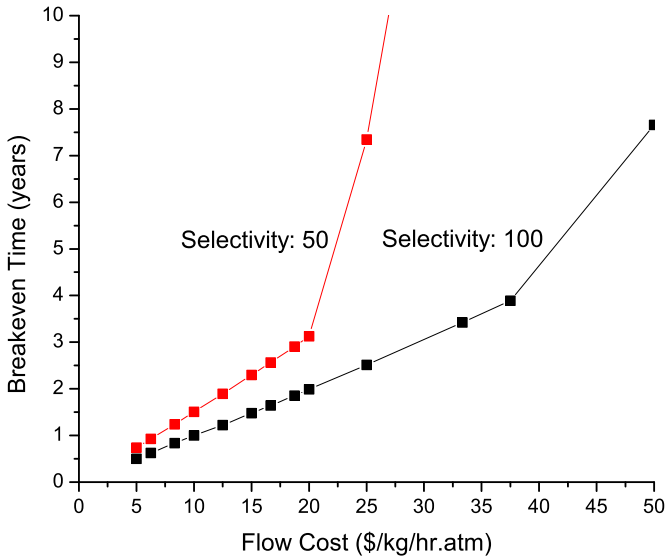

Figure 4.18: Breakeven time vs. flow cost for membranes with selectivity of 100 and 50

4.3.4 Conclusions

We have designed a novel hybrid system that combines a distillation column with a membrane unit to dehydrate corn derived ethanol. The distillation column is fed the fermentation effluent stream and produces a vapour product with an ethanol concentration of 56wt%. This is fed to a membrane unit which dehydrates the ethanol to the required 95wt% purity target. The overall ethanol recovery target of 99% is achieved by the use of a recycle stream. The required membrane performance targets are a selectivity of 100 and a flow cost less than \$42/kg/hr. An energy savings of approximately 3.74MW is achievable which corresponds to 24.6% of the total energy currently used in corn ethanol water distillation. Alternatively, a selectivity of 50 can be used in which case the upper bound flow cost was found to be \$22/kg/hr. This achieves an energy savings of 2.57MW compared to traditional distillation columns.

4.4 Case study 2: butane isomer separation

The second case study analyzed is the separation of butane isomers: normal and iso-butane. n-Butane is used for gasoline blending and for the production of ethylene and butadiene, both precursor molecules in the production of plastics. The separation of butane isomers is traditionally accomplished via a distillation process. This process is energy and capital intensive because of the closeness of the isomers' boiling points. The vapour-liquid equilibrium of the system is shown in figure 4.19. This figure highlights the deficiency of current distillation technologies when applied to this system because it clearly shows that a very small separation driving force is available. This points to examining the potential of a solution based on membrane technologies.

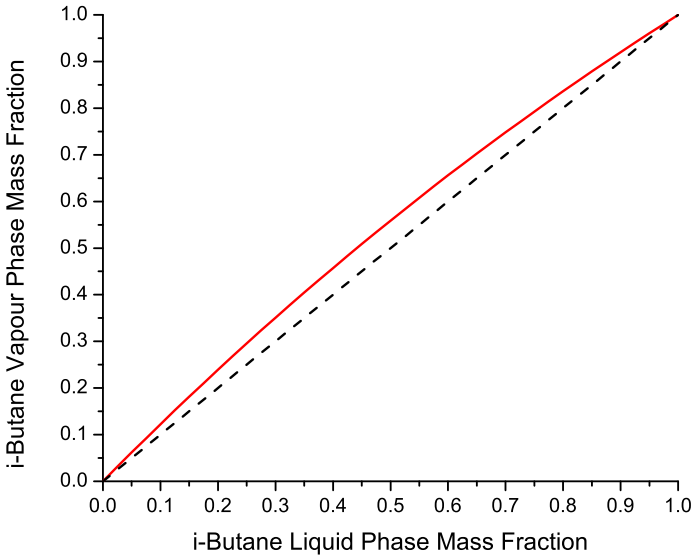

Figure 4.19: i-Butane vapour liquid equilibrium at 8.81 atm

4.4.1 Base case: distillation modelling results

The first task in this techno-economic analysis is to identify an industrially relevant base case. Distillation is the current industrial technology used to separate butane isomers. Typical industrial scale feed conditions are shown in table 4.1 [34].

An industrial scale distillation column was simulated using Aspen Plus. A schematic of the column is shown in figure 4.20. The number of trays, feed tray location and column

Table 4.1: Typical feed conditions for butane isomer separation

Pressure [atm]	8.81
Temperature [K]	343.3
Flow [kg/sec]	7.08
wt% n-Butane	0.697
wt% i-Butane	0.303

diameter are taken from the literature [34] and shown in table 4.2. It was found that n-butane is recovered in the bottoms of the column with a purity of 99.5 wt% and recovery of 98.6%. The column size data and the reboiler duty (10.24MW) and condenser duty (10.50MW) are used to estimate the capital and operating costs of the column according to the Guthrie correlations [18]. These are summarized in Table 4.3 which shows that this choice of technology is both energy and capital intensive.

Table 4.2: Industrial scale butane isomer separation distillation column size parameters

Column height	51.8m
Column diameter	2.9m
Total number of trays	74
Feed tray location	37

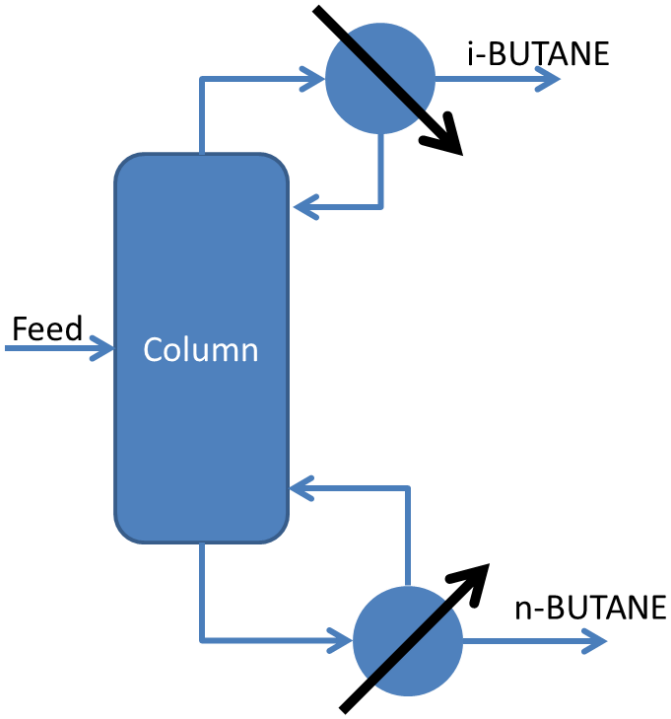

Figure 4.20: n-butane - i-butane distillation column schematic

Table 4.3: Operating and capital cost of distillation column for butane isomer separation

Annual Operating Cost (OPEX)	$2.11 MM
Capital Cost (CAPEX)	$2.20 MM

4.4.2 Single membrane unit process

A process composed of a single membrane unit shown in figure 4.21, is initially investigated as a possible solution to the energy and capital intensive distillation column used to separate butane isomers. Initially, a membrane with n-butane selectivity of 100 and n-butane permeance of 10kg/hr.m^2.atm is used as well as a sweep gas pressure of 1atm. An inert sweep gas of nitrogen flows on the permeate side at 1mol/sec. The membrane mass balance equations are the same as those described in section 4.2.

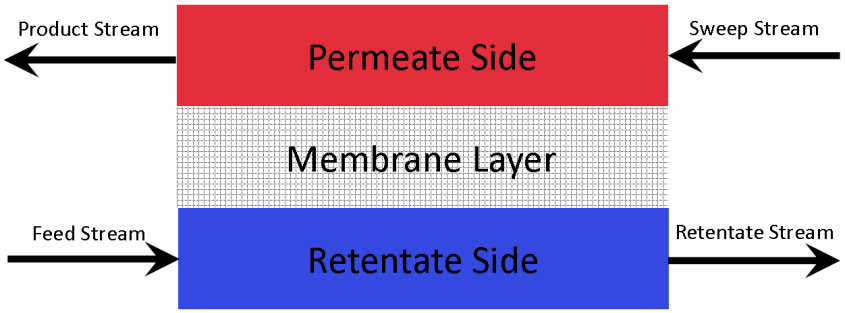

Figure 4.21: Schematic of membrane unit

Results for n-butane recovery and purity as a function of membrane area are shown in figure 4.22. The target recovery shown in the figure is the same recovery as that achieved in the distillation column. The purity achieved at this recovery is 97.4wt% which is lower than the 99.5wt% achieved with distillation. The required area for this separation is 653m^2.

The net present value (NPV) of the potential savings of this single membrane system over the traditional distillation based system can be calculated. A discount rate of 7% is assumed. The membrane is assumed to have a lifetime of 5 years and will cost 50% of the initial investment to replace. The NPV savings for different values of membrane costs are shown in figure 4.23. The NPV is calculated as follows:

$$NPV = \sum_{t=0}^{t=20} \frac{CF_t}{(1+r)^t} \tag{4.10}$$

where CF_t is the cash flow in year t and r is the discount rate. The value of CF_t will

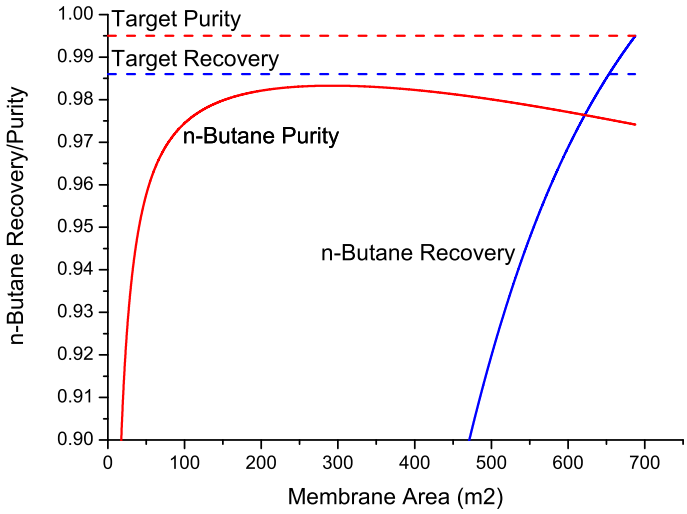

Figure 4.22: n-Butane recovery and product purity vs. membrane area for single membrane system. permeance: 10kg/hr.m^2.atm, selectivity: 100, target recovery: 98.6%, target purity: 99.5wt%

depend on the specific year. For year 0 the definition is as follows:

$$CF_0 = CAPEX_{dist} - CAPEX_{mem} - CAPEX_{vap} \tag{4.11}$$

where $CAPEX_{dist}$ is the CAPEX of the distillation based system calculated using the Guthrie correlations [18]. $CAPEX_{vap}$ is the CAPEX of a vapourizer needed to vapourize the feed stream which is assumed to be in the liquid state calculated using the Guthrie correlations [18] and equals \$0.87MM.

$CAPEX_{mem}$ is the CAPEX of the membrane system and defined as follows:

$$CAPEX_{mem} = A_{mem}C_{mem} \tag{4.12}$$

where A_{mem} is required membrane area, and C_{mem} is the membrane cost per square meter.

For all years greater than 0 and except years 5, 10, 15, and 20, which are years in which the membrane must be replaced, the cash flow is defined as follows:

$$CF_t = OPEX_{dist} - OPEX_{vap} \tag{4.13}$$

where $OPEX_{vap}$ is the operating cost of the vapourizer which was found, via Aspen Plus simulation, to be \$0.36MM. For years 5, 10, 15, and 20, the CAPEX associated with the replacement of the membrane unit is subtracted from the cash flow.

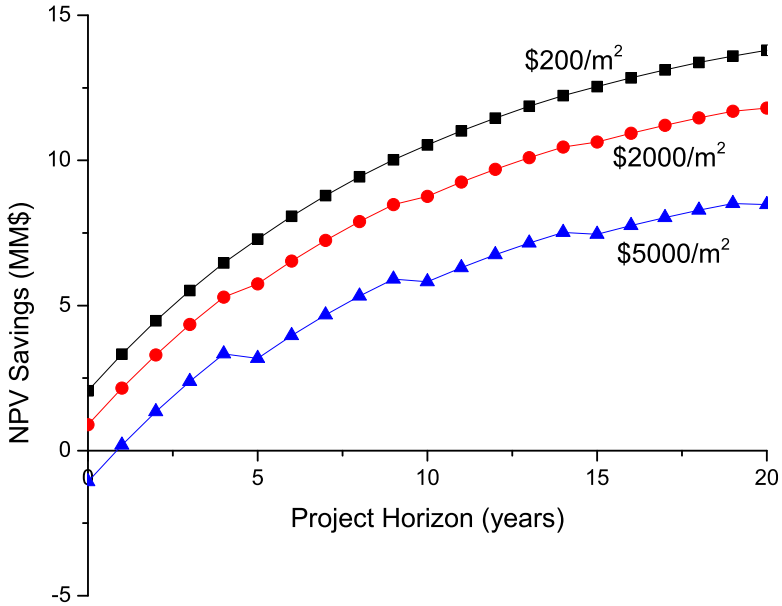

Figure 4.23: NPV of savings achieved by a single membrane unit system over distillation technology for different values of membrane cost

As can be seen in figure 4.23, significant savings can be achieved by replacing the distillation column with a membrane unit. However, as mentioned above the achieved product purity of a single membrane unit is below that achieved via distillation.

The specific product purity target will depend on the specific downstream application. Should a higher purity product be required, a system of cascading membrane has been shown to improve overall product purity without sacrificing product recovery [38] and will be investigated next.

4.4.3 Multi-membrane unit cascade process

A system composed of two membrane units was designed to improve the final product purity. The design consists of two membranes operated in series with each membrane's permeate stream being used as the next membrane's retentate feed as shown in figure 4.24. A compressor is used between the membranes to recompress the inter-membrane stream.

This compressor decouples the two membranes by allowing independent control over the second membrane's feed pressure. The key design parameter is the compressor outlet pressure as this will determine the pressure driving forces across the second membrane. Identical sweep stream pressures of 1atm are used in both membranes. The overall recovery (OR) is calculated as follows:

$$OR = R_1 R_2 \tag{4.14}$$

where R_i is the recovery in membrane i. Given that higher recoveries require larger membranes, an identical n-butane recovery is set for each membrane such that R_1 equals R_2 in equation 4.14. The n-butane recovery in each membrane is found, therefore, by taking the square root of the overall desired recovery (OR=98.6%).

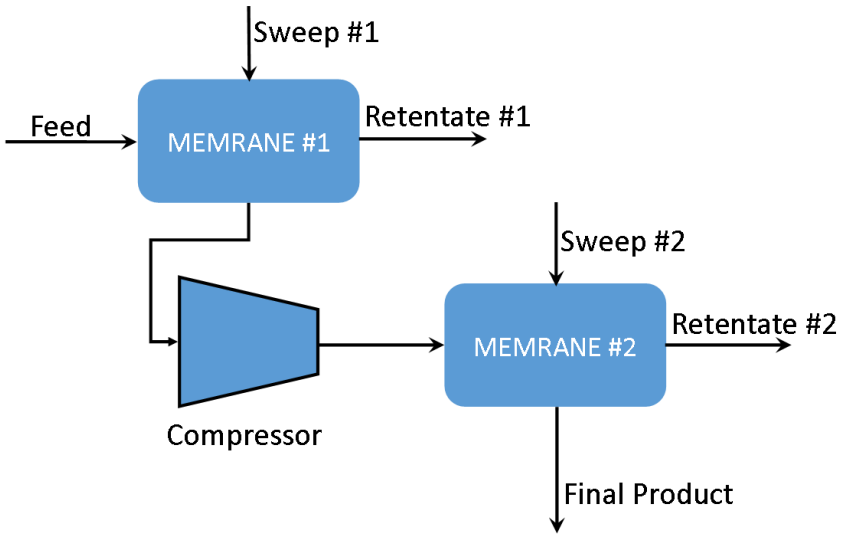

Figure 4.24: Process schematic of two membrane cascade system

The choice of optimal compressor outlet pressure is investigated in figure 4.25 which plots the total CAPEX (membrane CAPEX plus compressor CAPEX) against compressor outlet pressure for several values of membrane costs. The figure shows that as membrane costs increase the optimal compressor pressure increases. There is a trade-off between membrane cost (determined by area times costs) and compressor cost (increases with increasing outlet pressure). In all cases the first membrane is the same size as its feed and sweep pressures remain unchanged. The optimal compressor outlet pressures for the different membrane costs considered and associated CAPEX are shown in table 4.4.

The NPV savings projections for the two membrane system are shown in figure 4.26. These are calculated using the same methodology as for the single membrane system

Table 4.4: Optimal compressor outlet pressure and associated CAPEX breakdown for different membrane costs

Membrane Cost	Comp. Pressure	Mem.#1 Area	Mem.#2 Area	Compressor CAPEX	Total Mem. CAPEX	Total CAPEX
\$200/m^2	2atm	735m^2	2101m^2	\$0.85MM	\$0.57MM	\$1.42MM
\$500/m^2	3atm	735m^2	1000m^2	\$1.24MM	\$0.87MM	\$2.11MM
\$1000/m^2	4atm	735m^2	656m^2	\$1.52MM	\$1.39MM	\$2.91MM
\$2000/m^2	6atm	735m^2	389m^2	\$1.90MM	\$2.25MM	\$4.15MM
\$5000/m^2	8atm	735m^2	276m^2	\$2.18MM	\$5.06MM	\$7.23MM

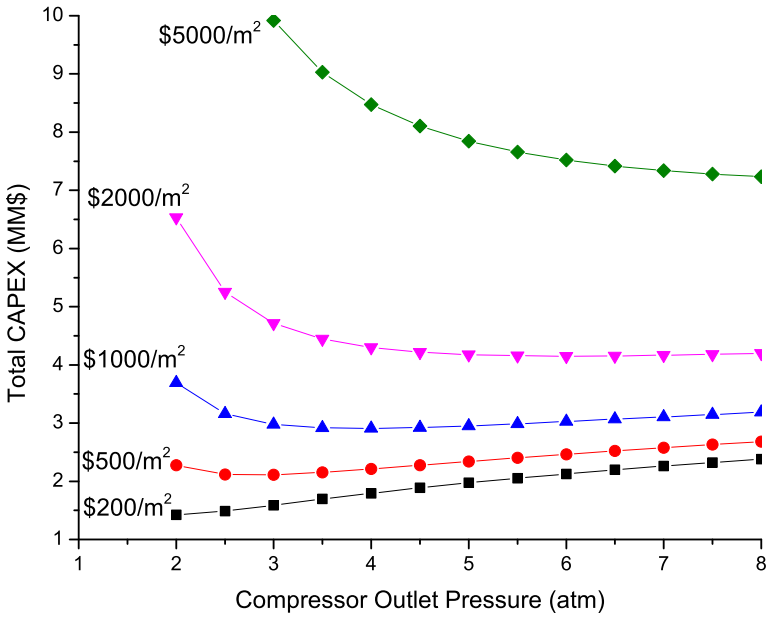

Figure 4.25: Total CAPEX for two membrane system against compressor outlet pressure for several values of membrane cost - n-Butane permeance: 10kg/hr.m^2.atm

but subtracting the CAPEX of the compressor from CF_0 and subtracting the compressor OPEX from CF_i for years i greater than 0. The compressor CAPEX is calculated using the Guthrie correlations [18] based on compressor horsepower calculated using Aspen Plus. The horsepower is used to calculated compressor OPEX assuming a cost of electricity of \$0.10/kWh and 8000hrs/year operation. The final product purity in this system was found to be 99.8wt% which is above that achieved during distillation.

A similar breakeven analysis as that carried out for the ethanol dehydration case study shows that using a maximum flow cost of \$200/kg/hr will result in systems with breakeven times less than three years. This flow cost corresponds to the \$2000/m^2 line in figure 4.26.

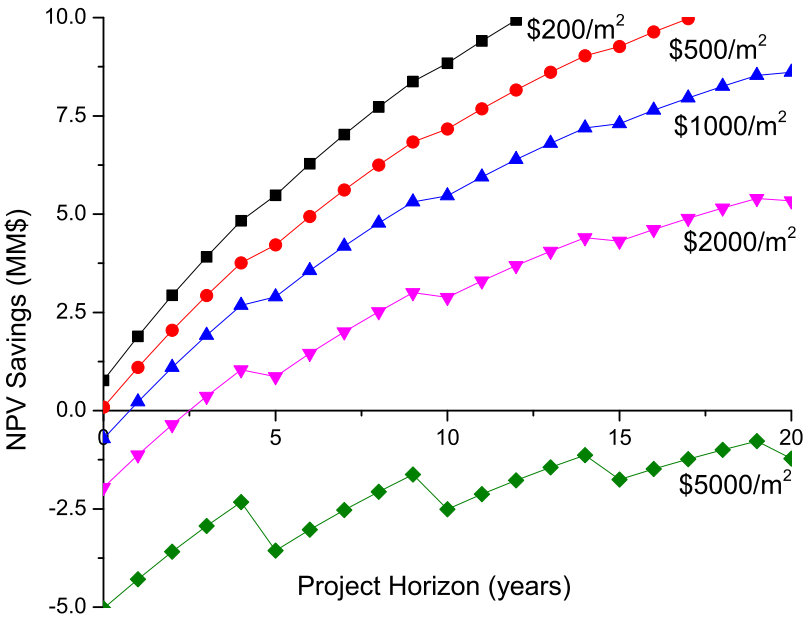

Figure 4.26: NPV savings projections of two membrane system for several values of membrane cost - n-Butane permeance: 10kg/hr.m^2.atm

4.4.4 Conclusions

The analyses presented in this section have shown that significant savings can be made using membrane-based systems rather than traditional distillation technology for the separation of butane isomers. Two membrane cascading systems that are capable of matching the product purity and recovery of distillation columns have been designed. A promising potential application of this novel technology has been shown throughout this study. Indeed, the work presented in this chapter has shown that economically attractive processes, that can outperform traditional technology, can be designed for a broad set of membrane performance criteria.

CHAPTER 5

Detailed Mathematical Modelling of Adsorption-Diffusion based Transport through Silica Support Zeolite Membranes

5.1 Introduction

Flux through zeolite membranes is driven by surface adsorption processes which are non-linear with respect to pressure [9]. Current membrane models (used in Chapter 4) define flux as the linear relationship between a fixed value of permeance and pressure as shown in equation 4.2. The need for a non-linear description of flux through a zeolite layer within a membrane unit is therefore imperative. To further illustrate the discrepancy between current membrane models and the real beheaviour of these systems, we present in figure 5.1 a sketch of a typical Langmuir adsorption curve in which two pairs of pressure values, namely, [P1, P2] and [P3, P4] are selected. Both pairs have the same pressure difference and therefore equation 4.2 would predict the same flux. However, the value of the coverage difference for both pairs is clearly different and, therefore, each pair would produce a different actual flux. This effect cannot be captured in pressure-driven flux models and can be significant in high recovery membrane units where large changes in partial pressures exist along the length of the unit. Indeed permeance and selectivity have been shown experimentally to depend on many other factors as well such as temperature,

pressure regimes, and feed conditions [11, 71].

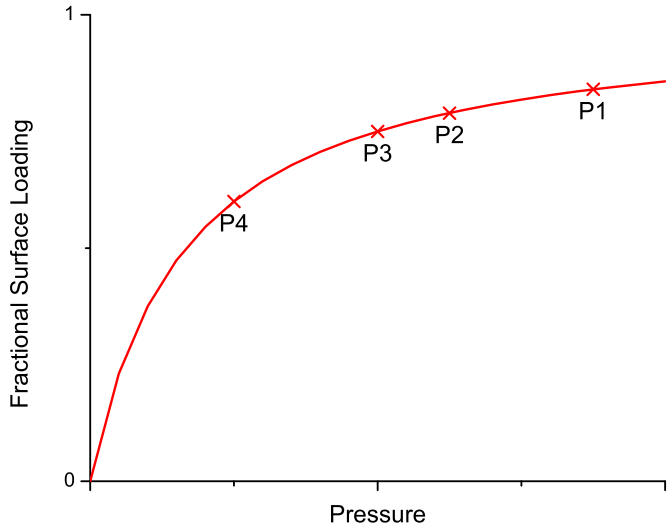

Figure 5.1: Sketch of typical Langmuir adsorption curve

The objective of this work is to formulate a model of the transport phenomena through a silica supported zeolite membrane which does not rely on estimates of selectivity and permeance. The newly developed model will include a detailed mathematical formulation of the adsorption and diffusion through the zeolite layer as well as diffusion through the support layer. The model of mass flow of each side of the membrane layer is also extended to include the effect of pressure drop. The combined model is able to predict membrane flux and selectivity based on pressure regimes, temperature and feed conditions and results in more accurate predictions of overall membrane performance.

The general mathematical description of transport phenomena (adsorption and diffusion) of compounds through zeolitic materials has been widely studied for a variety of industrially relevant compounds [33,35,39]. Within these generalized models the choice of adsorption isotherm model is crucial for accurate predictions. Three types of adsorption models exist of increasing computational complexity:

- Langmuir type models and multi-component extensions of these
- Ideal Adsorbed Solution Theory (IAST)
- Real Adsorbed Solution Theory (RAST)

The chosen model should be that which predicts experimental results with reasonable accuracy. The majority of previous research has focused on well mixed conditions (constant partial pressure conditions) on either side of the zeolite membrane layer. Only one contribution [68] was found that used adsorption-diffusion models to predict the flux through a membrane unit with axially dispersed partial pressures. This contribution used an extended Langmuir type isotherm to predict the beheaviour of membrane units in various configurations (co-current, counter-current, and recycle) used for the separation of methane-ethane and methane-propane mixtures.

5.2 Model development

The membrane module is modelled as a counter-current plug-flow membrane unit where the feed enters the retentate side, molecules permeate through the membrane and leave in the product stream on the shell side (permeate side). An inert sweep gas is used on the permeate side and assumed not to permeate through the membrane. A schematic of the membrane showing the support and membrane layers is shown in figure 5.2.

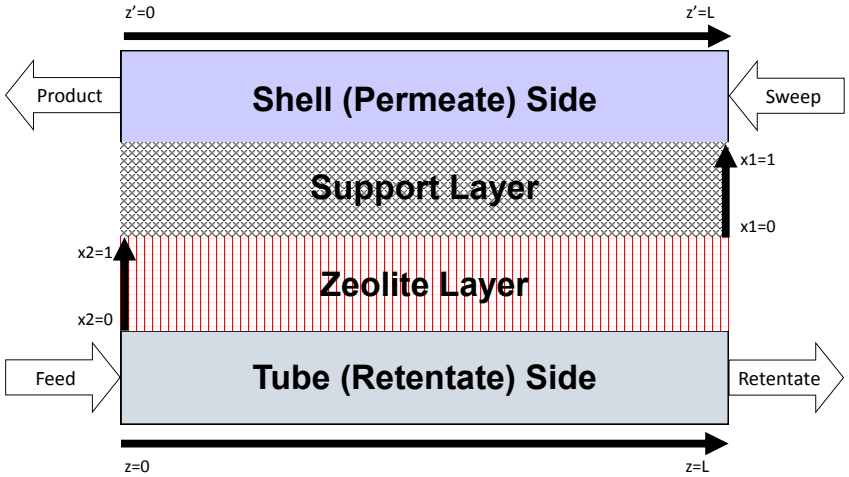

Figure 5.2: Schematic of silica supported zeolite membrane - not to scale

The membrane is divided into four sections:

1. retentate (tube) side
2. zeolite layer
3. silica support layer

4. permeate (shell) side

It is important to note that the term retentate side and tube side are used interchangeably and the same is true for permeate side and shell side.

Within each section, a different set of governing equations are solved in order to predict the overall transport of species through the support and zeolite layers. Appropriate boundary conditions are defined at the interfaces between the layers. The following assumptions are also made:

- isothermal operation
- ideal gas equation of state is used to calculate appropriate variables
- plug flow on each side of membrane
- total membrane area achieved by summation of a number of identical membrane units and feed is assumed evenly divided between each of these

5.2.1 Retentate and permeate section material balances

Dynamic mass balances are solved on both sides of the support-zeolite layer. The mass balances are formulated as follows:

$$\frac{dC_{k,i}}{dt} = \frac{4}{\pi dp^2}\frac{dF_{k,i}}{dz} - \frac{4}{dp}J_i \tag{5.1}$$

where $C_{k,i}$ is the mass concentration of species i on side k, $F_{k,i}$ is the component flow rate of component i on side k, dp is the diameter of the pipe, and J_i is the flux of species i. The pressure drop along the length of the membrane unit is modelled according to the Hagen-Poiseuille equation as follows [7]:

$$\frac{dP_k}{dz} = -\frac{8\mu_k {\dot{m}_k}^2}{\frac{dp^2}{4}\rho_k Ap} \tag{5.2}$$

where P is the total pressure on side k, $\dot{m}_k$ is the total mass flow rate on side k, μ_k is the viscosity of side k, and ρ_k is the total density of side k.

The following boundary conditions are applied:

$$F_{r,i}|_{z=0} = F^0_{r,i} \tag{5.3}$$

$$F_{p,i}|_{z'=L} = F^0_{p,i} \tag{5.4}$$

where L is the length of the membrane and $F^0_{k,i}$ is the feed flow rate of component i on side k.

The value of J_i, the flux of component i from tube side to shell side, is determined by solving an adsorption and diffusion model for each component through the support and zeolite layers described in section 5.2.2.

5.2.2 Zeolite membrane adsorption-diffusion and silica support molecular diffusion models

Nitish Mittal, a fellow member of the Daoutidis and Tsapatsis groups, has formulated a detailed mathematical model for describing the adsorption-diffusion through the zeolite membrane structure. The membrane structure consists of a zeolite layer grown on a porous silica support. Within the zeolite layer, the mixture adsorption is modelled using the Real Adsorption Solution Theory while the multi-component diffusion is based on Maxwell-Stefan equations. The permeation through the support layer is modelled using the combined effect of the Knudsen and molecular diffusion and viscous flow. These equations are then solved at each axial point along the membrane.

The transport through the zeolite layer of a binary system (molecules i and j) is governed by the generalized Maxwell-Stefan equation (GMS):

$$-\rho\frac{\theta_i}{RT}\nabla\mu_i = \sum_{j=1,j\neq i}^{n}\frac{q_jN_i - q_iN_j}{q_i^{sat}q_j^{sat}Đ_{ij}} + \frac{N_i}{q_i^{sat}Đ_i} \tag{5.5}$$

where the descriptions of each term are shown in table 5.1.

The first term:

$$-\rho\frac{\theta_i}{RT}\nabla\mu_i \tag{5.6}$$

corresponds to the adsorption isotherm and accounts for the driving force for transport of molecular i through the membrane. The second term:

$$\sum_{j=1,j\neq i}^{n}\frac{q_jN_i - q_iN_j}{q_i^{sat}q_j^{sat}Đ_{ij}} \tag{5.7}$$

Table 5.1: Definition of terms used in GMS model

Term	Definition
ρ	density of zeolite
θ_i	fractional surface loading of species i
R	universal gas constant
T	temperature
μ_i	chemical potential of species i
q_i	surface loading of species i
q_i^{sat}	saturation surface loading of species i
N_i	flux of species i
$Đ_i$	Maxwell-Stefan diffusion coefficient
$Đ_{ij}$	exchange coefficient

accounts for the interaction between molecule i and molecule j. The third term:

$$\frac{N_i}{q_i^{sat} Đ_i} \tag{5.8}$$

accounts for the interaction between molecule i and the zeolite layer.

Given individual Maxwell-Stefan diffusion coefficients, $Đ_i$ and $Đ_j$, the exchange coefficient, $Đ_{ij}$, is calculated according to the Vignes correlation as follows:

$$Đ_{ij} = Đ_i^{\frac{q_i}{q_i+q_j}} Đ_j^{\frac{q_j}{q_i+q_j}} \tag{5.9}$$

The Maxwell-Stefan diffusion coefficients, $Đ_i$, depend on the fractional surface loading, θ_i, as follows:

$$Đ_i = Đ_i^o(1-\theta_1)(1-\theta_2) \tag{5.10}$$

where $Đ_i^o$ is a temperature dependent parameter.

5.2.3 Boundary conditions between sections

Appropriate boundary conditions are used at the interface between the different sections of the membrane unit. Between the retentate side and zeolite layer, the following condition is applied:

$$\theta_i|_0 = f(P_i^{ret}, P_j^{ret}) \quad \forall \quad i \tag{5.11}$$

where P_i^{ret} is the partial pressure of component i on the retentate side and $f(P_i^{ret}, P_j^{ret})$ is the function that describes surface adsorption (Langmuir, IAST or RAST).

Between the zeolite and support layers, the following condition is applied:

$$N_i^{sup}|_0 = N_i^{mem}|_1 \quad \forall \quad i \tag{5.12}$$

such that the flux of species i in the membrane, N_i^{mem}, is equal to its flux in the support layer, N_i^{sup}, at the interface between these layers.

Finally, between support layer and permeate side, the following condition is applied:

$$P_i^{sup}|_1 = P_i^{perm} \quad \forall \quad i \tag{5.13}$$

where P_i^{sup} and P_i^{perm} are the partial pressures of component i in the support layer and on the permeate side, respectively.

5.3 Model formulation and simulation

The complete model incorporating each subsection mentioned above is solved using gPROMS v.3.6 assuming a 50 grid point discretization domain in each subsection. Each subsection is discretized according to a different method. A schematic of the membrane unit, showing the different axes used, is shown in figure 5.2. On the tube side a second order backwards finite difference method is used based on the z-axis shown in the figure 5.2, on the shell side a second order forward finite difference method is used on the z'-axis shown in figure 5.2. The z-axis and z'-axis are both based on the same set of grid points but are discretized according to different schemes because of where the boundary conditions are applied. The feed enters at $z' = L$ on the retentate side and therefore a forward finite difference method (with respect to z'-axis) is best suited. The opposite is true on the permeate side where the feed enters at $z = 0$ and therefore a backward finite difference method is best suited. The support and zeolite layers are discretized according to a fourth order centered finite difference method.

5.4 Results, analysis and discussion

The GMS model is used to predict the flux through the silica supported zeolite membrane layer based on partial pressures on either side which are themselve predicted from the flow models described in section 5.2.1. The combined model is called the adsorption-diffusion model compared to the models used in chpater 4 which predict flux based on pressure difference and are, therefore, called pressure driven flux models. Both models are applied to the butane isomer separation case study previously described in chapter 4. Nitish Mittal found that the RAST method for predicting zeolite surface adsorption is better suited for this butane isomer system than the Langmuir or IAST methods.

5.4.1 Adsorption-diffusion model results

The adsorption-diffusion model is solved for a variety of pressure regimes which are summarized in table 5.2. The feed concentrations of n-butane and i-butane are chosen to match those used in chapter 4 and shown in table 4.1.

Table 5.2: Conditions used in adsorption-diffusion model runs at 343K

Run Number	Tube Side Pressure (atm)	Shell Side Pressure (atm)
1	3	1
2	3	0.5
3	3	0.1
4	5	1
5	5	0.5
6	5	0.1
7	7	1
8	7	0.5
9	7	0.1

These conditions are used to generate figures 5.3 and 5.4 which, respectively, plot the membrane area required to recover 95% n-butane and the achieved product purity at this recovery against pressure difference across the membrane.

Figure 5.3 shows that as shell side (product side) pressure decreases, smaller membrane areas are required for the same tube side pressure (data with same colour/symbol in figure 5.3). Similarly, as tube side (feed side) pressure increases, smaller membrane areas are required for the same shell side (product side) pressure (data from same data label).

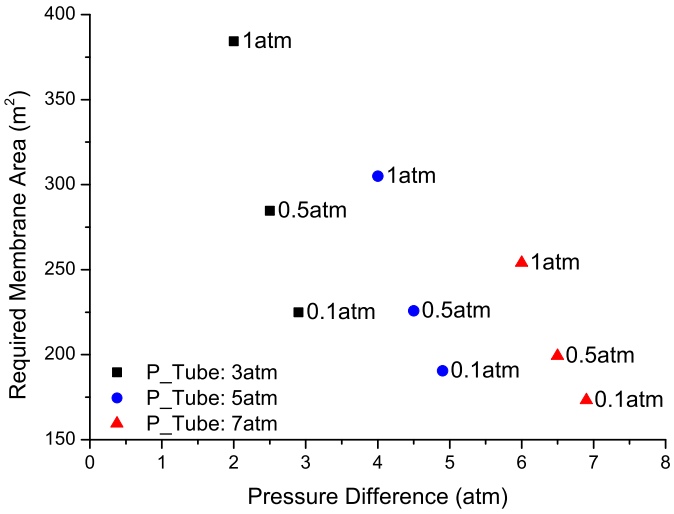

Figure 5.3: Required membrane area vs. pressure difference across membrane for different pressure regimes - data labels are shell side pressures

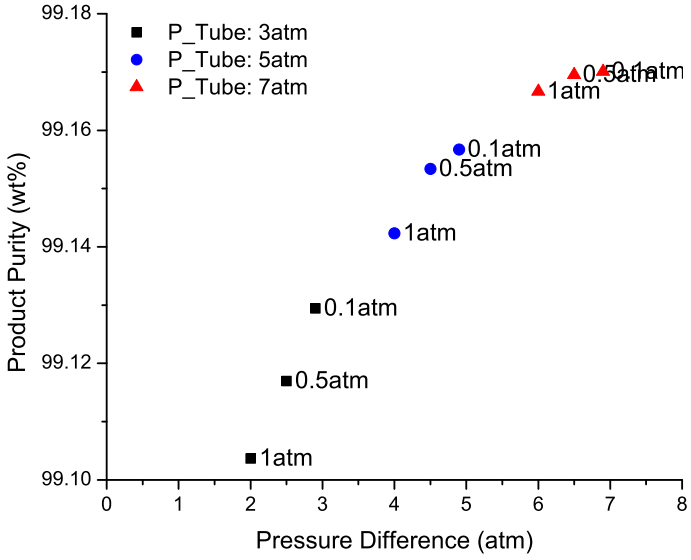

Figure 5.4: Achieved product purity vs. pressure difference across membrane for different pressure regimes - data labels are shell side pressures

Figure 5.4 shows that a monotonically increasing relationship exists between increasing pressure difference and increased achieved product purity.

5.4.2 Comparison results between adsorption-diffusion model and pressure driven flux model

It is instructive to investigate the differences in predicted membrane areas and product purities, two key operating characteristics, between simplified pressure-driven flux models (discussed in chapter 4) and the more complex adsorption-diffusion model developed in this chapter.

Before a comparison can be made, appropriate values of permeance and selectivity must be found from the adsorption-diffusion model and then used in the pressure driven flux models. The value of permeance ($\mathcal{P}_i$) is found by rearranging equation 4.2 as follows:

$$\mathcal{P}_i = \frac{J_i}{(P_{p,i} - P_{r,i})} \tag{5.14}$$

where J_i is the flux through the membrane predicted by the adsorption-diffusion model and $P_{k,i}$ is the partial pressure of species i on side k. Since the value of J_i predicted by the adsorption-diffusion model will varying along the axial dimension (z-axis) of the membrane unit, the value of $\mathcal{P}_i$ can be calculated at all points along the axial dimension as well.

The value of selectivity is defined as follows:

$$\alpha = \frac{J_n}{\Delta P_n} \Big/ \frac{J_{iso}}{\Delta P_{iso}} \tag{5.15}$$

where α is the selectivity, J_n and J_{iso} are the fluxes of n-butane and i-butane, respectively and ΔP_n and ΔP_{iso} are the partial pressure differences across the membrane of n-butane and i-butane. The value of α is found for all points along the axial dimension (z-axis) of the membrane unit.

Figures 5.5 and 5.6 show the permeance and selectivity, respectively, against membrane area and axial dimension at a feed side pressure of 5atm and product side pressure of 0.1atm. These figures show that significant variation in the parameters exists along both dimensions of axial length and membrane area.

In order to compare the pressure driven and adsorption-diffusion models, a single value of n-butane permeance and selectivity is needed. It is, therefore, necessary to take an average value of the parameters shown in figures 5.5 and 5.6. Two such averages can be considered, namely, an overall average over all axial and area dimensions or an axial

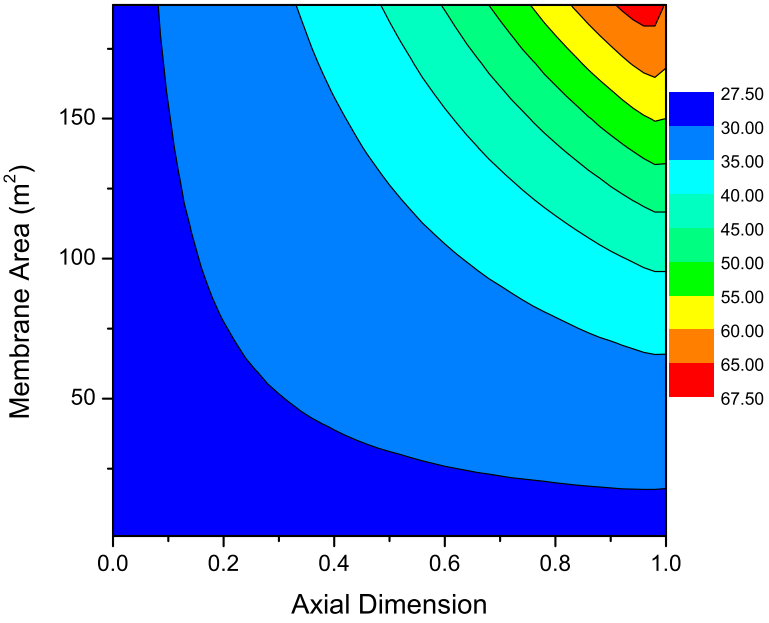

Figure 5.5: n-Butane permeance vs. membrane area and axial dimension
feed side pressure: 5atm, product side pressure: 0.1atm

average which is itself a function of membrane area.

Figure 5.7 shows the axially averaged n-butane permeance as a function of membrane area for three selected pressure regimes. Figure 5.8 shows axially averaged selectivity as a function of membrane area for three selected pressure regimes.

For the sake of an initial comparison, feed conditions of 5atm on the feed side and 0.1atm on the product side are selected. A comparison of predicted recovery is shown in figure 5.9 where two simple models are used. The first simple model is given the axially averaged value of n-butane permeance (44.18kg/hr.m^2) and selectivity (720.33) at the membrane area corresponding to the maximum recovery studied (95%); the second simple model is given the parameter values found by an overall average of n-butane permeance (35.53kg/hr.m^2) and selectivity (826.33).

It is observed that both simple models overestimate the required membrane area. This suggests that these pressure driven flux models, although easier to implement, cannot accurately predict the behaviour of membrane technologies over a wide range of membrane areas (and therefore recoveries) by only using a constant value of n-butane permeance and

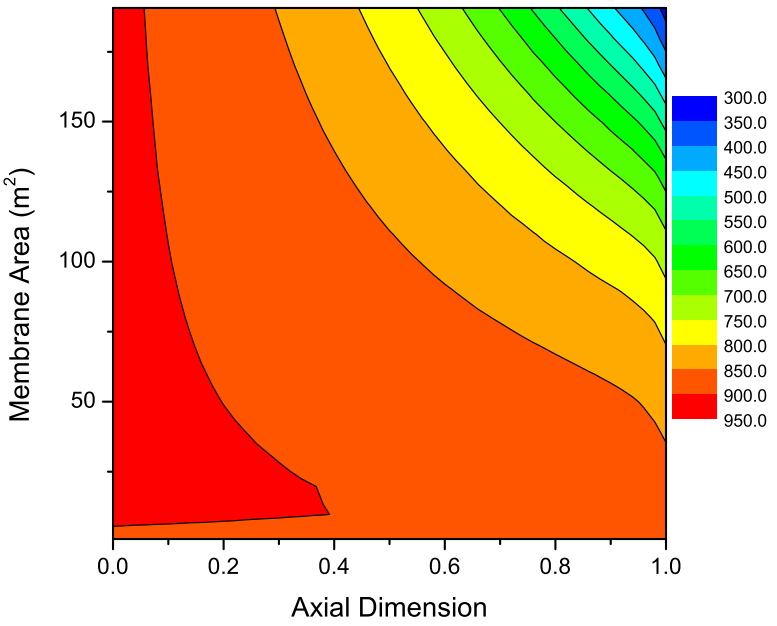

Figure 5.6: Selectivity vs. membrane area and axial dimension - feed side pressure: 5atm, product side pressure: 0.1atm

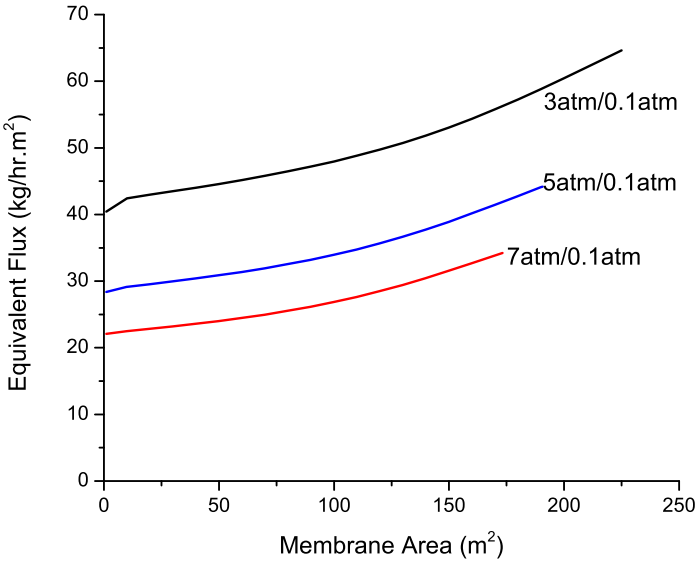

Figure 5.7: Average n-butane permeance vs. membrane area for three selected pressure regimes

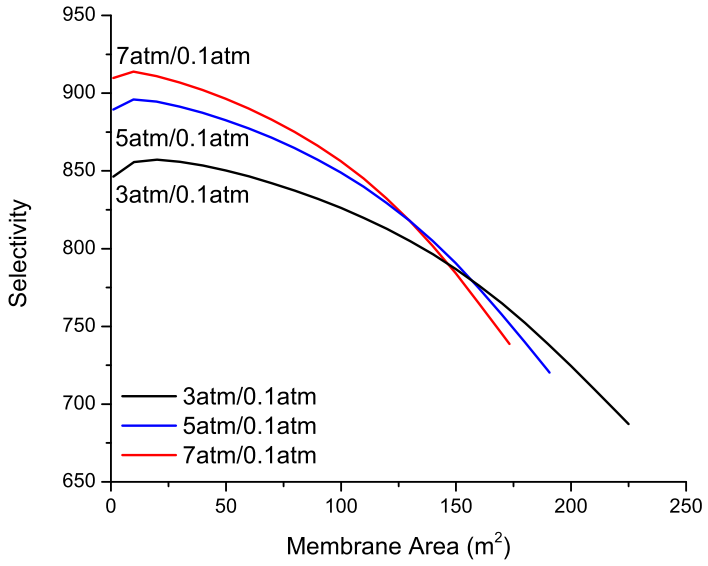

Figure 5.8: Average selectivity vs. membrane area for three selected pressure conditions

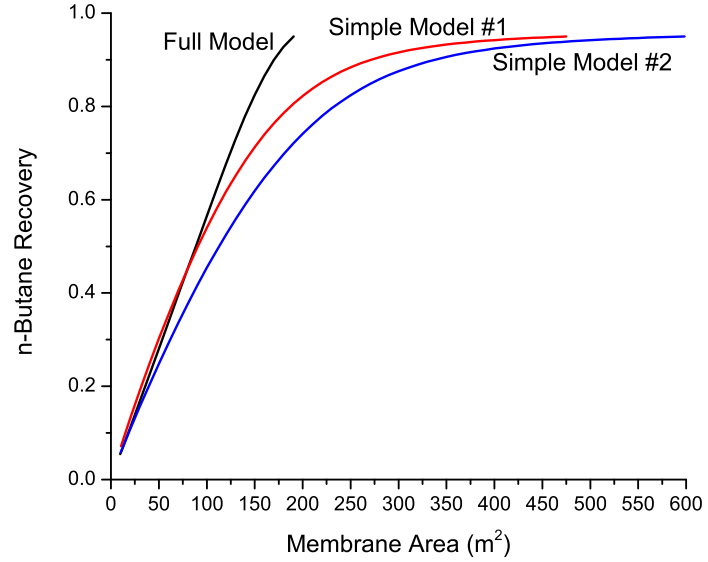

Figure 5.9: Comparison of n-butane recovery for simple and full models - feed side pressure: 5atm, product side pressure: 0.1atm - simple model#1 uses axially averaged parameters, simple model#2 uses overall averaged parameters

selectivity.

5.5 Conclusions

While these initial results suggest that the use of adsorption-diffusion models can better predict a membrane's performance than pressure-driven flux models, several key aspects have not yet been investigated. These include the effect of temperature which is expected to affect the prediction of flux and an investigation into multi-membrane systems which would build on the work presented in chapter 4 where each membrane is given the same permeance and selectivity.

The ability to predict a membrane unit's performance based exclusively on its feed pressures and temperatures is a significant development over traditional methods which use predetermined and fixed values of permeance and selectivity.

CHAPTER 6

Conclusions and Future Work

6.1 Conclusions

The work presented in this thesis applies principles and methods of Process Systems Engineering to tackle a set of problems related to the conversion of biomass resources to fuel and chemical products. The specific aim of the thesis was to address the energy use, environmental impact and economics of these processes and technologies.

The first of these problems, analyzed in chapter 2, focused on a facility location optimization problem of a novel super critical waste grease to biodiesel technology based in Greater London. This research has shown that small scale distributed production of biodiesel is economically feasible in a large city. Biodiesel production contributes to the reduction of CO_2 emissions from fossil fuel based diesel production and consumption. Perhaps more importantly, this process can help reduce cooking oil waste processing by converting it into biodiesel that is sourced, produced and sold locally.

A process synthesis problem was formulated for a multi-feedstock, multi-product biorefinery and analyzed in chapter 3. The base case solution, a variety of sensitivity analyses, multi-objective optimization, and Monte Carlo style analyses have shown that

biorefineries capable of producing fuels and chemicals allow biorefinery systems to be profitable under a wide range of material values and allow for the maximized utilization of the biomass feedstock towards the system's economic potential.

In chapter 4, a model of a novel hollow-fiber supported zeolite membrane technology is formulated and used to analyze the technical and economic feasibility of two proposed applications of this technology, namely, corn derived ethanol dehydration and butane isomer separation. For the ethanol dehydration case study, a novel hybrid system that combines a distillation column with a membrane unit has been designed and in order to maximize product recovery a recycle stream from the membrane's retentate stream back to the distillation column feed is included. The required membrane performance targets are a selectivity of 100 and a flow cost less than \$42/kg/hr. An energy savings of approximately 3.74MW is achievable which corresponds to 24.6% of the total energy currently used in corn ethanol distillation. For the butane isomer case study, the analyses have shown that significant savings can be made using membrane based systems rather than traditional distillation technology. Two membrane cascading systems that are capable of matching the product purity and recovery of distillation columns have been designed. The breakeven flow cost for this case study was found to be \$200/kg/hr. The work presented in chapter 4 has shown that economically attractive processes that outperform traditional technology can be designed for a broad set of membrane performance criteria.

Finally in chapter 5, a generalized Maxwell-Stefan model of the adsorption-diffusion beheaviour of butane isomers on zeolites was used to predict the flux through a silica supported zeolite membrane. Knudson and molecular diffusion as well as viscous flow are considered in the support layer. These are combined with plug-flow material balance equations for the retentate and permeate sides. The ability to predict a membrane unit's performance based exclusively on its feed pressures and temperatures is a significant development over traditional methods which use predetermined and fixed values of permeance and selectivity.

6.2 Future Work

6.2.1 Process synthesis of biorefineries: integration with facility location optimization

The biorefinery process synthesis work presented in chapter 3 has shown that biorefineries offer a potentially lucrative use for the biomass resources available; however, the analysis assumed a plentiful supply of biomass feedstocks and a limitless demand for the biofuels and bio-chemicals produced. This assumption can be lifted and the effect of limited demand for certain products and limited supply of certain feeds can be incorporated. A study of the impact of limited supply and demand would further improve the understanding of how biorefinery systems can be optimally designed given real world limitations.

In reality, whilst the supply of biomass feedstocks is both limited and seasonal and the demand for the biorefinery's products is also limited, the supply and demand is also geographically distributed. Clearly, different biomass types are more or less prevalent in certain regions of the United States, and the same can be true for the biorefinery's products. For example, a precursor molecule produced at the biorefinery must be delivered to an existing facility suitable for its upgrading. This delivery incurs a cost and environmental impact associated with the transport of products from the biorefinery to the upgrading facility. Similarly, transport of biomass feedstocks from the farm to the biorefinery also incurs economic and environmental costs.

These supply chain considerations ultimately lead to the creation of facility location and process synthesis model where each facility is optimally designed for its specific location. This integration of supply chain and process design considerations enables the creation of a complete decision making tool which spans both the enterprise and facility time and length domains.

6.2.2 Zeolite membrane modelling

The work presented in chapter 5 suggest that the use of adsorption-diffusion models can better predict a membrane's performance than pressure-driven flux models; however, several key aspects have not yet been investigated. The effect of temperature on membrane performance has yet to be investigated. Lower temperatures are expected

to produce lower fluxes but higher selectivities [76]. This can have significant impact on multi-membrane systems which have not yet been investigated using the adsorption-diffusion based models. For example, in chapter 4 a two unit system with inter-membrane recompression was considered and compression costs were found to contribute significantly to the total capital and operating costs; therefore, investigating the effect that an inter-membrane heater or cooler produces on the system's performance and costs will prove insightful. This may improve the overall economics of these systems. Finally, more accurate predictions of membrane flux and selectivity and therefore performance will lead to faster development of this novel technology and ultimately the benefits of reduced energy consumption that this technology promises will be achieved faster, safer, and cheaper.

Bibliography

[1] C. Akerberg and G. Zacchi. An economic evaluation of the fermentative production of lactic acid from wheat flour. *Bioresource Technology*, 75:119–126, 2000.

[2] G. L. Authority. Website: Fast food city - mayor urges action on healthier eating, url: http://www.london.gov.uk/media/press_releases_mayoral/fast-food-city-%e2%80%93-mayor-urges-action-healthier-eating, accessed november 2012, November 2012.

[3] R. W. Baker. Future directions of membrane gas separation technology. *Industrial and Engineering Chemistry Research*, 41:1393–1411, 2002.

[4] R. C. Baliban, J. A. Elia, and C. A. Floudas. Toward novel hybrid biomass, coal, and natural gas processes for satisfying current transportation fuel demands, 1: Process alternatives, gasification modeling, process simulation, and economic analysis. *Industrial & Engineering Chemistry Research*, 49:7343–7370, 2010.

[5] R. C. Baliban, J. A. Elia, and C. A. Floudas. Biomass to liquid transportation fuels (BTL) systems: process synthesis and global optimization framework. *Energy & Environmental Science*, 6(1):267–287, 2013.

[6] R. E. Baron, J. H. Porter, and O. H. Hammond. *Chemical equilibria in carbon-hydrogen-oxygen systems.* The MIT Press, Massachusetts, USA, 1976.

[7] R. B. Bird, W. E. Stewart, and E. N. Lightfoot. *Transport Phenomena.* John Wiley & Sons., 2002.

[8] A. Bridgwater. Renewable fuels and chemicals by thermal processing of biomass. *Chemical Engineering Journal*, 91(2-3):87–102, Mar. 2003.

[9] S. Brunauer, L. S. Deming, W. E. Deming, and E. Teller. On a theory of the van der waals adsorption of gases. *Journal of the American Chemical Society*, 67(7):1723–1732, 1940.

[10] P. D. Camargo, S. Tangermann, R. Moehler, R. Johnson, C. Hebebrand, A. Swinbank, D. Orden, G. Kutas, and M. Gifford. IPC Position Paper Biofuel and Biomass Subsidies in the U . S ., EU and Brazil: Towards a Transparent System of Notification. Technical Report September, International Food and Agricultural Trade Policy Council, 2010.

[11] P. D. Chapman, T. Oliveira, A. G. Livingston, and K. Li. Membranes for the dehydration of solvents by pervaporation. *Journal of Membrane Science*, 318(1-2):5–37, 2008.

[12] A. Corma, O. D. L. Torre, M. Renz, and N. Villandier. Production of High-Quality Diesel from Biomass Waste Products. *Angewandte Chemie International Edition*, 50:2375–2378, Jan. 2011.

[13] P. Daoutidis, A. J. Kelloway, W. A. Marvin, S. Rangarajan, and A. I. Torres. Process systems engineering for biorefineries: new research vistas. *Current Opinion in Chemical Engineering*, 2:442–447, 2013.

[14] P. Daoutidis, W. A. Marvin, S. Rangarajan, and A. I. Torres. Engineering Biomass Conversion Processes: A Systems Perspective. *AIChE Journal*, 59:3–18, 2013.

[15] P. Daoutidis, W. A. Marvin, S. Rangarajan, and A. I. Torres. Engineering Biomass Conversion Processes: A Systems Perspective. 59(1):3–18, 2013.

[16] W. De Jong and G. Marcotullio. Overview of Biorefineries based on Co-Production of Furfural, Existing Concepts and Novel Developments. *International Journal of Chemical Reactor Engineering*, 8, 2010.

[17] U. M. Diwekar. *Introduction to Applied Optimization*. New York: Springer, 2008.

[18] J. M. Douglas. *Conceptual design of chemical processes*. New York: McGraw Hill, 1988.

[19] S. R. Fore, W. Lazarus, P. Porter, and N. Jordan. Economics of small-scale on-farm use of canola and soybean for biodiesel and straight vegetable oil biofuels. *Biomass and Bioenergy*, 35(1):193–202, Jan. 2011.

[20] S. R. Fore, P. Porter, and W. Lazarus. Net energy balance of small-scale on-farm biodiesel production from canola and soybean. *Biomass and Bioenergy*, 35(5):2234–2244, May 2011.

[21] T. Fortenbery. Biodiesel feasibility study: an evaluation of biodiesel feasibility in Wisconsin. *Staff Paper Series*, (481), 2005.

[22] B. Freedman and E. Pryde. Variables affecting the yields of fatty esters from transesterified vegetable oils. *Journal of the American Oil*, 61(10):1638–1643, 1984.

[23] P. Gallezot. Conversion of biomass to selected chemical products. *Chemical Society reviews*, 41(4):1538–1558, Feb. 2012.

[24] F. Group. Website: World membrane separation technologies to 2017 - industry market research, url: http://www.freedoniagroup.com/world-membrane-separation-technologies.html, accessed march 2015, March 2015.

[25] K. Guthrie and W. Grace. Data and techniques for preliminary capital cost estimating. *Chemical Engineering*, 76:114–142, 1969.

[26] D. J. Hayes, S. Fitzpatrick, M. Hayes, and J. R. H. Ross. The biofine process - production of levulinic acid, furfural, and formic acid from lignocellulosic feedstocks. In *Biorefineries-Industrial Processes and Products: Status Quo and Future Directions*. Wiley-VCH Verlag GmbH, 2008.

[27] W. Hettinga, H. Junginger, S. Dekker, M. Hoogwijk, A. McAloond, and K. Hicks. Understanding the reductions in us corn ethanol production costs: An experience curve approach. *Energy Policy*, 37:190–203, 2009.

[28] J. Hill, E. Nelson, D. Tilman, S. Polasky, and D. Tiffany. Environmental, economic, and energetic costs and benefits of biodiesel and ethanol biofuels. *Proceedings of the National Academy of Sciences of the United States of America*, 103(30):11206–10, July 2006.

[29] K. Hofvendahl and B. Hahn-Hägerdal. Factors affecting the fermentative lactic acid production from renewable resources(1). *Enzyme and microbial technology*, 26(2-4):87–107, Feb. 2000.

[30] ICIS.com. Chemical price reports. 2011.

[31] J. Jae, G. A. Tompsett, Y.-C. Lin, T. R. Carlson, J. Shen, T. Zhang, B. Yang, C. E. Wyman, W. C. Conner, and G. W. Huber. Depolymerization of lignocellulosic biomass to fuel precursors: maximizing carbon efficiency by combining hydrolysis with pyrolysis. *Energy & Environmental Science*, 3(3):358–365, 2010.

[32] B. Kamm and M. Kamm. Biorefineries - Multi Product Processes. *White Biotechnology*, (January):175–204, 2007.

[33] F. Kapteijn and R. Moulijn, J.A.and Krishna. Diffusion of binary mixtures in zeolites: Molecular dynamics simulations versus maxwell-stefan theory. *Chemical Engineering Science*, 55:2923–2930, 2000.

[34] K. T. Klemola and J. K. Ilme. Distillation efficiencies of an industrial-scale i-butane/n-butane fractionator. *Industrial and Engineering Chemistry Research*, 35:4579–4586, 1996.

[35] R. Krishna. Diffusion of binary mixtures in zeolites: Molecular dynamics simulations versus maxwell-stefan theory. *Chemical Physics Letters*, 326:477–484, 2000.

[36] J. R. Kwiatkowski, A. J. McAloon, F. Taylor, and D. B. Johnston. Modeling the process and costs of fuel ethanol production by the corn dry-grind process. *Industrial Crops and Products*, 23:288–296, 2006.

[37] T. Leathers. Bioconversions of maize residues to value-added coproducts using yeast-like fungi. *FEMS Yeast Research*, 3(2):133–140, Apr. 2003.

[38] J. Marriott and E. Sørensen. The optimal design of membrane systems. *Chemical Engineering Science*, 58(22):4991–5004, 2003.

[39] J. G. Martinek, T. Q. Gardner, R. D. Noble, and J. L. Falconer. Modeling transient permeation of binary mixtures through zeolite membranes. *Industrial and Engineering Chemistry Research*, 45(17):6032–6043, 2006.

[40] W. A. Marvin, S. Rangarajan, and P. Daoutidis. Automated Generation and Optimal Selection of Biofuel-Gasoline Blends and Their Synthesis Routes. *Energy and Fuels*, 2013.

[41] C. V. McNeff, L. C. McNeff, B. Yan, D. T. Nowlan, M. Rasmussen, A. E. Gyberg, B. J. Krohn, R. L. Fedie, and T. R. Hoye. A continuous catalytic system for biodiesel production. *Applied Catalysis A: General*, 343(1-2):39–48, July 2008.

[42] S. Murat Sen, C. A. Henao, D. J. Braden, J. A. Dumesic, and C. T. Maravelias. Catalytic Conversion of Lignocellulosic Biomass to Fuels: Process Development and Technoeconomic Evaluation. *Chemical Engineering Science*, 67(1):57–67, July 2011.

[43] P. E. Murillo-Alvarado, J. M. Ponce-Ortega, M. Serna-González, A. J. Castro-Montoya, and M. M. El-Halwagi. Optimization of Pathways for Biorefineries Involving the Selection of Feedstocks, Products, and Processing Steps. *Industrial & Engineering Chemistry Research*, 52(14):5177–5190, Apr. 2013.

[44] D. K. S. Ng. Automated targeting for the synthesis of an integrated biorefinery. *Chemical Engineering Journal*, 162(1):67–74, Aug. 2010.

[45] N. P. Nghiem, K. B. Hicks, and D. B. Johnston. Integration of succinic acid and ethanol production with potential application in a corn or barley biorefinery. *Applied Biochemistry and Biotechnology*, 162(7):1915–1928, Nov. 2010.

[46] P. Nigam and D. Singh. Processes for Fermentative Production of Xylitol - a Sugar Substitute. *Process Biochemistry*, 30(2):117–124, 1995.

[47] D. J. O'Brien, L. H. Roth, and A. J. McAloon. Ethanol production by continuous fermentation-pervaporation: a preliminary economic analysis. *Journal of Membrane Science*, 166:105–111, 2000.

[48] R. Perry and D. Green. *Perry's Chemical Engineers' Handbook.* New York: McGraw-Hill, 2008.

[49] V. Pham and M. M. El-Halwagi. Process synthesis and optimization of biorefinery configurations. *AIChE Journal*, 58(4), 2011.

[50] D. W. Rackemann, W. O. S. Doherty, and T. Crops. The conversion of lignocellulosics to levulinic acid. *Biofuels, Bioproducts and Biorefining*, pages 198–214, 2011.

[51] S. Rangarajan, A. Bhan, and P. Daoutidis. Rule-Based Generation of Thermochemical Routes to Biomass Conversion. *Industrial & Engineering Chemistry Research*, 49(21):10459–10470, Nov. 2010.

[52] N. Sammons, W. Yuan, and M. Eden. A systematic framework for biorefinery production optimization. *Proceedings of the 18th European Symposium on Computer Aided Process Engineering*, pages 1077–1082, 2008.

[53] N. Sammons, W. Yuan, M. Eden, B. Aksoy, and H. Cullinan. Optimal biorefinery product allocation by combining process and economic modeling. *Chemical Engineering Research and Design*, 86(7):800–808, July 2008.

[54] E. J. Santibanez-Aguilar, J. B. Gonz, M. Serna-gonz, and M. M. El-halwagi. Optimal Planning of a Biomass Conversion System Considering Economic and Environmental Aspects. *Industrial & Engineering Chemistry Research*, pages 8558–8570, 2011.

[55] Sartec. Prices and equipment sizes. *Personal communication with Sartec, Inc.*, 2011.

[56] H. Song and S. Y. Lee. Production of succinic acid by bacterial fermentation. *Enzyme and Microbial Technology*, 39(3):352–361, July 2006.

[57] N. Sridhar and D. Hill. Carbon dioxide utilization: Electrochemical conversion of co2 - opportunities and challenges. Technical report, DNV Research and Innovation, Position Paper, 2011.

[58] G. Stephanopoulos. Process Systems Engineering: From Solvay to the 21st Century. A History of Development, Successes and Prospects for the Future. *Computer Aided Chemical Engineering*, 27:149–155, 2009.

[59] P. R. Stuart and M. M. El-Halwagi. *Integrated Biorefineries: Design, Analysis and Optimization.* CRC Press, 2013.

[60] M. Tawarmalani and N. V. Sahinidis. A polyhedral branch-and-cut approach to global optimization. *Mathematical Programming*, 103(2):225–249, May 2005.

[61] D. H. S. Tay, H. Kheireddine, D. K. S. Ng, M. M. El-Halwagi, and R. R. Tan. Conceptual Synthesis of Gasification-Based Biorefineries Using Thermodynamic Equilibrium Optimization Models. *Industrial & Engineering Chemistry Research*, 50(18):10681–10695, Sept. 2011.

[62] D. H. S. Tay, D. K. S. Ng, H. Kheireddine, and M. M. El-Halwagi. Synthesis of an integrated biorefinery via the C-H-O ternary diagram. *Clean Technologies and Environmental Policy*, 13(4):567–579, Mar. 2011.

[63] D. H. S. Tay, D. K. S. Ng, N. E. Sammons, and M. R. Eden. Fuzzy Optimization Approach for the Synthesis of a Sustainable Integrated Biorefinery. *Industrial & Engineering Chemistry Research*, 50(3):1652–1665, Feb. 2011.

[64] TradingCharts.com. Soybean oil weekly commodity futures price chart. 2011.

[65] R. Turton. *Analysis, synthesis, and design of chemical processes*. Upper Saddle River, N.J. Prentice Hall, 2009.

[66] O. P. van Vliet, A. P. Faaij, and W. C. Turkenburg. Fischer-Tropsch diesel production in a well-to-wheel perspective: A carbon, energy flow and cost analysis. *Energy Conversion and Management*, 50(4):855–876, Apr. 2009.

[67] L. M. Vane and F. R. Alvarez. Membrane assisted vapor stripping: energy efficient hybrid distillation: Vapor permeation process for alcohol-water separation. *Journal of Chemical Technology & Biotechnology*, 1287:1275–1287, 2008.

[68] P. Vareltzis, E. Kikkinides, and M. Georgiadis. On the optimization of gas separation processes using zeolite membranes. *Chemical Engineering Research and Design*, 81(5):525–536, 2003.

[69] G. Vicente, M. Martínez, and J. Aracil. Integrated biodiesel production: a comparison of different homogeneous catalysts systems. *Bioresource technology*, 92(3):297–305, May 2004.

[70] G. Vicente, M. Martínez, and J. Aracil. Optimisation of integrated biodiesel production. Part II: a study of the material balance. *Bioresource technology*, 98(9):1754–61, July 2007.

[71] Z. Vroon, r. K. Keize, M. Gilde, H. Verweij, and A. Burggraaf. Transport properties of alkanes through ceramic thin zeolite mfi membranes. *Journal of Membrane Science*, 113(2):293–300, 1996.

[72] T. Werpy, G. Petersen, A. Aden, and J. Bozell. Top Value Added Chemicals From Biomass. Volume 1 - Results of Screening for Potential Candidates From Sugars and Synthesis Gas. Technical report, Pacific Northwest National Laboratory (PNNL) and National Renewable Energy Laboratory (NREL), 2004.

[73] G. Wiltsee. Urban Waste Grease Resource Assessment. Technical report, National Renewable Energy Laboratory, 1998.

[74] M. M. Wright and R. C. Brown. Distributed processing of biomass to bio-oil for subsequent production of Fischer-Tropsch liquids. *Biofuels, Bioproducts and Biorefining*, pages 229–238, 2008.

[75] M. M. Wright, D. E. Daugaard, J. A. Satrio, and R. C. Brown. Techno-economic analysis of biomass fast pyrolysis to transportation fuels. *Fuel*, 89:S2—-S10, 2010.

[76] G. Xomeritakis, S. Nair, and M. Tsapatsis. Transport properties of alumina-supported mfi membranes made by secondary (seeded) growth.

[77] Q. Xue, T. J. Heindel, and R. O. Fox. A CFD model for biomass fast pyrolysis in fluidized-bed reactors. *Chemical Engineering Science*, 66(11):2440–2452, June 2011.

[78] Z. Yuan, B. Chen, and R. Gani. Applications of process synthesis: Moving from conventional chemical processes towards biorefinery processes. *Computers & Chemical Engineering*, 49:217–229, Feb. 2013.

[79] J. G. Zeikus, M. K. Jain, and P. Elankovan. Biotechnology of succinic acid production and markets for derived industrial products. *Applied Microbiology and Biotechnology*, 51(5):545–552, May 1999.

[80] K. Zhang, R. Lively, C. Zhang, W. Koros, and R. Chance. Investigating the intrinsic ethanol/water separation capability of zif-8: an adsorption and diffusion study. *The Journal of Physical Chemistry C*, 117:7214–7225, 2013.

[81] R. W. R. Zwart and H. Boerrigter. High Efficiency Co-production of Synthetic Natural Gas (SNG) and Fischer-Tropsch (FT) Transportation Fuels from Biomass. *Energy & Fuels*, 19(2):591–597, Mar. 2005.